



# New constraints on the early formation of the Western Dharwar Craton (India) from igneous zircon U-Pb and Lu-Hf isotopes

Martin Guitreau, Samuel B. Mukasa, Lorne Loudin, Sajeew Krishnan

## ► To cite this version:

Martin Guitreau, Samuel B. Mukasa, Lorne Loudin, Sajeew Krishnan. New constraints on the early formation of the Western Dharwar Craton (India) from igneous zircon U-Pb and Lu-Hf isotopes. *Precambrian Research*, 2017, 302, pp.33-49. 10.1016/j.precamres.2017.09.016 . hal-04432083

**HAL Id: hal-04432083**

**<https://hal.science/hal-04432083>**

Submitted on 1 Feb 2024

**HAL** is a multi-disciplinary open access archive for the deposit and dissemination of scientific research documents, whether they are published or not. The documents may come from teaching and research institutions in France or abroad, or from public or private research centers.

L'archive ouverte pluridisciplinaire **HAL**, est destinée au dépôt et à la diffusion de documents scientifiques de niveau recherche, publiés ou non, émanant des établissements d'enseignement et de recherche français ou étrangers, des laboratoires publics ou privés.

# New constraints on the early formation of the Western Dharwar Craton (India) from igneous zircon U-Pb and Lu-Hf isotopes

## **Highlights:**

- We present new U-Pb and Lu-Hf isotope data for igneous zircons from the WDC (75 characters)
- We found the oldest granitoid of the WDC which is a 3411 Ma peraluminous orthogneiss (85 characters)
- This orthogneiss is suggested to mark the beginning of the WDC formation (72 characters)
- Our results reveal that ancient crust up to 3607 Ma is present as inherited zircons (83 characters)
- No crust older than 3410 Ma was involved in the WDC formation prior to ~3200 Ma (79 characters)

1 New constraints on the early formation of the Western Dharwar  
2 Craton (India) from igneous zircon U-Pb and Lu-Hf isotopes

3

4 Martin Guitreau<sup>1,2,3\*</sup>, Samuel B. Mukasa<sup>1,4</sup>, Lorne Loudin<sup>1,5</sup>, Sajeew Krishnan<sup>6</sup>

5

6 <sup>1</sup> CEPS-Department of Earth Sciences, University of New Hampshire, James Hall, 56  
7 College Road, Durham, NH 03824, USA

8 <sup>2</sup> School of Earth and Environmental Sciences, The University of Manchester,  
9 Williamson building, Oxford road, Manchester, M13 9PL, UK

10 <sup>3</sup> Université Clermont Auvergne, Laboratoire Magmas et Volcans, IRD, CNRS, UMR  
11 6524, 6 avenue Blaise Pascal, 63178 Aubière, France

12 <sup>4</sup> Department of Earth Sciences, University of Minnesota, Pillsbury Hall, 310 Pillsbury  
13 Drive SE, Minneapolis, MN 55455, USA

14 <sup>5</sup> Gemological Institute of America, Inc., 50 W 47th Street, New York, NY 10036, USA

15 <sup>6</sup> Centre for Earth Sciences, Indian Institute of Science, Bangalore 560 012, India

16 \* Corresponding author: martin.guitreau@uca.fr

17

18 Keywords: Western Dharwar Craton, zircon U-Pb geochronology, Lu-Hf isotope  
19 system, continents, Archean

20

21 Word count: abstract = 344; Main text = 10492; Figures = 9 (+ 6 in supplementary)  
22 and Tables = 4 (+6 in supplementary); refs = 124

23

24

**Abstract:**

The Western Dharwar Craton (WDC) is an Archean crustal segment for which the earliest stages of development have remained poorly constrained because the oldest identified lithologies are chronologically indistinguishable despite vastly different compositions and origins (i.e.,  $3352 \pm 110$  Ma Sargur-group komatiites and  $3342 \pm 6$  Ma Hassan-Gorur TTG gneiss). Indication for older crust come from ancient detrital zircons (3450-3610 Ma), although their genetic link to the WDC is purely conjectural. In order to bring new understanding to early development of the WDC, we studied orthogneisses around the Holenarsipur Schist Belt (HSB) for their petrography, major-oxide concentrations, zircon U-Pb geochronology, and Lu-Hf isotope systematics. Our results reveal that the WDC igneous record contains crust older than 3350 Ma in the form of a  $3410.8 \pm 3.6$  Ma granitic gneiss and inherited zircons with ages ranging from  $3295 \pm 18$  to  $3607 \pm 16$  Ma that were found within a  $3178 \pm 10$  Ma trondhjemitic gneiss and a biotite-rich enclave found within it. The presence of muscovite and the peraluminous signature of the granitic gneiss, in spite of mildly-depleted Hf isotopic signature ( $\epsilon_{\text{Hf}} = +2.2 \pm 0.6$  at 3410.8 Ma), suggest that this sample formed by reworking of a felsic precursor with short crustal residence time, possibly marking the beginning of WDC formation. The oldest inherited zircons display variable  $\epsilon_{\text{Hf}}$  ranging from +10.4 at 3414 Ma to -2.3 at 3607 Ma that did not seem to have influenced the Hf isotopic composition of granitoids of the WDC that formed between 3200 and 3410 Ma, except perhaps in the Sargur area. We suggest that the WDC formed remote from continental crust until a crustal block containing >3410 Ma zircons was accreted to it ~3200 My ago. This event resulted in the stabilization of the WDC which is marked by diapiric granitoids to which the 3178 Ma trondhjemitic gneiss belongs.



After 3200 Ma, the crustal block together with granitoids formed between 3410 and 3200 Ma buffered the Hf isotopic signature of newly formed granitoids, hence, indicating that, by then, the WDC already was a stable continental segment.

## 1. Introduction:

The Western Dharwar Craton (WDC; Southern India) is amongst the best-preserved pieces of Archean crust and therefore has been well studied (e.g., Naqvi and Rogers, 1987; Bouhallier et al., 1995; Chardon et al., 2008; Ramakrishnan, 2009; Dey, 2013; Jayananda et al., 2015). It has recorded multiple episodes of magmatic and volcanic activity as well as several sedimentary cycles and tectonic events that started in the Paleoproterozoic (~3400 Ma) and ended around the Archean-Proterozoic transition (~2500 Ma), although later metamorphic events have also occurred (e.g., Naqvi and Rogers, 1987; Bhaskar Rao et al., 1992; Meen et al., 1992; Miller et al., 1996; Table 1). Despite a large number of studies, including recent ones, having addressed the question of the evolution of the Dharwar craton (e.g., Naqvi and Rogers, 1987; Chadwick et al., 2000; Jayananda et al., 2008; Lancaster et al., 2015), there still is uncertainty in the timing and the nature of WDC's first crust formation. This is because the two oldest known lithologies appear coeval within analytical uncertainty, and yet have vastly different compositions. These units are the  $3352 \pm 110$  Ma Sargur-group komatiites (Jayananda et al., 2008) and the Hassan-Gorur gneisses, ranging from dioritic amphibolites to typical TTGs (e.g., Beckinsale et al., 1980; Bhaskar Rao et al., 1991; Naqvi et al., 2009; Jayananda et al., 2015). These orthogneisses have been dated at  $3358 \pm 66$  Ma by Beckinsale et al., (1980), and more recently refined to  $3342 \pm 6$  Ma by Jayananda et al. (2015). Yet, zircons from detrital metasediments (i.e., quartzites and conglomerates; Nutman et al., 1992; Lancaster et al., 2015; Bhaskar Rao et al., 2008; Sarma et al., 2012)

75 reveal the presence of sialic crust as old as  $3542 \pm 9$  to  $3634 \pm 10$  Ma in the vicinity of  
76 WDC between  $\sim 3300$  My and  $\sim 2500$  My ago, as deduced from the estimated age of  
77 deposition for the studied detrital sediments of the WDC ([Table 1](#)). Some of the Nd  
78 isotopic signatures displayed by Hassan-Gorur gneisses are consistent with the  
79 involvement of pre-existing crust in their genesis ([Jayananda et al., 2015](#)), but closed-  
80 system evolution of the Sm-Nd isotope system in these gneisses cannot be verified.  
81 Therefore, the actual age of the oldest generations of WDC's peninsular gneisses  
82 remains uncertain (e.g., [Jayananda et al., 2008, 2015](#); [Naqvi et al., 2009](#); [Dey, 2013](#);  
83 [Lancaster et al., 2015](#)), while it bears a great deal on our understanding of the early  
84 history of the Dharwar Craton.

85         Zircons derived from terranes adjacent, or accreted, to a craton, after its major  
86 stages of formation, can contribute to the local detrital zircon record. Interestingly,  
87 neighboring Bastar and Bundelkhand cratons, as well as the Coorg Block, contain old  
88 gneisses dated at  $3509 \pm 14$  Ma ([Sarkar et al., 1993](#)),  $3561 \pm 11$  Ma ([Ghosh, 2004](#)),  
89  $3582.6 \pm 4$  Ma ([Rajesh et al., 2009](#)),  $3550.9 \pm 5.9$  Ma ([Kaur et al., 2014](#)), and  $3502 \pm$   
90  $11$  Ma ([Santosh et al., 2016](#)). Rare ancient zircon cores have also been found in TTG  
91 gneisses from the Karwar Block ( $3473$ - $3601$  Ma; [Ishwar-Kumar et al., 2013](#)). However,  
92 while WDC's oldest detrital zircons show coherent Hf isotopic signatures (see [Sarma](#)  
93 [et al., 2012](#); [Lancaster et al., 2015](#)), they generally differ from those of their coeval  
94 igneous counterparts from Coorg Block and Bundelkhand Craton's oldest gneiss  
95 ([Santosh et al., 2016](#); [Kaur et al., 2014](#)), possibly indicating a different origin.  
96 Quartzites and greywackes in which Paleoarchean detrital zircons have been found, are  
97 assumed to have been deposited at respective ages of  $\sim 3300$ - $3200$ ,  $\sim 2900$  Ma, and  
98  $\sim 2500$  Ma (e.g., [Nutman et al., 1992](#); [Bhaskar Rao et al., 1992, 2008](#); [Peucat et al.,](#)  
99 [1995](#); [Sarma et al., 2012](#); [Hokada et al., 2013](#); [Table 1](#)). Therefore, it remains uncertain

if the ages indicated by detrital zircons accurately depict the age of the oldest crusts involved in development of the WDC.

To shed new light on the context of early formation of the Western Dharwar Craton, we have conducted a field survey of some of the oldest generations of peninsular gneisses in the Hassan-Gorur area. Here, we report on two felsic gneisses and an enclave found within one of them, as well as on their zircon U-Pb ages and Hf isotopic signatures. Our new results considered with available data on the WDC bring important constraints on the early development of the WDC.

## **2. Geological background**

The Dharwar craton (Southern India) is subdivided into a western (WDC) and an eastern (EDC) part that are separated by a major shear zone along the Chitradurga greenstone belt (“Ch” in Fig. 1), and a N-S trending intrusion composed of late Archean K-rich granites (i.e., Closepet batholith; e.g., [Moyen et al., 2003](#); [Fig. 1](#)). Most of the rocks of the EDC exhibit Neoarchean ages, whereas those found in the WDC have protoliths dated at ~2500 and up to ~3360 Ma (e.g., [Beckinsale et al., 1980](#); [Naqvi and Rogers, 1987](#); [Meen et al., 1992](#); [Bhaskar Rao et al., 1992](#); [Jayananda et al., 2008, 2015](#); [Sarma et al., 2012](#); [Dey, 2013](#)). The Dharwar craton had been northwardly tilted, probably sometime between 2400 and 1600 Ma ([Ramakrishnan, 2009](#)), and therefore displays an almost entire conformable crustal sequence characterized by a continuous increase in metamorphic grade from greenschist to granulite toward South (e.g., [Pichamuthu, 1965](#); [Rollinson et al., 1981](#); [Hansen et al., 1985](#); [Raase et al., 1986](#)). Tonalite-trondhjemite-granodiorite (TTG) gneisses, locally named peninsular gneisses, make up the basement of the WDC and dominantly crop out in the southern regions (Fig. 1). These orthogneisses are intercalated with highly deformed supracrustal

sequences of the ~3.4-3.0 Ga Sargur group (e.g., [Naqvi and Rogers, 1987](#); [Yoshida et al., 1994](#); [Jayananda et al., 2008, 2015](#)) that were equilibrated in high-metamorphic grade in the late-Archean (i.e., ~8kbar and ~700-750°C around 2430 Ma; [Janardhan et al., 1982](#); [Raith et al., 1983](#); [Jayananda et al., 2013](#)). Both the Peninsular gneisses and the Sargur group are unconformably overlain by the 2.9-2.5 Ga Dharwar supergroup ([Table 1](#)), which is less deformed and less metamorphosed than the Sargur group. Therefore, the oldest remnants are located in the South, in high-grade metamorphic conditions, and the youngest, less metamorphosed greenstones, are located in northern regions of the WDC ([Fig. 1](#)). Some younger granites (2700-2500 Ma) are also found throughout the WDC (e.g., [Taylor et al., 1984](#); [Meen et al., 1992](#)). The general dome-and-basin structure exhibited by the WDC have been documented in several studies that concluded that denser greenstone belts sunk into the basement gneisses by sagduction (e.g., [Bouhallier et al., 1993, 1995](#); [Chardon et al., 1996, 1998](#)).

Supracrustal (greenstone) belts are very abundant in the WDC and they contain either one or both volcano-sedimentary groups (e.g. [Hokada et al., 2013](#)); the Sargur group (~3350-3000 Ga) and the Dharwar supergroup (2900-2500 Ga), the latter of which is further sub-divided into Chitradurga (upper section) and Bababudan groups (lower section) based on lithologies and ages (e.g., [Naqvi and Rogers, 1987](#); [Ramakrishnan, 2009](#); [Table 1](#)). Sargur Group volcanic sequences are dominated by komatiites and tholeiitic basalts, with subordinate felsic lava flows, whereas the Dharwar Supergroup volcanics contain abundant tholeiitic to felsic volcanics with subordinate komatiitic basalts. Sediments composing Sargur and Dharwar groups are conglomerate, quartzite, pelite, carbonate, and banded iron formation. According to [Ramakrishnan \(2009\)](#), the Sargur Group occurs in two types of lithological association, namely: (i) linear ultramafic-mafic belts containing subordinate clastic sediments and

BIF (e.g. Nuggihalli, Nagamangala and Krishnarajpet), and (ii) scattered ultramafic-mafic enclaves associated with quartzite-carbonate-pelite-BIF assemblage (e.g. Sargur and Mercara). The same author, together with [Chadwick et al. \(1989\)](#), indicates that the Dharwar sequence consists of three lithological packages that are, in the ascending order, (1) a basal quartz-pebble conglomerate with amygdular metabasalt alternations, local felsic volcanics, and banded-iron formation (BIF), which correspond to the Bababudan Group, (2a) a polymict conglomerate, quartzite, pelite, carbonate, and Mn/Fe formations that define the Vanivilas Subgroup of the Chitradurga Group, (2b) pillowed metabasalts, felsic volcanics, and BIF which form the Ingaldhal Subgroup of the Chitradurga Group, and (3) a greywacke turbidite, a polymict conglomerate, and a BIF horizon that correspond to the Ranibennur Subgroup of the Chitradurga Group.

The peninsular gneisses exhibit ages from 3360 to 3000 Ma and are somewhat heterogeneous in age and composition (e.g., [Beckinsale et al., 1980](#); [Rogers et al., 1986](#); [Bhaskar Rao et al., 1991](#); [Jayananda et al., 2015](#)). Multiple generations of peninsular gneisses have been identified and classified using different criteria (e.g., [Janardhan et al., 1978](#); [Bhaskar Rao et al., 1983](#); [Naqvi et al., 1983](#); [Monrad, 1983](#)) but the most commonly used classification has been that of [Monrad \(1983\)](#), which is mainly based on geochemistry. The latter author, through the example of the Hassan District (Karnataka), proposed a low-Rb group (~3360-3200 Ma), a low-Al group (~3200-3100 Ma), a high-Al group (~3000 Ma) and a post-tectonic group (~3000-2900 Ma) corresponding to massive diapiric bodies (e.g., Halekote trondhjemite, Chikmagalur granite; [Stroh et al., 1983](#); [Taylor et al., 1984](#); [Meen et al., 1992](#)). A recent study (i.e., [Jayananda et al., 2015](#)) refined the classification of peninsular gneisses around the Hassan district as follows: older TTG gneisses, which contain a low-Al and high-Al group (3340-3280 Ma), younger trondhjemites, including Halekote-type, (3230-3200

Ma), eastern gneisses (3100 Ma) and the Chikmagalur granite (3150 Ma). The older TTG gneisses have chemical characteristics suggesting that they formed by partial melting of essentially undepleted heterogeneous mafic crusts at shallow depth and high pressure, for the low-Al and high-Al group, respectively. In addition, older TTG gneisses indicate possible interaction with pre-existing crust during emplacement. Similar mafic sources can account for the formation of the trondhjemites (e.g., Halekote-type) with significant interaction with pre-existing crust as testified to by the presence of inherited zircon cores (e.g., [Jayananda et al., 2015](#)). The eastern gneisses more likely represent shallow level melting of depleted mafic sources subsequently contaminated by older TTG gneisses (low-Al type), whereas the Chikmagalur granite most likely originate from partial melting of newly formed TTG crust at lower crustal level.

In a craton-wide compilation of available Nd isotope data, [Dey, \(2013\)](#) proposed that the WDC formed through essentially juvenile addition (mafic and felsic) between 3360 and 3000 Ma ( $\epsilon_{\text{Nd}} = +1.5$  to  $+6.4$ ), followed by dominantly mafic crust addition between 2900 and 2600 Ga ( $\epsilon_{\text{Nd}} = -0.3$  to  $+0.4$ ), and major crust reworking at 2600-2500 Ma, accompanied by minor juvenile input. A recent study dealing with detrital zircon U-Pb and Lu-Hf isotope systematics ([Lancaster et al., 2015](#)) concluded that there had been significant juvenile crust extraction from  $\sim 3.3$  to 2.7 Ga and cratonization at  $\sim 3.0$  Ga in the WDC. These authors also suggested continuous extraction of mantle melts from as far back as 3.7 Ga to 3.3 Ga, which matches ages of some detrital zircons ([Table 1](#) and references therein) but are mostly absent from the igneous record.

### 3. Sampling strategy and sample description

Samples analyzed in this study were collected in two separate locations around the Holenarsipur Schist Belt (HSB; Fig. 2; Table 2) because this area hosts WDC's oldest peninsular gneisses reported so far (e.g., Beckinsale et al., 1980; Bhaskar Rao et al., 1991; Meen et al., 1992; Jayananda et al., 2015). The HSB area consists of volcano-sedimentary successions that mostly belong to the Sargur group (e.g., Peucat et al., 1995; Jayananda et al., 2008) and that sunk by sagduction into 3350-3300 Ma peninsular gneisses (e.g., Beckinsale et al., 1980; Bouhallier et al., 1993; Jayananda et al., 2015). Both peninsular gneisses and the HSB were intruded by Halekote trondhjemites ~3200 My ago (e.g., Taylor et al., 1984; Jayananda et al., 2015). Most of the gneisses analyzed in previous studies were collected in quarries (e.g., Beckinsale et al., 1980; Bhaskar Rao et al., 1991; Jayananda et al., 2015), hence possibly missing the oldest generations of peninsular gneisses. Consequently, we have purposely sampled gneisses both inside, and outside quarries where, however, outcrops are limited. Nevertheless, we made every effort to collect fresh samples, free of any altered surfaces.

### **3.1. Field occurrence of orthogneiss 13DC12**

Sample 13DC12 is a fine-grained and massive to very weakly foliated brownish orthogneiss collected from meter- to decameter-scale outcrops protruding from weathered soils (Fig. 3A). Medium-grained pegmatite veins, which belong to only one identifiable generation, crosscut the orthogneiss (Fig. 3A), but these were avoided in collecting sample 13DC12. As summarized in Table 2, this sample is composed dominantly of quartz, plagioclase, K-Feldspar (microcline), but also contains biotite, muscovite, and very few opaque phases (e.g., oxide, sulfide). At the hand-sample scale some rare 1-5 mm octahedral metallic phases are also visible. In thin section (see Figs.

3B and 3C), quartz consists of medium-sized to large xenomorphs that sometimes contain smaller euhedral to subhedral quartz grains, likely recrystallized statically. Plagioclase often appears as medium to large sub-euhedral to xenomorphic crystals showing variable degrees of sericitization. K-Feldspar is commonly found as small xenomorphs intercalated between larger quartz or plagioclase grains, although big crystals can sometimes be found. Biotite is always present as small subhedral crystals, often altered into chlorite. In places, zircon is visible within biotite because of the halo generated through radioactive decay of zircon-hosted U and Th. Muscovite forms bigger crystals than biotite and they are often subhedral. Although the rock appears massive to weakly foliated, and displays a granoblastic texture (Figs. 3B and 3C), bands of grain-size reduction down to a factor of ~5, are visible at the thin section scale. However, no noticeable change in mineralogy is observed in these bands.

### 3.2. Field occurrence of orthogneiss 13DC13

Sample 13DC13 is a fresh, grey, and fine-grained orthogneiss (Fig. 3D), that is massive to weakly foliated. In contrast to the field occurrence of orthogneiss 13DC12, this sample was collected in a large (~500 x 500 m) active quarry (Fig. 3D; Table 2) throughout which the outcrops are homogeneous. It is, nevertheless, crosscut by multiple generations of pegmatite veins of various sizes and spatial distribution (Fig. 3D), and some biotite-rich enclaves ranging in size from ~5 x 2 to ~30 x 10 cm can also be found sparsely distributed within it. Sample 13DC13 is composed essentially of plagioclase, quartz, K-Feldspar (microcline), biotite, and muscovite (Table 2). In thin section (see Figs. 3E and 3F), quartz appears as medium-sized and relatively fresh xenomorphs. Plagioclase show little sericitization and also occurs as subhedral crystals to xenomorphs of substantial size, in contrast to K-Feldspar which is commonly small



with the exception of some rare large and fresh xenomorphs that are likely secondary. Biotite is more abundant than in the orthogneiss 13DC12 and crystals are usually subhedral and fresh (no or very little alteration into chlorite). Zircon halos are visible in some biotite crystals. Muscovite is slightly less abundant than biotite but has a similar habitus and size. Both biotite and muscovite seem to have been co-genetically crystallized as they form coherent masses of interspersed crystals. Almost no opaque phase can be seen in thin section. Sample 13DC13 is characterized by a granoblastic texture visible in thin section (Figs. 3E and 3F).

### **3.3. Biotite-rich enclave (13DC15)**

Sample 13DC15 is a fresh ~20 x 10 cm biotite-rich enclave found in the orthogneiss that 13DC13 represents. Due to its high-biotite content, this type of enclave is very often deeply weathered and friable but the ongoing work in the quarry exhumed some fresh samples such as 13DC15. This rock contains approximately 70% biotite (sometimes turned into chlorite), 10% quartz, 10% plagioclase, and 10% of various minerals (e.g., K-Feldspar, muscovite, opaque phases; Table 2).

## **4. Analytical details**

### **4.1. Major and minor element analysis**

Major- and minor-oxide results are given in Table S1. Measurements were done by ICP-AES (Jobin-Yvon ULTIMA C) at the Laboratoire Magmas et Volcans (Clermont-Ferrand, France). The rock standard BHVO-1 was also analyzed so as to determine the precision and accuracy of the measurements. Major- and minor-oxide concentrations were within <1% up to 5% of consensus values (Flanagan, 1976; Abbey, 1983;

Govindaraju, 1994) whereas analytical precisions were better than 1% for both major and minor oxides, except for P<sub>2</sub>O<sub>5</sub> concentration which had 3% uncertainty.

#### 4.2. Zircon U-Pb geochronology by LA-ICP-MS

Zircon crystals were separated at the University of Colorado (Boulder, CO, USA) using standard mineral separation techniques (see Mojzsis et al., 2003). The most optically clear zircon grains devoid of cracks and inclusions were selected and mounted in epoxy together with fragments of the zircon standards AS3 (1099.1 ± 0.5 Ma; Paces and Miller, 1993) and 91500 (1065.4 ± 0.3 Ma; Wiedenbeck et al., 1995). The selected crystals were euhedral to subhedral, pale pink to orange, and transparent to slightly cloudy. The spots analyzed on each grain were selected based on internal textures as revealed by cathodoluminescence (CL) images acquired at the University of New Hampshire using a Tescan Lyra 3 scanning electron microscope.

Zircon U-Pb analyses were carried out by LA-ICP-MS at the University of New Hampshire (UNH). Details regarding operating conditions are given in Table S2 and results can be found in Table 3, and the supplementary Tables S3 and S4. A gold trap was used to lower <sup>204</sup>Hg interferences on <sup>204</sup>Pb and, hence, more accurately detect the presence of common Pb. Measurements were started ~5s after the beginning of the ablation to allow a steady flow of the aerosol from the laser to the mass spectrometer. Time-resolved signals were carefully monitored throughout each and every analysis to ensure optimization and data reproducibility. Further, because of down-hole fractionation, we used the t<sub>0</sub> intercept method based on data regression through linearly shifting isotopic ratios as a function of time (see Košler and Sylvester, 2003; Fisher et al., 2010). Both <sup>207</sup>Pb/<sup>235</sup>U and <sup>206</sup>Pb/<sup>238</sup>U ratios were measured, but the former was only used as a quality check by comparing it to <sup>207</sup>Pb/<sup>235</sup>U calculated from measured

$^{206}\text{Pb}/^{238}\text{U}$  and  $^{207}\text{Pb}/^{206}\text{Pb}$ , as well as a  $^{238}\text{U}/^{235}\text{U}$  of 137.88. Decay constant used are the followings:  $^{238}\lambda = 1.55125 \cdot 10^{-10}$ ,  $^{235}\lambda = 9.8485 \cdot 10^{-10}$  (Jaffey et al., 1971), and  $^{232}\lambda = 4.9475 \cdot 10^{-11}$  (Le Roux and Glendenin, 1963).  $^{207}\text{Pb}/^{206}\text{Pb}$  ages were calculated using iterative convergence. The ISOPLLOT program (Ludwig, 2008) was used to display the processed data on Concordia diagrams and to determine the sample ages. We further measured semi-quantitative (no internal standardization) concentrations of Pb, U, and Th, by using AS3 as an external standard (Paces and Miller, 1993). Finally,  $^{232}\text{Th}/^{238}\text{U}$  ratios were calculated from  $^{208}\text{Pb}/^{206}\text{Pb}$  values and determined  $^{207}\text{Pb}/^{206}\text{Pb}$  ages.

91500 zircon standard was analyzed as an unknown throughout the session for quality check. The weighted average  $^{207}\text{Pb}/^{206}\text{Pb}$  and upper-intercept U-Pb age obtained for 91500, over the course of this study, were both  $1061.6 \pm 7.1$  Ma ( $2\sigma$ ;  $n = 10$ ; Fig. S1). These ages agree well within uncertainty with the commonly accepted ID-TIMS age of  $1065.4 \pm 0.3$  Ma (Wiedenbeck et al., 1995). 91500 zircon standard Pb, U, and Th mean concentrations determined over the course of this study gave  $14.4 \pm 2.1$  ( $2\sigma$ ;  $n = 10$ ),  $66.3 \pm 7.9$ , and  $23.0 \pm 4.5$  ppm (Table S3), respectively. These values are in reasonably good agreement with the respective recommended values of  $15 \pm 4$  ( $2\sigma$ ),  $80 \pm 16$ , and  $29.9 \pm 4.2$  ppm (Wiedenbeck et al., 2004), which are means of analyses performed in 5 different laboratories. The mean calculated  $^{232}\text{Th}/^{238}\text{U}$  obtained for 91500 was  $0.37 \pm 0.01$  ( $2\sigma$ ;  $n = 10$ ; Table S3), which is in agreement with values of  $0.3444 \pm 0.0018$  ( $2\sigma$ ), determined by Wiedenbeck et al. (1995) on 2 zircon fragments, and  $0.38 \pm 0.09$  determined by numerous LA-ICP-MS analyses (Wiedenbeck et al., 2004).

### 4.3. Zircon Lu-Hf isotope analysis by LA-MC-ICP-MS

Lu-Hf isotope analyses were done by LA-MC-ICP-MS at Laboratoire Magmas et Volcans (LMV), Clermont-Ferrand (France). Details regarding the operating conditions are given in [Table S2](#) and results can be found in [Tables 3](#), [S5](#), and [S6](#). Lu-Hf isotope measurements were done using the cup configuration recommended by [Fisher et al. \(2014a\)](#). The Yb and Hf instrumental mass biases used to correct data were determined using  $^{173}\text{Yb}/^{171}\text{Yb}$  normalized to the value of 1.132685 ([Chu et al., 2002](#)) and  $^{179}\text{Hf}/^{177}\text{Hf}$  normalized to the value of 0.7325 ([Stevenson and Patchett 1990](#)). It was further assumed that Lu fractionation followed that of Yb ([Fisher et al., 2014a](#)). A value of 0.79618 for  $^{176}\text{Yb}/^{173}\text{Yb}$  ([Chu et al., 2002](#)) and 0.02655 for  $^{176}\text{Lu}/^{175}\text{Lu}$  ([Fisher et al., 2014a](#)) were used to correct data for the isobaric interferences of  $^{176}\text{Yb}$  and  $^{176}\text{Lu}$  on  $^{176}\text{Hf}$ . In order to monitor instrumental fractionation and data quality, zircon standards 91500, MudTank, Plešovice, and R33 were measured multiple times over the course of the LA-MC-ICP-MS analyses. Lu-Hf isotope analyses were done on top of the pits developed by ablation during the U-Pb isotope analyses in order to acquire linked information. Much like for U-Pb isotope analyses, time-resolved signals were carefully monitored throughout each and every analysis. The  $^{176}\text{Lu}$  decay constant of [Scherer et al. \(2011\)](#) and [Söderlund et al. \(2004\)](#), which is  $1.867 \cdot 10^{-11}$ , was used to calculate initial Hf isotopic compositions. Uncertainties associated with the radiogenic-ingrowth correction were propagated using the algorithms of [Ickert \(2013\)](#). Epsilon notations were derived from normalization to the Bulk Silicate Earth (BSE) Lu-Hf isotopic parameters published by [Iizuka et al. \(2015\)](#).

Obtained mean  $^{176}\text{Hf}/^{177}\text{Hf}$  for 91500, MudTank, Plešovice, and R33 were  $0.282299 \pm 0.000018$  ( $2\sigma$ ;  $n=16$ ),  $0.282501 \pm 0.000017$  ( $2\sigma$ ;  $n=17$ ),  $0.282472 \pm 0.000013$  ( $2\sigma$ ;  $n=7$ ), and  $0.282757 \pm 0.000039$  ( $2\sigma$ ;  $n=9$ ), respectively ([Table S5](#); [Fig. S2](#)). These values are well within uncertainty of the accepted values of  $0.282308 \pm$

0.000006 (Blichert-Toft, 2008) for 91500,  $0.282507 \pm 0.000006$  (Woodhead and Hergt, 2005) for MudTank,  $0.282482 \pm 0.000012$  (Sláma et al., 2008) for Plešovice, and  $0.282764 \pm 0.000014$  (Fisher et al., 2014b) for R33. Determined  $^{176}\text{Yb}/^{177}\text{Hf}$  and  $^{176}\text{Lu}/^{177}\text{Hf}$  for these zircon standards also comply well with those recommended by other authors (Table S5; e.g., Fisher et al., 2014a, 2014b).

## 5. Results

### 5.1. Orthogneiss 13DC12 composition and ages

This sample is characterized by high silica content (74 wt%), moderately high  $\text{Al}_2\text{O}_3$  (13.9 wt%), similar  $\text{Na}_2\text{O}$  and  $\text{K}_2\text{O}$  contents (3.9 and 4.3 wt%, respectively), and low  $\text{Fe}_2\text{O}_3$  (1.47 wt%),  $\text{CaO}$  (0.95 wt%),  $\text{MgO}$  (0.19 wt%),  $\text{TiO}_2$  (0.11 wt%),  $\text{P}_2\text{O}_5$  (0.11 wt%), and  $\text{MnO}$  (0.02 wt%) (Table S1). On an Ab-An-Or normative plot (O'Connor, 1965; Barker, 1979), sample 13DC12 falls in the granite field (Fig. 4A). Major elements further indicate that sample 13DC12 has a peraluminous character ( $\text{A}/\text{CNK}$  and  $\text{A}/\text{NK} > 1$ ; Table S1; Fig. 4B). In addition, it can be seen in Figure 4C that 13DC12 plots at the high-silica end of the domain that characterizes calc-alkalic rock suites, more specifically in the field of Bt- and two-mica granites and on the edge of the field for TTG. Similarly, in the ternary diagram proposed by Laurent et al. (2014) for classification of Archean granitoids, 13DC12 falls in a zone where the fields for Bt- and two-mica granites and hybrid granites overlap (Fig. 4D). Finally, Figure 4E shows that 13DC13 major element concentrations comply with those of melts produced by partial melting of tonalites.

Zircons recovered from this sample have similar habits but exhibit variable internal structures, as revealed by CL images, ranging from simple oscillatory zoning to patchy and/or chaotic domains resembling alteration/recrystallization textures (Fig.

S3). This is in line with the U-Pb data being concordant to highly discordant. Similarly, U and Th concentrations vary from relatively low (<300 ppm for U and <100 ppm for Th; Tables 3 and S4) to high (>1000 ppm; Tables 3 and S4) and positively correlate with degrees of discordance with a change of slope beyond ~1000 ppm U. Measured  $^{207}\text{Pb}/^{206}\text{Pb}$  ages do not show any correlation with discordance in the range 0-40% where they vary between  $3310 \pm 15$  and  $3425 \pm 18$  Ma (Table 3 and S4), but steadily decrease from  $3235 \pm 14$  to  $2696 \pm 11$  Ma between 40 and 71% discordance. The only truly concordant data correspond to two analyses done on the crystal labelled “13DC12\_5” which gave ages of  $3413 \pm 7$  and  $3410 \pm 4$  Ma. The oldest  $^{207}\text{Pb}/^{206}\text{Pb}$  ages determined on 13DC12’s zircon population are in excellent agreement with the age of this concordant zircon. When used together these ages define an upper intercept age and weighted average  $^{207}\text{Pb}/^{206}\text{Pb}$  age of  $3410.8 \pm 3.6$  and  $3408.6 \pm 3.6$  Ma, respectively (Fig. 6). All other zircons taken together, define a single broad Discordia with upper- and lower-intercepts at  $3440 \pm 39$  and  $576 \pm 90$ , respectively (Fig. 6C). Note that the upper-intercept age is consistent, within uncertainty, with that determined from oldest and least discordant zircons. No global correlation is observed between Th/U ratios, which for the vast majority fall within the common range of magmatic zircons (e.g., Wang et al., 2011; Kirkland et al., 2015), and other chemical nor isotopic parameters. None of the observed internal structures indicate the presence of xenocrystic cores, nor of overgrowths (Fig. S3).

Zircons from the granitic gneiss exhibit high  $^{176}\text{Yb}/^{177}\text{Hf}$  and  $^{176}\text{Lu}/^{177}\text{Hf}$  values that are strongly correlated with each other (Table S6). Also, both ratios correlate positively with the measured  $^{176}\text{Hf}/^{177}\text{Hf}$  values, which vary between  $0.280685 \pm 0.000032$  and  $0.281124 \pm 0.000029$ . This correlation almost vanishes when  $^{176}\text{Yb}/^{177}\text{Hf}$  and  $^{176}\text{Lu}/^{177}\text{Hf}$  are plotted against initial  $^{176}\text{Hf}/^{177}\text{Hf}$  (calculated using determined

$^{207}\text{Pb}/^{206}\text{Pb}$  ages) because these latter all agree within error-bars except for two data points which exhibit the most radiogenic  $^{176}\text{Hf}/^{177}\text{Hf}$  (Tables 3 and S4; Fig. 5). These two errant data points resulted from analyses done on two separate crystals (zircons #1 and #2) that exhibit advanced discordance (Tables 3 and S4) and that have been analyzed twice. The other analyses done on these crystals show initial Hf isotopic compositions that comply well with the general Hf isotope initials, especially with those determined on the concordant zircon 13DC12\_5 (i.e.,  $^{176}\text{Hf}/^{177}\text{Hf} = 0.280635 \pm 0.000018$  and  $0.280625 \pm 0.000015$ ). If all initial  $^{176}\text{Hf}/^{177}\text{Hf}$  are calculated at the age given by the concordant crystal, the positive correlation between  $^{176}\text{Yb}/^{177}\text{Hf}$  and  $^{176}\text{Hf}/^{177}\text{Hf}$ , as well as between  $^{176}\text{Lu}/^{177}\text{Hf}$  and  $^{176}\text{Hf}/^{177}\text{Hf}$  completely vanishes. Broad positive correlations are observed between U concentration and  $^{176}\text{Lu}/^{177}\text{Hf}$ , and therefore  $^{176}\text{Yb}/^{177}\text{Hf}$ .

## 5.2. Orthogneiss 13DC13 composition and ages

This sample has high  $\text{SiO}_2$  content (72.6 wt%), high  $\text{Al}_2\text{O}_3$  (15 wt%), relatively high  $\text{Na}_2\text{O}$  (4.9 wt%) and  $\text{CaO}$  (1.82 wt%), moderately low  $\text{K}_2\text{O}$  (2.5 wt%) and  $\text{Fe}_2\text{O}_3$  (1.69 wt%), and low  $\text{MgO}$  (0.50 wt%),  $\text{TiO}_2$  (0.27 wt%),  $\text{P}_2\text{O}_5$  (0.08 wt%), and  $\text{MnO}$  (0.02 wt%) (Table S1). On an Ab-An-Or normative plot (O'Connor, 1965; Barker, 1979), sample 13DC13 falls in the trondhjemite field (Fig. 4). Major elements further indicate that sample 13DC13 has a peraluminous character, much like 13DC12 ( $\text{A}/\text{CNK}$  and  $\text{A}/\text{NK} > 1$ ; Table S1). Figure 4C shows that 13DC13 plots at the high-silica end of the domain that characterizes calc-alkalic rock suites, where the field for TTG and Bt- and two-mica granites overlap. Similarly, in the ternary diagram proposed by Laurent et al. (2014) for the classification of late-Archean granitoids (Fig. 4D), 13DC13 plots where the fields for Bt- and two-mica granites, hybrid granites, and TTG overlap. Finally, in

Figure 4E 13DC13 fall in the compositional range of melts produced by partial melting of tonalities but near the boundary with low-K and high-K mafic rocks.

Zircons from this sample show variable crystal habits from stubby to elongated, and exhibit very different types of internal structures as revealed by CL images (Fig. S4). For example, zircon #5 exhibits a concentrically zoned dark and bright core with sinuous outlines surrounded by an oscillatory-zoned outer part. Zircon #11 has a homogeneous and barely zoned core surrounded by a darker and more chaotic outer rim. In this zircon, part of the core seems to have been resorbed and replaced by the same zircon material as that forming the outer rim. Similar to 13DC12 zircons, those from 13DC13 universally show a correlation between degrees of discordance and U, as well as Th, contents, which respectively vary from a few hundred to a few thousand ppm, and from a few tens to a few hundred ppm (Tables 3 and S4). Measured  $^{207}\text{Pb}/^{206}\text{Pb}$  ages vary between  $3441 \pm 16$  (5% discordant) and  $2836 \pm 20$  Ma (80% discordant) (Fig. 7), and a broad correlation is observed between degrees of discordance and  $^{207}\text{Pb}/^{206}\text{Pb}$  ages. Zircons from sample 13DC13 do not define a single Discordia but instead a funnel-shaped discordance pattern on a Concordia plot with upper-intercept ages ranging from ~3100 to ~3450 Ma (Fig. S5).

Zircons from the trondhjemitic gneiss with Th/U below 0.2 yield dates from 3355 down to 2964 Ma, whereas zircons with Th/U values that characterize the common magmatic range (>0.2-0.8; e.g., Wang et al., 2011; Kirkland et al., 2015) exhibit less variability and older dates (~3450-3320 Ma). Finally, zircons with Th/U >1 exhibit younger dates of 3278-2836 Ma (Tables 3 and S4; Fig.S5).

Determined  $^{176}\text{Lu}/^{177}\text{Hf}$  and  $^{176}\text{Yb}/^{177}\text{Hf}$  for zircons from the trondhjemitic gneiss are moderately low (Tables 3 and S6; Fig. 7) and strongly correlated with each



other. Initial Hf isotope ratios show modest variability between  $0.280717 \pm 0.000022$  and  $0.280860 \pm 0.000016$  and do not correlate with any elemental or isotopic parameter.

### 5.3. Biotite-rich enclave (13DC15)

Only two zircons have been recovered from the biotite-rich enclave 13DC15 and they both show simple oscillatory zoning in CL images (Fig. S6). Each zircon has been dated twice (see Tables 3 and S4 and Fig. S6). The first zircon (i.e., 13DC15\_1) gave  $^{207}\text{Pb}/^{206}\text{Pb}$  ages of  $3473 \pm 21$  Ma (2% discordant) and  $2973 \pm 30$  Ma (23% discordant).  $^{176}\text{Yb}/^{177}\text{Hf}$  and  $^{176}\text{Lu}/^{177}\text{Hf}$  determined on the same crystal are both low and close to each other (Tables 3 and S5). In contrast to the differences exhibited by U-Pb ages, the two measured  $^{176}\text{Hf}/^{177}\text{Hf}$  are in excellent agreement within uncertainty, which is also the case for the initial ratios (i.e.,  $0.280477 \pm 0.000022$  and  $0.280487 \pm 0.000013$ ; Tables 3 and S6; Fig. 8).

The two U-Pb analyses performed on the second zircon crystal are very consistent with each other and gave respective  $^{207}\text{Pb}/^{206}\text{Pb}$  ages of  $3603 \pm 23$  Ma (9% discordant) and  $3610 \pm 23$  Ma (11% discordant). Determined  $^{176}\text{Yb}/^{177}\text{Hf}$  and  $^{176}\text{Lu}/^{177}\text{Hf}$  are both low and close to each other (Tables 3 and S6), and the two measured  $^{176}\text{Hf}/^{177}\text{Hf}$  are in excellent agreement within uncertainty, which is also the case for the initial ratios (i.e.,  $0.280374 \pm 0.000019$  and  $0.280373 \pm 0.000021$ ; Tables 3 and S6; Fig. 8).

The oldest ages, obtained for 13DC15\_1a, 2a, and 2b, are associated with Th/U ratios in the common magmatic range, whereas the significantly discordant data of 13DC15\_1b, which indicates a  $^{207}\text{Pb}/^{206}\text{Pb}$  age of 2973 Ma, is coupled to a Th/U below 0.2 (Tables 3 and S6).

## 6. Discussion

### 6.1. Origin of studied orthogneisses based on petrographic observations and geochemical data

#### 6.1.1. Granitic gneiss (13DC12)

One of the most notable petrographic observation that one can make in 13DC12 is the presence of significant amounts of muscovite which is a strong indicator for the crustal origin of granites (e.g., [Barbarin, 1999](#)). This is reinforced by the peraluminous flavor of this sample ([Fig. 4B](#)) together with the fact that it plots in the field of crustally-derived granites (i.e., Bt- and two-mica granites) in some key geochemical diagrams for late-Archean granitoids ([Figs 4C and 4D](#)). Finally, the major element composition of 13DC12 matches well with that of melts expected from partial melting of tonalitic sources with possible involvement of metasediments ([Figs 4E](#)). Taken altogether, we consider that petrographic and geochemical observations point to a dominant crustal origin for the protolith of the granitic gneiss 13DC12.

#### 6.1.2. Trondhjemitic gneiss (13DC13)

The sample 13DC13 also contains significant amounts of muscovite that points to a crustal contribution to the formation of 13DC13 protolith. This is consistent with the peraluminous signature of this sample ([Fig. 4B](#)) together with the fact that it plots in the field of crustally-derived granites (i.e., Bt- and two-mica granites) and hybrid granites in some key geochemical diagrams for late-Archean granitoids ([Figs 4C and 4D](#)). Much as for 13DC12, the major element content in 13DC13 matches well with that of melts expected from partial melting of tonalitic sources with probable involvement of mafic sources (low-K and/or high-K; [Figs 4E](#)). Consequently, we

interpret petrographic and geochemical observations made on the trondhjemitic gneiss 13DC13 as evidence for its dominant crustal origin.

## 6.2. Interpretation of the zircon U-Pb ages and primary Hf isotopic signatures

### 6.2.1. Granitic gneiss (13DC12)

As illustrated in [Figure 5](#), zircons from granitic gneiss sample 13DC12 display large variations in  $^{207}\text{Pb}/^{206}\text{Pb}$  ages, but only a small variation in initial  $^{176}\text{Hf}/^{177}\text{Hf}$ . This behavior is quite common in old zircons (e.g., [Patchett, 1983](#); [Gerdes and Zeh, 2009](#); [Guitreau et al., 2012](#)) and can be attributed to different sensitivities to perturbation of the U-Pb and Lu-Hf isotope systems by thermal means and/or fluid activity (e.g., [Lenting et al., 2010](#)). Because all data points, except for 13DC12\_1a, comply with the closed-system evolution model for the Lu-Hf isotope system in the analyzed crystals – based on the measured  $^{176}\text{Lu}/^{177}\text{Hf}$  ([Figure 5](#)) – the observed variability in initial  $^{176}\text{Hf}/^{177}\text{Hf}$  is not considered to be geological. Rather, this variability is the result of under-correction of radiogenic  $^{176}\text{Hf}$  ingrowth that merely derives from the use of  $^{207}\text{Pb}/^{206}\text{Pb}$  ages that are younger than the actual crystallization ages. Zircons from the granitic gneiss, therefore, form a single population. The age of  $3410.8 \pm 3.6$  Ma ([Fig. 6A](#)) determined using the most concordant, and oldest least discordant zircons, is hence interpreted to be the actual crystallization age of this zircon population, and by extension that of 13DC12. [Figure 5](#) shows that zircons used to establish this age also provide very consistent initial  $^{176}\text{Hf}/^{177}\text{Hf}$  of  $0.280631 \pm 0.000018$ , which translates into an  $\epsilon_{\text{Hf}}$  of  $+2.2 \pm 0.6$  at 3410.8 Ma ([Table 4](#)), and that we interpret as best reflecting the Lu-Hf isotope systematic of sample 13DC12. The upper-intercept age obtained from zircons that underwent post-crystallization U-Pb disturbance (i.e.,  $3440 \pm 39$  Ma) ([Fig. 6C](#)) is in agreement, within uncertainty, with the established crystallization age for

520 13DC12, reinforcing the notion that there is a single zircon population in the granitic  
521 gneiss. Finally, the lower-intercept age of  $576 \pm 90$  Ma (Fig. 6C) that is interpreted as  
522 the timing of Pb-loss in some of 13DC12 zircons, matches well with metamorphic  
523 episodes recorded by rocks of the WDC and the southern granulite province (e.g.,  
524 Bhaskar Rao et al., 1992; Miller et al., 1996; Meißner et al., 2002; Santosh et al., 2006).  
525 This date corresponds to widespread Pan-African metamorphic events in the southern  
526 continents which previously comprised the supercontinent Gondwana (e.g., Yoshida et  
527 al., 1996; Meert, 2003; Santosh et al., 2005, 2006; Sato et al., 2011).

528         The age and initial Hf isotopic signature of zircons from the granitic gneiss  
529 sample 13DC12 match well with those of ancient detrital zircons from the WDC  
530 analyzed by Sarma et al. (2012), Lancaster et al. (2015) and Maibam et al. (2016), which  
531 are presented in Figure 9. These authors rationally interpreted this slightly positive  
532 initial  $\epsilon_{\text{Hf}}$  signature as marking juvenile crust addition. However, if one assumes that  
533  $\sim 3410$  Ma detrital zircons were derived from lithologies similar to the granitic gneiss  
534 studied herein, which is the only rock  $>3350$  Ma identified so far in the WDC, then, the  
535 positive  $\epsilon_{\text{Hf}}$  signatures become misleading because sample 13DC12 is interpreted as a  
536 crust reworking product based on petrographic and geochemical arguments (see *section*  
537 *5.1.1*). This example illustrates the fact that Hf isotopic signatures cannot  
538 unambiguously discriminate between juvenile addition and crustal reworking when  
539 used alone in the detrital zircon record. However, positive  $\epsilon_{\text{Hf}}$  in a crustally-derived  
540 granitoid indicates that its precursor had a crustal residence time that was short enough  
541 so that its Hf isotopic composition was still close to that of its mantle source when it  
542 got reworked. In the absence of constraints on the nature of this precursor and its mantle  
543 source, we can speculate on lower- and upper-limits for crustal residence time by,  
544 respectively, assuming that the minimum time-span between emplacement and

reworking of a granitic unit is on the order of  $\sim 10$  My, and by calculating two-stage model ages (e.g., Blichert-Toft and Albarède, 2008; Hawkesworth et al., 2010). In order to minimize issues inherent to model ages (e.g., Arndt and Goldstein, 1987; Laurent and Zeh, 2015; Payne et al., 2016), we have used end-members from a large range of crustal  $^{176}\text{Lu}/^{177}\text{Hf}$  which characterize average Archean TTGs (0.004; Guitreau et al., 2012) and average continental crust (0.015; Griffin et al., 2004). Assuming a mantle source similar to the arc-mantle ( $\epsilon_{\text{Hf}} = +13.3$ ; Dhuime et al., 2011; Iizuka et al., 2013), the calculated model ages range from 3466 to 3492 Ma. If, instead, a depleted mantle source (DM) similar to that of MORB ( $\epsilon_{\text{Hf}} = +17$ ; Chauvel and Blichert-Toft, 2001) is assumed, the model ages become 3503 to 3545 Ma. We cannot conclude on the actual residence time of the precursor to 13DC12 but we note that it can range from  $\sim 10$  to  $\sim 130$  My and is, hence, relatively short and included in the range displayed by the oldest detrital zircons (e.g., Nutman et al., 1992; Sarma et al., 2012; Lancaster et al., 2015; Maibam et al., 2016) and igneous zircons (this study) of the WDC.

### 6.2.2. Trondhjemitic gneiss (13DC13)

Internal textures associated with variable U-Pb ages, Th/U, and initial Hf isotopic compositions in 13DC13 zircons (Figs. 7 and S5) led us to conclude that there is more than one population in this sample, each variably affected by post-crystallization disturbance(s). In order to characterize these populations, we have determined Discordia lines at the scale of each zircon every time analyses done on a same crystal showed consistent initial  $^{176}\text{Hf}/^{177}\text{Hf}$  and that  $^{207}\text{Pb}/^{206}\text{Pb}$  ages correlated with degrees of U-Pb discordance. Otherwise,  $^{207}\text{Pb}/^{206}\text{Pb}$  ages and their associated initial  $^{176}\text{Hf}/^{177}\text{Hf}$  were considered separately. Doing so results in the emergence of five groups (Table 4).

The first one is represented by three zircon crystals in which the laser-ablation spots were located in zones that we interpreted as xenocrystic cores because they appear as rounded and/or resorbed domains surrounded by oscillatory-zoned outerparts in CL images (Fig. S4). These three zircons exhibit ages of  $3468 \pm 41$  (upper-intercept zircon #4),  $3456 \pm 20$  (upper-intercept zircon #7), and  $3414 \pm 23$  Ma (concordant  $^{207}\text{Pb}/^{206}\text{Pb}$  zircon #12) that are associated with respective initial Hf isotopic compositions of  $0.280742 \pm 0.000014$ ,  $0.280721 \pm 0.000017$ , and  $0.280860 \pm 0.000016$ . These latter are equivalent to  $\epsilon_{\text{Hf}}$  of  $+7.5 \pm 0.5$ ,  $+6.4 \pm 0.6$ , and  $+10.4 \pm 0.6$  (Table 4), respectively.

The second group is represented by three crystals in which laser-ablation measurements were done in domains resembling xenocrystic cores much like for the first group and that gave ages of  $3342 \pm 19$  (upper-intercept zircon #5),  $3356 \pm 25$  (upper-intercept zircon #11), and  $3359 \pm 110$  (upper-intercept zircon #3). The initial Hf isotopic signatures obtained on the same locations are  $0.280720 \pm 0.000018$ ,  $0.280733 \pm 0.000012$ , and  $0.280778 \pm 0.000016$  (Table 4), respectively, which translates into  $\epsilon_{\text{Hf}}$  values of  $+3.7 \pm 0.6$ ,  $+4.5 \pm 0.4$ , and  $+6.1 \pm 0.6$ .

The third group is represented by only one crystal that gave an age of  $3295 \pm 18$  Ma (grain #6; Fig. S4). This crystal has very reproducible initial Hf isotopic compositions (Table 3) that, when calculated at 3295, give a weighted average of  $0.280752 \pm 0.000010$  which is equivalent to an  $\epsilon_{\text{Hf}}$  of  $+3.7 \pm 0.4$ .

The fourth group exhibits ages of  $3170 \pm 32$  and  $3179 \pm 11$  Ma that have been obtained in oscillatory-zoned outer margins of two different crystals. The corresponding initial  $^{176}\text{Hf}/^{177}\text{Hf}$  are  $0.280756 \pm 0.000013$  and  $0.280822 \pm 0.000011$ , which gives  $\epsilon_{\text{Hf}}$  of  $+0.8 \pm 0.5$  and  $+3.4 \pm 0.4$ , respectively (Table 4).

The fifth group corresponds to an age of  $3101 \pm 25$  Ma that was obtained from two analyses done in one very elongated zircon (Fig. S5). Initial Hf isotopic signature

for this zircon is  $0.280739 \pm 0.000021$ , which is equivalent to an  $\epsilon_{\text{HF}}$  of  $-1.4 \pm 0.7$  (Table 4).

The calculated lower-intercept ages for the identified Discordia lines, different from  $\sim 0$  Ma, form two groups with one ranging from  $542 \pm 160$  to  $749 \pm 90$  Ma and another poorly constrained one from  $969 \pm 770$  to  $1792 \pm 640$  Ma, which is due to the limitedly discordant data that define the Discordia lines. The accuracy of the latter group is debatable. However, the first group exhibit ages very compatible with that observed for the granitic gneiss (Fig. 6C) and that comply well with known Pan-African metamorphic events that occurred in southern India (e.g., Bhaskar Rao et al., 1992; Miller et al., 1996).

We interpret the trondhjemitic gneiss (13DC13) to have been emplaced at  $3178 \pm 10$  Ma, which is the average age of the fourth group, because it corresponds to the age of oscillatory zoned outer margins. Older ages, which are for the most part located in identifiable xenocrystic cores are interpreted as inherited. The age of the fifth group is assumed to be metamorphic because of the internal texture of the crystal and its high Th/U of  $\sim 1.2$ , which is often seen in zircons that formed during high-temperature metamorphism (e.g., Vavra et al., 1999; Möller et al., 2003). This is consistent with the finding of Jayananda et al. (2015) that titanite recovered from neighboring 3200 Ma Halekote-type trondhjemite exhibit ages ranging from 3217 to 3091 Ma, and that these authors interpreted as marking a ca. 3100 Ma metamorphic event in the area around the HSB. We note that the estimated age of crystallization for the trondhjemitic gneiss is close to that of the Chikmagalur granite, which crops out south from the Bababudan belt (Fig. 1; Jayananda et al., 2015), and to that of diapiric trondhjemites observed in the Holenarsipur Schist Belt (Figs. 1 and 2; Jayananda et al., 2015). The inherited zircon ages of 3295, 3342-3359, and 3414 Ma match well with, respectively, a  $3298 \pm 7$  Ma

volcanic flow identified within the HSB by [Peucat et al., \(1995\)](#), the  $3342 \pm 6$  Ma Hassan-Gorur gneiss studied by [Beckinsale et al., \(1980\)](#), [Bhaskar Rao et al., \(2008\)](#), and [Jayananda et al. \(2015\)](#), and the  $3410.8 \pm 3.6$  Ma granitic gneiss (13DC12) from this study. Further, the  $\epsilon_{\text{Hf}}$  of +4 to +7 determined by [Bhaskar Rao et al. \(2008\)](#) for a  $3346 \pm 10$  Ma Gorur gneiss match very well with the values of +3.7 to +6.1 obtained for inherited zircons of the second group, which gave ages of 3342 to 3359 Ma. However, the  $\epsilon_{\text{Hf}}$  signature of the granitic gneiss (13DC12),  $+2.2 \pm 0.6$ , differs significantly from that of the 3414-Ma zircon (i.e.,  $+10.4 \pm 0.6$ ) which indicates that although coeval, they did not record the same event. Finally, the trondhjemitic gneiss zircons dated at 3456-3468 Ma do not correspond to any known lithology in the WDC, although such old zircons have been found as detrital crystals (e.g., [Nutman et al., 1992](#); [Sarma et al., 2012](#); [Lancaster et al., 2015](#); [Maibam et al., 2016](#)). These oldest detrital zircons exhibit less radiogenic Hf isotope signatures than the inherited ones studied herein.

The trondhjemitic gneiss (13DC13) is petrographically similar to the Halekote trondhjemites and Chikmagalur granite, which also contain primary muscovite according to descriptions provided in [Jayananda et al. \(2015\)](#). Given all these similarities, as well as the fact that the trondhjemitic gneiss has been sampled in a zone of low strain resembling the central part of a diapir ([Fig. 2](#); [Bouhallier et al., 1993](#)), we propose that it is related to the diapiric trondhjemites of the WDC, which are known to contain enclaves of older rocks (e.g., [Naqvi and Rogers, 1987](#); [Meen et al., 1992](#); [Jayananda et al., 2015](#)), such as the Bt-rich enclave (13DC15) which itself contains older zircons. [Stroh et al. \(1983\)](#) interpreted these diapiric granitoids as markers of WDC stabilization through removal of heat-producing radioactive elements from the lower crust by reworking. This interpretation is supported by data recently presented in



Jayananda et al. (2015), who also concluded that the dome-and-basin structure of the WDC had been acquired during the emplacement of these trondhjemites ~3200 My ago. This process of stabilization of Archean continental crust has also been suggested for other cratons (e.g., Schoene et al., 2008). When evolutionary paths for felsic and mafic lithologies are taken into account (see Fig. 9), the  $\epsilon_{\text{Hf}}$  signatures of the trondhjemitic gneiss 13DC13, represented by the fourth group ( $+0.8 \pm 0.5$  and  $+3.4 \pm 0.4$  at 3178 Ma; Table 4) can be accounted for by the reworking of various crustal lithologies represented by inherited zircons older than 3200 Ma within 13DC13. Therefore, this Hf isotope variability could be indicative of isotopic heterogeneity within the magma parental to 13DC13 which originated from distinct crustal sources involved during anatexis and/or acquired through interactions with various crustal lithologies. However, we cannot rule out some mixing between unrelated domains because the two analyzed crystals both contained two zones with slightly different Hf isotope signatures (Fig. 6 and S5). According to the  $^{176}\text{Hf}/^{177}\text{Hf}$  of the corresponding domains (Tables 4 and S6), the  $\epsilon_{\text{Hf}}$  values mentioned above (i.e., +0.8 and +3.4) could be interpreted as, respectively, minimum and maximum values for the fourth group. Nevertheless, whether or not this heterogeneity is real or analytical is not important for the rest of the discussion. Yet, we note that the Hf isotopic signatures of 13DC13 cognate zircons match very well with those of coeval zircons from all detrital zircon datasets for the WDC (Fig. 9).

The first group (3414-3468 Ma) has  $\epsilon_{\text{Hf}}$  signatures more radiogenic than coeval zircons from the detrital record (Fig. 9) implying that either the original host-rocks of zircons from the first group were rare or they were not available for sampling at the surface at the time of sedimentation. These high values (+6 to +10) imply that a strongly depleted mantle source was tapped during the formation of the magma parental to

zircons from the first group. Such highly depleted source is rare in the Archean and mostly limited to boninites and komatiites (e.g., Hoffmann et al., 2010; Nebel et al., 2014; Hoffmann and Wilson, 2017).

### 6.2.3. Biotite-rich enclave (13DC15)

The two zircon crystals recovered from this sample show remarkably simple Lu-Hf isotope systematics between the two analyses performed in each zircon (Fig. 8). However, the first zircon (13DC15\_1) exhibit a significant variation in age in spite of consistent initial Hf isotopic compositions (Fig 8). This consistency likely indicates that U-Pb systematics have been disturbed at some point in this zircon's evolution. This is also consistent with the fact that oldest zircon  $^{207}\text{Pb}/^{206}\text{Pb}$  age is associated with a Th/U value that falls within the common magmatic range whereas the youngest age (i.e., 2973 Ma; Table 3) is associated with a Th/U <0.2 that can be interpreted as resulting from metamorphism. The oldest age determined for 13DC15\_1 is not strictly concordant and, therefore, we have fitted a Discordia line through the two U-Pb analyses, which gave upper- and lower-intercept ages of  $3499 \pm 29$  and  $1719 \pm 190$  Ma, respectively (Fig. S6). Note that the upper-intercept age overlaps within uncertainty with the oldest  $^{207}\text{Pb}/^{206}\text{Pb}$  age determined for this zircon (13DC15\_1). U-Pb ages are very consistent in the second crystal which gives a combined crystallization age of  $3607 \pm 16$  Ma (Fig. S6).

Average initial  $^{176}\text{Hf}/^{177}\text{Hf}$  for the two zircons analyzed (i.e., 13DC15\_1 and 13DC15\_2) are  $0.280476 \pm 0.000011$  and  $0.280374 \pm 0.000014$ , respectively, which correspond to  $\epsilon_{\text{Hf}}$  values of  $-1.3 \pm 0.4$  and  $-2.3 \pm 0.5$  at 3499 and 3607 Ma, respectively (Table 4).

The zircons from the biotite-rich enclave exhibit not only ages >3400 Ma but, contrary to zircons from other samples studied herein, negative initial  $\varepsilon_{\text{Hf}}$  that, hence, suggest that the magmas parental to these zircons originated from, or were buffered by, crustal lithologies with long crustal residence times. Using an arc-mantle source (see *section 5.1.1*) and assuming that the precursor can be either felsic ( $^{176}\text{Lu}/^{177}\text{Hf} = 0.004$ ) or mafic ( $^{176}\text{Lu}/^{177}\text{Hf} = 0.022$ ), calculated two-stage model ages (e.g., [Blichert-Toft and Albarède, 2008](#); [Hawkesworth et al., 2010](#)) are 3684 and 3891 Ma for zircon #1, and 3821 and 4060 Ma for zircon #2. If instead we use a depleted mantle source (see *section 5.1.1*), the model ages become 3713 and 3937 Ma for zircon #1, and 3846 and 4094 Ma for zircon #2. Finally, using BSE composition from [Iizuka et al. \(2015\)](#) for the mantle source of the precursors we obtain ages of 3558 and 3649 Ma for zircon #1, and 3715 and 3880 Ma for zircon #2. These model ages are too variable and rely on too unconstrained assumptions to be interpreted as are but nevertheless illustrate the fact that very old crust, up to 4000 Ma, could have been involved in the formation of the magma parental to 13DC15 zircons.

### 6.3. Early formation of the Western Dharwar Craton

Our new results, though limited, bring important constraints that can be used in combination with previous studies to discuss the early formation of the WDC in terms of sources involved. We can further compare these latter to the latest models for WDC formation (e.g., [Jayananda et al., 2008, 2015](#); [Lancaster et al., 2015](#)) to speculate on the geological setting of WDC early formation. **Figure 9** presents our results in the context of detrital zircon datasets available for the WDC and that have been used to depict the big-picture evolution of the WDC (i.e., [Sarma et al., 2012](#); [Lancaster et al., 2015](#); [Maibam et al., 2016](#)). **Figure 9** also includes the age range for Sargur-group komatiites

(Jayananda et al., 2008) and U-Pb ages alongside  $\epsilon_{\text{Hf}}$  for Gorur gneiss from Bhaskar Rao et al., (2008). It can be seen that all zircons analyzed in this study have detrital equivalents, except for the most radiogenic zircons from 13DC13's first group (3414-3468 Ma; Fig. 9). Although essentially consistent, slight differences can be observed between the ages and  $\epsilon_{\text{Hf}}$  displayed in the detrital records of Figure 9, which likely arise from distinct catchment basins and possibly the number of analyses. The early formation of the WDC can be divided into three time-periods: (1) pre-3400 Ma, (2) 3400-3200 Ma, (3) post-3200 Ma.

Zircons older than 3400 Ma exhibit large variations in  $\epsilon_{\text{Hf}}$  signatures (Fig. 9) testifying to various sources which likely points to different contexts of formation for their parental granitoids. These sources are mantle domains with ancient depletion history, mantle domains with moderately depleted signatures that are equivalent to those observed in WDC granitoids formed during the second period, and enriched crusts of possibly old ages (up to 4000 Ma). Most zircons that testify to this period are inherited crystals in the 3178 Ma trondhjemitic gneiss (13DC13) and detrital zircons from the Sargur-group, which have deposition ages estimated between 3100 and 3300 Ma. The role of the source to these zircons parental granitoids is discussed later on.

In the time-span 3400-3200 Ma, all detrital zircon records show positive  $\epsilon_{\text{Hf}}$  varying within the same restricted range, except for zircons from the Sargur Schist Belt (Lancaster et al., 2015) which, nevertheless, also show a restricted range but around chondritic values. This indicates that during this time-period, granitoids were sourced in a common mantle domain that had mildly-depleted to near-chondritic Hf isotopic compositions, with limited or no continental influence, similar to global data for TTGs presented by Guitreau et al. (2012). In Figures 9B and 9D, an enhanced variability of  $\epsilon_{\text{Hf}}$  is visible around 3250-3200 Ma and is associated with a shift towards negative

values that can be seen in Figures 9C and 9D. Moreover, the ~3220 Ma granitic clast analyzed in Maibam et al. (2016) contains pre-3400 Ma zircons that have  $\epsilon_{\text{Hf}}$  similar to that of the granitic sample (13DC12) from this study (Fig. 9D). These features can be accounted for by reworking of WDC's oldest lithologies, buffering of newly formed magmas by older lithologies, and/or a continental influence similar to what can be seen in Svecofennian provinces of northern Sweden (e.g., Öhlander et al., 1993), the Kohistan-Ladakh arc (e.g., Bouilhol et al., 2013), and the Sunda-Banda arc (e.g., Elburg et al., 2005; Herrington et al., 2011), for example.

After ~3200 Ma, all datasets, but that for Bababudan-group sediments for which there is no data younger than 3200 Ma (Lancaster et al., 2015), exhibit a drift of  $\epsilon_{\text{Hf}}$  towards increasingly negative values as age decreases. The deposition age of the sediments from which detrital zircons were recovered are not well constrained, except for the Gadag Greenstone Belt (Sarma et al., 2012). Sargur-group sediments are assumed to have been deposited between ~3300 and ~3100 Ma depending on their location within the WDC and the way the sedimentation age was estimated (e.g., Nutman et al., 1992; Ramakrishnan et al., 1994; Peucat et al., 1995; Sarma et al., 2012; Hokada et al., 2013). When minimum deposition ages are taken into account (Fig. 9), the major part of the drifts in  $\epsilon_{\text{Hf}}$  through time appear artificial for datasets related to Sargur-group sediments because most ages are younger than that of deposition and are most likely related to ancient U-Pb disturbance and/or recrystallization as noted by Lancaster et al. (2015). It is interesting to note that datasets from Lancaster et al. (2015) and Maibam et al. (2016) contain zircons with ages and  $\epsilon_{\text{Hf}}$  that comply well with the fifth group of the trondhjemitic gneiss (13DC13) and that we interpreted as metamorphic (Figs. 9C and 9D). This example illustrates the fact that detrital zircons are very powerful at unveiling big-picture information about the continental crust

formation and evolution but they can also provide ambiguous information because evolution patterns of crustal segments (e.g., [Zeh et al., 2011](#); [Laurent and Zeh, 2015](#)) and artificial trends resulting from ancient Pb-loss look the same in  $\epsilon_{\text{Hf}}$  versus age diagrams, as already pointed out elsewhere (e.g., [Amelin et al., 2000](#); [Guitreau and Blichert-Toft, 2014](#); [Payne et al., 2016](#)). As a consequence, we have not considered detrital zircon data for ages younger than 3100 Ma. Yet, the drift observed in [Sarma et al. \(2012\)](#) dataset is real and is also visible with data from the Eastern Dharwar craton (e.g., [Maibam et al., 2016](#)). This indicates that after ~3200 Ma, the WDC magmatic events dominantly involved crust reworking processes and/or buffering of magmas by dominant lithologies, not unlike what was proposed by [Laurent and Zeh \(2015\)](#) for the Pietersburg block. This is consistent with conclusions of [Bhushan and Sahoo \(2010\)](#) and [Maibam et al. \(2011\)](#) that stable continental crust was formed in the WDC prior to 3 Ga. Further, [Taylor et al. \(1984\)](#) and [Jayananda et al. \(2015\)](#) concluded from major and trace elements, as well as Sr, Pb, and Nd isotopes that granitoids younger than 3200 Ma contained a pre-existing crust component.

Sargur-group komatiites have long been considered as the oldest units of the WDC (e.g., [Naqvi, 1983](#)) until the discovery of detrital zircons as old as 3600 Ma by [Nutman et al. \(1992\)](#). The best age estimate for these komatiites is  $3352 \pm 110$  Ma ([Jayananda et al., 2008](#)), which is, hence, not precise enough to conclude on the actual role of these ultramafic rocks in the early development of the WDC. Nevertheless, [Naqvi et al. \(1983\)](#) and [Jayananda et al. \(2008\)](#) noted that some of the oldest identifiable generations of peninsular gneisses intruded into the surrounding greenstones of the HSB, hence, indicating that most of the peninsular gneisses are younger than Sargur-group komatiites. [Jayananda et al. \(2008, 2016\)](#) concluded from elemental and isotopic geochemistry that Sargur-group komatiites formed remote from continental crust.

793 Therefore, these authors proposed that komatiites of the Sargur group formed in an  
794 oceanic-plateau-like environment and were accreted to a continental nucleus that  
795 contained lithologies represented by the >3400 Ma detrital zircons (e.g., [Kunugiza et](#)  
796 [al., 1996](#); [Jayananda et al., 2008](#)). This scenario is not unlike what was proposed for  
797 other Precambrian terranes (e.g., [Boher et al., 1992](#); [Puchtel et al., 1999](#); [Rey et al.,](#)  
798 [2003](#); [Guitreau et al., 2012](#); [Martin et al., 2014](#)), and it is consistent with our  
799 observations for the WDC. Recently, [Baes et al. \(2016\)](#) illustrated using numerical  
800 modeling that the fact that the emplacement of a mantle plume in the lithosphere could  
801 initiate subduction. We propose a similar scenario whereby the emplacement of an  
802 oceanic plateau, comprising the Sargur-group komatiites, initiated subduction beneath  
803 it that resulted in the generation of the oldest peninsular gneisses. We further propose  
804 that this subduction acted as a “conveyor belt” that induced the accretion to this oceanic  
805 plateau of oceanic arcs, smaller oceanic plateaus and crustal segments much like it has  
806 been proposed for North America (e.g., [Hoffman, 1988](#); [Whitmeyer and Karlstrom,](#)  
807 [2007](#)), the Svecofennian Orogen (e.g., [Weihed et al., 2005](#); [Guitreau et al., 2014](#)) and  
808 the Kohistan-Ladakh arc (e.g., [Bouilhol et al., 2013](#)). The accretion to the oceanic  
809 plateau of several oceanic arcs and smaller oceanic plateaus would account for the  
810 various unrelated chemical and isotopic signatures of peninsular gneisses found  
811 throughout the WDC (e.g., [Bhaskar Rao et al., 1983](#); [Monrad, 1983](#); [Naqvi et al., 2009](#);  
812 [Jayananda et al., 2015](#)). Further, this scenario can account for the low- and high-  
813 pressure sources for peninsular gneisses identified by [Jayananda et al. \(2015\)](#) because  
814 the size and buoyancy of these mafic-ultramafic segments can control the modality of  
815 subduction (i.e., fast or low; shallow or steep). Accretion of oceanic arcs and oceanic  
816 plateaus could also account for the short-crustal residence time of sources to peninsular  
817 gneisses, as interpreted by [Bhaskar Rao et al. \(1991\)](#), [Jayananda et al. \(2015\)](#), and as

concluded for sample 13DC12 (this study). We surmise that accretion of oceanic arcs could induce crustal reworking which would be consistent with the fact that some of the oldest granitoids of the WDC have peraluminous characteristics despite Nd and Hf isotope signatures similar to mildly depleted mantle sources (Jayananda et al., 2015; this study). If we interpret the granitic gneiss 13DC12 as the reworking product of oceanic arc granitoids during accretion to an oceanic plateau represented by Sargur-group komatiites, then, the sample 13DC12 gives a minimum age of 3410 Ma for this oceanic plateau and the initiation of the WDC growth. The role of ancient crust represented by 3500-3600 Ma zircons is hard to understand and needs further investigation. However, it appears from Figure 9 that such ancient crust did not influence the  $\epsilon_{\text{Hf}}$  signatures of granitoids in the catchment basins of sediments from Bababudan, Chitradurga, and Gadag Schist belt before ~3200 Ma. In contrast, sediments in the Sargur Schist Belt had a distinct catchment basin as testified to by the  $\epsilon_{\text{Hf}}$  of detrital zircons in Figure 9C. The granitoids parental to these latter zircons appear to have been possibly influenced by 3500-3600 Ma crust, as represented by zircons from 13DC15, earlier than 3200 Ma. Further, the granitoids parental to these latter could have been part of the catchment basin of Sargur Schist Belt sediments. However, the large uncertainty on detrital zircon ages in Figure 9C, prevents accurate conclusions to be drawn. Nevertheless, we see the absence of influence of the ancient crust, represented by zircons from 13DC15, in the  $\epsilon_{\text{Hf}}$  signatures of most of detrital zircons from the WDC (Fig. 9) as an argument in favor of the absence of this ancient crust in the vicinity of the HSB prior to ~3200 Ma. We suggest that a large crustal block containing 3500-3600 Ma zircons was accreted to the WDC around 3200 Ma, which initiated the stabilization of, at least, portions of the WDC (e.g., HSB) and the buffering of newly formed magmas by dominant enriched lithologies represented by 3400-3200



Ma peninsular gneisses and 3600-3400 Ma granitoids (Fig. 9). This event marked a change in the growth style of the WDC that is substantiated by the drift of detrital zircons  $\varepsilon_{\text{Hf}}$  values (Fig. 9) which could correspond, at least in part, to hidden crustal growth (see Laurent and Zeh, 2015; Payne et al., 2016; Couzinié et al., 2016). Remnants of this crustal block, which is intrinsic to the WDC record, may be in the vicinity of the HSB but more likely around the Sargur Schist Belt.

In order to reconstruct the detailed tectono-magmatic history of the WDC and test models for its geological setting, future work will have to focus on documenting ages and signatures of peninsular gneisses in greater details, as well as understanding their stratigraphic relationships and spatial distribution. One important aspect to target is the role of the ancient crust identified herein. Doing so will help refine the above-explained scenario and its local variations that can account for differences in Hf isotopic signatures exhibited by the various detrital zircon records shown in Figure 9. Finally, the same work will have to be conducted in supracrustal belts in order to clarify their origin and relationships with peninsular gneisses.

## 7. Conclusions

We have studied the petrography of a Western Dharwar Craton granitic gneiss and trondhjemitic gneiss, as well as a Bt-rich enclave within the latter, and measured their zircon U-Pb ages and Lu-Hf isotope systematics to shed new light on crustal formation processes during the early formation of the WDC. Our study reveals that crust older than the oldest known granitoid of the WDC (3342-Ma Hassan-Gorur gneiss; Beckinsale et al., 1980; Jayananda et al., 2015), which was known from the detrital zircon record (e.g., Nutman et al., 1992), is also present in the igneous record in the form of a  $3410.8 \pm 3.6$  Ma granitic gneiss and inherited zircons, with ages up to 3607

868  $\pm 16$  Ma, in a 3178 Ma trondhjemitic gneiss and a mica-rich enclave found within this  
869 trondhjemite. Hf isotopic signatures indicate short-crustal residence time for the  
870 precursor to the granitoids parental to analyzed zircons, except for the oldest ones that  
871 could have been sourced from Eoarchean-Hadean precursor(s).

872 Our results compared with similar data for detrital zircons from four locations  
873 throughout the WDC allow three time periods to be distinguished. The first one is pre-  
874 3400 Ma and exhibit multiple zircon  $\epsilon_{\text{Hf}}$  signatures (very depleted to slightly enriched;  
875  $\epsilon_{\text{Hf}}$  of +10.4 to -2.3) testifying to the involvement of several distinct sources in the  
876 formation of pre-3400 Ma units. The second period is from 3400 to 3200 Ma and  
877 corresponding zircons display either mildly-depleted or near-chondritic Hf isotopic  
878 signatures, depending on the sampling location of sediments, that vary within a  
879 restricted range throughout this period. This indicates involvement of a common  
880 juvenile source with limited or no continental influence until  $\sim 3200$  Ma, when the third  
881 period started. This latter is characterized by dominant crust reworking or buffering of  
882 newly formed granitoids by pre-existing ones, which translates into a drift of  $\epsilon_{\text{Hf}}$   
883 signatures towards increasingly negative values. We propose a scenario updated from  
884 that of [Jayananda et al. \(2008\)](#) for the early formation of the WDC in which the arrival  
885 of a mantle plume in the upper-mantle gave rise to an oceanic plateau that contained  
886 Sargur-group komatiites. The formation of this oceanic plateau triggered subduction on  
887 its edges in a way similar to that described in models from [Baes et al. \(2016\)](#). The  
888 subducted oceanic-like crust acted as a conveyor belt that dragged crustal blocks in the  
889 vicinity of the oceanic plateau which included short-lived oceanic arcs and small  
890 oceanic plateaus which ultimately contributed to the growth of the WDC. We suggest  
891 that this subduction started at least 3410 My ago and lasted until at least 3200 Ma when  
892 a continental block containing the granitoids parental to the  $>3410$  Ma zircons got

accreted to the WDC, hence, inducing its stabilization. The WDC further grew and evolved but newly formed granitoids were buffered by, or sourced in, dominant lithologies of the WDC.

#### **Acknowledgements:**

We thank Steve Mozjasis and the CRiO group for help with zircon separation, Nancy Cherim and Mark Townley for help with CL image acquisition, Julia G. Bryce and Maria F. Fahnestock for technical help at UNH. Jean-Louis Paquette and Abdel-Mouhcine Gannoun are thanked for assistance with analyses at the Laboratoire Magmas et Volcans. We are grateful to Claire Fonquernie and Mhammed Benbakkar for rock crushing and major-oxide analyses at Laboratoire Magmas et Volcans. Discussions with Hervé Martin helped improve the present manuscript. Martin Guitreau acknowledges financial support from Matthias Willbold through NERC grant R117299 and the Région Auvergne through the Auvergne Fellowship program. This is a Laboratory of Excellence ClerVolc contribution. The University of New Hampshire supported this research project through start-up funds granted to Dr. Samuel B. Mukasa. Last but not least, we would like to thank Randall Parrish for efficient editorial handling as well as Tsuyoshi Iizuka, Sukanta Dey, and an anonymous reviewer for insightful comments that helped improve this manuscript.

#### **References**

Abbey, S., 1983. Studies in "Standard Samples" of Silicate Rocks and Minerals 1969-1982. Canadian Geological Survey Paper 83-15, p. 114.

916 Amelin, Y., Lee, D.-C., Halliday, A.N., 2000. Early–middle archaean crustal evolution  
 917 deduced from Lu–Hf and U–Pb isotopic studies of single zircon grains.  
 918 *Geochimica et Cosmochima Acta* 64, 4205–4225.

919 Arndt, N.T., Goldstein, S.L., 1987. Use and abuse of crust-formation ages. *Geology* 15,  
 920 893-895.

921 Baes, M., Gerya, T., Sobolev, S.V., 2016. 3-D thermos-mechanical modeling of plume-  
 922 induced subduction initiation. *Earth and Planetary Science Letters* 453, 193-  
 923 203.

924 Barbarin, B., 1999. A review of the relationships between granitoid types, their origins  
 925 and their geodynamic environments. *Lithos* 46, 605-626.

926 Barker, F., 1979. Trondhjemites: definition, environment and hypotheses of origin. In:  
 927 Barker, F. Ed., *Trondhjemites, Dacites and Related Rocks*. Elsevier,  
 928 Amsterdam, pp. 1–12.

929 Beckinsale, R.D., Drury, S.A., Holt, R.W., 1980. 3300-Myr old gneisses from the South  
 930 Indian Craton. *Nature* 283, 469–470.

931 Bhaskar Rao, Y.J., Beck, W., Murthy, V.R., Charan, S.N., Naqvi, S.M., 1983. Geology,  
 932 geochemistry and age of metamorphism of Archaean grey gneisses around  
 933 Channarayapatna Hassan district, Karmataka, South India. *Geological Society*  
 934 *of India Memoirs* 4, 309–328.

935 Bhaskar Rao, Y.J., Naha, K., Srinivasan, R., Gopalan, K., 1991. Geology, geochemistry  
 936 and geochronology of the Archaean Peninsular Gneiss around Gorur, Hassan  
 937 District, Karnataka, India. *Proceedings of the Indian Academy of Science* 100,  
 938 399-412.

939 Bhaskar Rao, Y.J., Sivaraman, T.V., Pantulu, G.V.C., Gopalan, K., Naqvi, S.M., 1992.  
 940 Rb–Sr ages of late Archean metavolcanics and granites, Dharwar craton, South

941 India and evidence for Early Proterozoic thermotectonic event. *Precambrian*  
942 *Research* 59, 145–170.

943 Bhaskar Rao, Y.J., Griffin, W.L., Ketchum, J., Pearson, N.J., Beyer, E., O'Reilly, S.Y.,  
944 2008. An outline of juvenile crust formation and recycling history in the  
945 Archaean Western Dharwar craton, from zircon in situ U-Pb dating and Hf-  
946 isotopic compositions. *Goldschmidt conference abstracts* p.81.

947 Blichert-Toft, J., 2008. The Hf isotopic composition of zircon reference material 91500.  
948 *Chemical Geology* 253, 252-257.

949 Blichert-Toft, J., Albarède, F., 2008. Hafnium isotopes in Jack Hills zircons and the  
950 formation of the Hadean crust. *Earth and Planetary Science Letters* 265, 686-  
951 702.

952 Bhushan, S.K., Sahoo, P., 2010. Geochemistry of clastic sediments from Sargur  
953 supracrustals and Bababudan group, Karnataka: Implications on Archaean  
954 Proterozoic boundary. *Journal of the Geological Society of India* 75, 829-840.

955 Boher, M., Abouchami, W., Michard, A., Albarede, F., Arndt, N.T., 1992. Crustal  
956 growth in West-Africa at 2.1 Ga. *Journal of Geophysical Research* 97, 345–369.

957 Bouhallier, H., Choukroune, P., Ballèvre, M., 1993. Diapirism, bulk homogeneous  
958 shortening and transcurrent shearing in the Archaean Dharwar craton: The  
959 Holenarsipur area, southern India. *Precambrian Research* 63, 43-58.

960 Bouhallier, H., Chardon, D., Choukroune, P., 1995. Strain patterns in Archaean dome-  
961 and-basin structures: The Dharwar craton (Karnataka, South India). *Earth and*  
962 *Planetary Science Letters*, 135, 57-75.

963 Bouilhol, P., Jagoutz, O., Hanchar, J.M., Dudas, F.O., 2013. Dating the India-Eurasia  
964 collision through arc magmatic records. *Earth and Planetary Science Letters*  
965 366, 163-175.

966 Chadwick, B., Ramakrishnan, M., Vasudev, V.N., Viswanatha, M.N., 1989. Facies  
 967 distribution and structure of a Dharwar volcano-sedimentary basin: Evidence  
 968 for late Archaean transpression in south India. *Journal of the Geological Society*  
 969 of London 146, 825-834.

970 Chadwick, B., Vasudev, V.N., Hedge, G.V., 2000. The Dharwar craton, southern India,  
 971 interpreted as the result of Late Archaean oblique convergence. *Precambrian*  
 972 *Research* 99, 91-111.

973 Chardon, D., Choukroune, P., Jayananda, M., 1996. Strain patterns, décollement and  
 974 incipient sagducted greenstone terrains in the Archaean Dharwar craton (south  
 975 India). *Journal of structural geology* 18, 991-1004.

976 Chardon, D., Choukroune, P., Jayananda, M., 1998. Sinking of the Dharwar Basin  
 977 (South India): implications for Archaean tectonics. *Precambrian Research* 91,  
 978 15-39.

979 Chardon, D., Jayananda, M., Chetty, T.R.L., Peucat, J.-J., 2008. Precambrian  
 980 continental strain and shear zone patterns; South Indian case. *Journal of*  
 981 *Geophysical Research* 113, 1-16.

982 Chauvel, C., Blichert-Toft, J., 2001. A hafnium isotope and trace element perspective  
 983 on melting of the depleted mantle. *Earth and Planetary Science Letters* 190,  
 984 137–151.

985 Chu, N., Taylor, R.N., Chavagnac, V., Nesbitt, R.W., Boella, R.M., Milton, J.A.,  
 986 German, C.R., Bayon, G., Burton, K., 2002. Hf isotope ratio analysis using  
 987 multi-collector inductively coupled plasma mass spectrometry: an evaluation of  
 988 isobaric interference corrections. *Journal of Analytical Atomic Spectrometry*  
 989 17, 1567–1574.

990 Couzinié, S., Laurent, O., Moyen, J.-F., Zeh, A., Bouilhol, Villaros, A., 2016. Post-  
 991 collisional magmatism: crustal growth not identified by zircon Hf-O isotopes.  
 992 Earth and Planetary Science Letters 456, 182-195.

993 Dey, S., 2013. Evolution of the Archaean crust in the Dharwar craton: The Nd isotope  
 994 record. Precambrian Research 227, 227-246.

995 Dhuime, B., Hawkesworth, C., Cawood, P.A., 2011. When continents formed, Science  
 996 331, 154-155.

997 Elburg, M.A., Foden, J.D., van Bergen, M.J., Zulkarnain, I., 2005. Australia and  
 998 Indonesia in collision: geochemical sources of magmatism. Journal of  
 999 Volcanology and Geothermal Research 140, 25–47.

1000 Fisher, C.M., Longerich, H.P., Jackson, S.E., Hanchar, J.M., 2010. Data acquisition and  
 1001 calculation of U-Pb isotopic analyses using laser ablation (single collector)  
 1002 inductively coupled plasma mass spectrometry. Journal of Analytical Atomic  
 1003 Spectrometry 25, 1905-1920.

1004 Fisher, C.M., Vervoort, J.D., Hanchar, J.M., 2014a. Guidelines for reporting zircon Hf  
 1005 isotopic data by LA-MC-ICP-MS and potential pitfalls in the interpretation of  
 1006 these data. Chemical Geology 363, 125–133.

1007 Fisher, C.M., Vervoort, J.D., DuFrane, S.A., 2014b. Accurate Hf isotope  
 1008 determinations of complex zircons using the “laser ablation split stream”  
 1009 method. Geochemistry Geophysics Geosystem 15, 121-139.

1010 Flanagan, F.J., 1976, Descriptions and Analysis of Eight New USGS Rock Standards,  
 1011 U.S. Geological Survey Professional Paper 840, p. 192.

1012 Gerdes, A., Zeh, A., 2009. Zircon formation versus zircon alteration – New insights  
 1013 from combined U-Pb and Lu-Hf in-situ LA-ICP-MS analyses, and

1014 consequences for the interpretation of Archean zircon from the Central Zone of  
 1015 the Limpopo Belt. *Chemical Geology* 261, 230-243.

1016 Ghosh, J.G., de Wit, M., Zartman, R.E., 2004. Age and tectonic evolution of  
 1017 Neoproterozoic ductile shear zone in the Southern Granulite Terrain of India,  
 1018 with implications for Gondwana studies. *Tectonics* 23, 1-38.

1019 Govindaraju, K., 1994, 1994 Compilation of Working Values and Descriptions for 383  
 1020 Geostandards, *Geostandards Newsletter*, 18:1-158.

1021 Griffin, W.L., Belousova, E.A., Shee, S.R., Pearson, N.J., O'Reilly, S.Y., 2004.  
 1022 Archean crustal evolution in the northern Yilgarn Craton: U-Pb and Hf-isotope  
 1023 evidence from detrital zircons. *Precambrian Research* 131, 231-282.

1024 Guitreau, M., Blichert-Toft, J., 2014. Implications of discordant U-Pb ages on Hf  
 1025 isotope studies of detrital zircons. *Chemical Geology* 385, 17-25.

1026 Guitreau, M., Blichert-Toft, J., Martin, H., Mojzsis, S.J., Albarède, F., 2012. Hafnium  
 1027 isotope evidence from Archean granitic rocks for deep mantle origin of  
 1028 continental crust. *Earth and Planetary Science Letters* 337–338, 211–223.

1029 Guitreau, M., Blichert-Toft, J., Billström, K., 2014. Hafnium isotope evidence for  
 1030 early-Proterozoic volcanic arc reworking in the Skellefte district (northern  
 1031 Sweden) and implications for the Svecofennian orogeny. *Precambrian Research*  
 1032 252, 39-52.

1033 Hawkesworth, C., Dhuime, B., Pietranik, A., Cawood, P., Kemp, T., and Storey, C.,  
 1034 2010, The generation and evolution of the continental crust: *Journal of the*  
 1035 *Geological Society* 167, 229–248.

1036 Herrington, R.J., Scotney, P.M., Roberts, S., Boyce, A.J., Harrison, D., 2011. Temporal  
 1037 association of arc–continent collision, progressive magma contamination in arc



1038 volcanism and formation of gold-rich massive sulphide deposits on Wetar  
1039 Island (Banda arc). *Gondwana Research* 19, 583–593.

1040 Hokada, T., Horie, K., Satish-Kumar, M., Ueno, Y., Nasheeth, A., Mishima, K.,  
1041 Shiraishi, K., 2013. An appraisal of Archaean supracrustal sequences in  
1042 Chitradurga Schist Belt, western Dharwar craton, southern India. *Precambrian*  
1043 *Research* 227, 99–119.

1044 Hoffman, P., 1988. United Plates of America, the birth of a craton: early  
1045 Proterozoic assembly and growth of Laurentia. *Annual Reviews in Earth and*  
1046 *Planetary Science*. 16, 543–603.

1047 Hoffmann, J.E., Münker, C., Polat, A., König, S., Mezger, K., Rosing, M.T., 2010.  
1048 Highly depleted Hadean mantle reservoirs in the sources of early Archean arc-  
1049 like rocks, Isua supracrustal belt, southern West Greenland. *Geochimica et*  
1050 *Cosmochimica Acta* 74, 7236-7260.

1051 Hoffmann, J.E., Wilson, A.H., 2017. The origin of highly radiogenic Hf isotope  
1052 compositions in 3.33 Ga Comondale komatiite lavas (South Africa). *Chemical*  
1053 *Geology* 455, 6-21.

1054 Ickert, R., 2013. Algorithms for estimating uncertainties in initial radiogenic isotope  
1055 ratios and model ages. *Chemical Geology* 340, 131–188.

1056 Iizuka, T., Campbell, I.H., Allen, C.M., Gill, J.B., Maruyama, S., Makoka, F., 2013.  
1057 Evolution of the African continental crust as recorded by U–Pb, Lu–Hf and O  
1058 isotopes in detrital zircons from modern rivers. *Geochimica et Cosmochimica*  
1059 *Acta* 107, 96–120.

1060 Iizuka, T., Yamaguchi, T., Hibiya, Y., Amelin, Y., 2015. Meteorite zircon constraints  
1061 on the bulk Lu-Hf isotope composition and early differentiation of the Earth.  
1062 *Proceedings of the National Academy of Science* 112, 5331-5336.

1063 Ishwar-Kumar, C., Windley, B.F., Horie, K., Kato, T., Hokada, T., Itaya, T., Yagi, K.,  
1064 Gouzu, C., Sajeev, K., 2013. A Rodinian suture in western India: New insights  
1065 on India-Madagascar correlations. *Precambrian Research* 236, 227-251.

1066 Jaffey, A.H., Flynn, K.F., Glendenin, L.E., Bentley, W.C., Essling, A.M., 1971.  
1067 Precision measurement of half-lives and specific activities of <sup>235</sup>U and <sup>238</sup>U.  
1068 *Physical Reviews C* 4, 1889.

1069 Janardhan, A.S., Srikantappa, C., Ramachandra, H.M., 1978. The Sargur schist  
1070 complex – An Archaean high-grade terrane in southern India. In: B.F.  
1071 Windley and S.M. Naqvi (Eds.) *Archaean Geochemistry*, Elsevier, Amsterdam,  
1072 pp. 127-149.

1073 Janardhan, A.S., Newton, R.C., Hansen, E.C., 1982. The transformation of amphibolite  
1074 facies gneiss to charnockite in southern Karnataka and northern Tamil Nadu,  
1075 India. *Contributions to Mineralogy and Petrology* 79, 130-149.

1076 Jayananda, M., Kano, T., Peucat, J.-J., Channabasappa, S., 2008. 3.35 Ga komatiite vol-  
1077 canism in the western Dharwar craton: constraints from Nd isotopes and  
1078 wholerock geochemistry. *Precambrian Research* 162, 160–179.

1079 Jayananda, M., Tsutsumi Y., Miyazaki, T., Gireesh, R.V., Kapfo, K.-u., Tushipokla,  
1080 Hidaka, H., Kano, T., 2013. Geochronological constraints on Meso- and  
1081 Neoarchean regional metamorphism and magmatism in the Dharwar craton,  
1082 southern India. *Journal of Asian Earth Sciences* 78, 18-38.

1083 Jayananda, M., Chardon, D., Peucat, J.-J., Tushipokla, Fanning, C.M., 2015. Paleo- to  
1084 Mesoarchean TTG accretion and continental growth in the western Dharwar  
1085 craton, Southern India: Constraints from SHRIMP U-Pb zircon geochronology,  
1086 whole-rock geochemistry and Nd-Sr isotopes. *Precambrian Research* 268, 295-  
1087 322.

1088 Jayananda, M., Duraiswami, R.A., Aadhiseshan, K.R., Gireesh, R.V., Prabhakar, B.C.,  
 1089 Kafo, K.-u, Tushipokla, Namratha, R., 2016. Physical volcanology and  
 1090 geochemistry of Palaeoarchaeon komatiite lava flows from the western Dharwar  
 1091 craton, southern India: implications for Archaean mantle evolution and crustal  
 1092 growth. *International geology review* 58, 1569-1595.

1093 Kaur, P., Zeh, A., Chaudhri, N., 2014. Characterisation and U-Pb-Hf isotope record of  
 1094 the 3.55 Ga felsic crust from the Bundelkhand Craton, northern India.  
 1095 *Precambrian Research* 255, 236-244.

1096 Kirkland, C.L., Smithies, R.H., Taylor, R.J.M., Evans, N., McDonald, B., 2015. Zircon  
 1097 Th/U ratios in magmatic environs. *Lithos* 212-215, 397-414.

1098 Košler, J., Sylvester, P.J., 2003. Present trends and the Future of Zircon in  
 1099 Geochronology: Laser Ablation ICPMS. *Zircon. Reviews in Mineralogy and*  
 1100 *Geochemistry*, 53, 243–275.

1101 Kunugiza, K., Kato, Y., Kano, T., Takaba, Y., Kuruma, I., Sohma, T., 1996. An  
 1102 Archaean tectonic model of the Dharwar craton, Southern India: the origin of  
 1103 the Holenarsipur greenstone belt (Hassan district, Karnataka) and  
 1104 reinterpretation of the Sargur-Dharwar relationship. *Journal of Southeast Asian*  
 1105 *Earth Sciences* 14, 149-160.

1106 Lancaster, P.J., Dey, S., Storey, C.D., Mitra, A., and Bhunia, R.K., 2015. Contrasting  
 1107 crustal evolution processes in the Dharwar craton: insights from detrital zircon  
 1108 U-Pb and Hf isotopes. *Gondwana Research* 28, 1361-1372.

1109 Laurent, O., Martin, H., Moyon, J.F., Doucelance, R., 2014. The diversity and evolution  
 1110 of late-Archaean granitoids: Evidence for the onset of “modern-style” plate  
 1111 tectonics between 3.0 and 2.5 Ga. *Lithos* 205, 208-235.

1112 Laurent, O., Zeh, A., 2015. A linear Hf isotope-age array despite different granitoid  
 1113 sources and complex Archean geodynamics: Example from the Pietersburg  
 1114 block (South Africa). *Earth and Planetary Science Letters* 430, 326-338.

1115 Lenting, C., Geisler, T., Gerdes, A., Kooijman, E., Scherer, E.E., Zeh, A., 2010. The  
 1116 behavior of the Hf isotope system in radiation-damaged zircon during  
 1117 experimental hydrothermal alteration. *American Mineralogist* 95, 1343–1348.

1118 Le Roux, L.J., Glendenin, L.E., 1963. Half-life of  $^{232}\text{Th}$ . In: National Conference on  
 1119 Nuclear Energy, Application of Isotopes and Radiation. Proceedings of the  
 1120 National Conference on Nuclear Energy held in Pretoria, April 5–8 1963. South  
 1121 African Atomic Energy Board, Pelindaba, pp. 83–94.

1122 Ludwig, K.R., 2008. User's Manual for Isoplot 3.6, a Geochronological Toolkit for  
 1123 Microsoft Excel. Berkeley Geochronology Center Special Publication 4.

1124 Maibam, B., Goswami, J.N., Srinivasan, R., 2011. Pb–Pb zircon ages of Archean  
 1125 metasediments and gneisses from the Dharwar craton, southern India:  
 1126 implications for the antiquity of the eastern Dharwar craton. *J. Earth Syst. Sci.*  
 1127 120 (4), 643–661.

1128 Maibam, B., Gerdes, A., Goswami, J.N., 2016. U-Pb and Hf isotope records in detrital  
 1129 and magmatic zircon from eastern and western Dharwar craton, southern India:  
 1130 Evidence for coeval Archean crustal evolution. *Precambrian Research* 275,  
 1131 496-512.

1132 Moyen, J.-F., Martin, H., 2012. Forty years of TTG research. *Lithos* 148, 312–336.

1133 Martin, H., Moyen, J.-F., Guitreau, M., Blichert-Toft, J., Le Pennec, J.-L., 2014. Why  
 1134 Archean TTG cannot be generated by MORB melting in subduction zones.  
 1135 *Lithos* 198-199, 1-13.

- 1136 Meißner, B., Deters, P., Srikantappa, C., Köhler, H., 2002. Geochronological evolution  
1137 of the Moyar, Bhavani and Palghat shear zones of Southern India: Implications  
1138 for east Gondwana correlations. *Precamb. Res.*, 114, 149-175.
- 1139 Meen, J.K., Rogers, J.J.W., Fullagar, P.D., 1992. Lead isotopic compositions in  
1140 the western Dharwar craton, southern India: evidence for distinct middle  
1141 Archaean terranes in a late Archaean craton. *Geochim. Cosmochim. Acta* 56,  
1142 2455–2470.
- 1143 Meert, J.G., 2003. A synopsis of events related to the assembly of eastern Gondwana.  
1144 *Tectonophysics* 362, 1-40.
- 1145 Miller, J.S., Santosh, M., Pressley, R.A., Clements, A.S., Rogers, J.J.W., 1996. A Pan-  
1146 African thermal event in southern India. *Journal of Southeast Asian Earth*  
1147 *Sciences* 14, 127-136.
- 1148 Mojzsis, S.J., Devaraju, T.C., Newton, R.C., 2003. Ion microprobe U-Pb age  
1149 determinations on zircon from the late Archean granulite facies transition zone  
1150 of Southern India. *Journal of Geology* 111, 407-425.
- 1151 Möller, A., O'Brien, P.J., Kennedy, A., Kröner, A., 2003. Linking growth episodes of  
1152 zircon and metamorphic textures to zircon chemistry: an example from the  
1153 ultra-high temperature granulites of Rogaland (SW Norway). *Geological*  
1154 *Society, London, Special Publications* 220, 65-81.
- 1155 Monrad, 1983. Evolution of sialic terranes in the vicinity of the Holenarasipur belt,  
1156 Hassan district, Karnataka, India. *Geological Society of India Memoirs* 4, 343–  
1157 364.
- 1158 Moyen et al., 2003. Syntectonic granite emplacement at different structural levels: the  
1159 Closepet granite, South India. *Journal of Structural Geology* 25, 611-631.

1160 Naqvi, S.M., 1983. Early Precambrian clastic metasediments of Dharwar greenstone  
 1161 belts; Implications to sial-sima transformation processes. Geological Society of  
 1162 India Memoirs 4, 220-236.

1163 Naqvi, S.M., Divakara Rao, V., Hussain, S.M., Narayana, B.L., Nirmal Charan, S.,  
 1164 Govil, P.K., Bhaskar Rao, Y.J., Jafri, S.H., Rama Rao, P., Balram, V., Masood  
 1165 Ahmad, Pantulu, K.P., Gnaneswar Rao, Subba Rao, D.V., 1983. Geochemistry  
 1166 of gneisses from Hassan district and adjoining areas, Karnataka, India.  
 1167 Geological Society of India Memoirs 4, 401-413.

1168 Naqvi, S.M., Ram Mohan, M., Rana Prathap, J.G., Srinivasa Sarma, D., 2009. Adakite–  
 1169 TTG connection and fate of Mesoarchean basaltic crust of Holenarsipur  
 1170 nucleus, Dharwar Craton, India. Journal of Asian Earth Sciences 35, 416–434.

1171 Naqvi and Rogers, 1987. Precambrian Geology of India. Oxford monographs on  
 1172 Geology and Geophysics 6.

1173 Nutman, A.P., Chadwick, B., Ramakrishnan, M., Viswanatha, M.N., 1992. SHRIMP  
 1174 U-Pb ages of detrital zircon in Sargur supracrustal rocks in western Karnataka,  
 1175 southern India. Journal of the Geological Society of India 39, 367–374.

1176 Nebel, O., Campbell, I.H., Sossi, P.A., van Kranendonk, M.J., 2014. Hafnium and iron  
 1177 isotopes in early Archean komatiites record a plume-driven convection cycle in  
 1178 the Hadean Earth. Earth and Planetary Science Letters 397, 111–120.

1179 O'Connor, J.T., 1965. A classification for quartz-rich igneous rocks based on feldspar  
 1180 ratios. U.S. Geological Survey Professional Paper, 525(B): 79-84.

1181 Öhlander, B., Skiöld, T., Elming, S.-Å., BABEL working group, Claesson, S.,  
 1182 Niska, D.H., 1993. Delineation and character of the Archaean-Proterozoic  
 1183 boundary in northern Sweden. Precambrian Res. 64, 67–84.

1184 Paces, J.B. and Miller, J.D.Jr, 1993, Precise U-Pb ages of Duluth Complex and related  
1185 mafic intrusions, Northeastern Minnesota: geochronological insights to  
1186 physical, petrogenetic, paleomagnetic, and tectonomagmatic processes  
1187 associated with the 1.1 Ga Midcontinent Rift System. *Journal of Geophysical*  
1188 *Research* 98, 13997-14013.

1189 Patchett, P.J., 1983. Importance of the Lu–Hf isotopic system in studies of planetary  
1190 chronology and chemical evolution. *Geochimica et Cosmochimica Acta* 47, 81–  
1191 91.

1192 Payne, J.L., McInerney, D.J., Barovich, K.M., Kirkland, C.L., Pearson, N.J., Hand, M.,  
1193 2016. Strengths and limitations of zircon Lu–Hf and O isotopes in modelling  
1194 crustal growth. *Lithos* 248–251, 175–192.

1195 Peucat et al., 1995. Age of the Holenarsipur greenstone belt, relations with the  
1196 surrounding gneisses (Karnataka, South India). *Journal of Geology* 103, 701-  
1197 710.

1198 Puchtel, I.S., Hofmann, A.W., Amelin, Y.V., Garbe-Schönberg, C.-D., Samsonov,  
1199 A.V., Shchipansky, A.A., 1999. Combined mantle plume-island arc model for  
1200 the formation of the 2.9 Ga Sumozero-Kenozero greenstone belt, SE Baltic  
1201 Shield: Isotope and trace element constraints. *Geochimica et Cosmochimica*  
1202 *Acta* 63, 3579-3595.

1203 Raase, P., Raith, M., Ackermant, D., Lal, R.K., 1986. Progressive metamorphism of  
1204 mafic rocks from greenschist to granulite facies in the Dharwar craton of South  
1205 India. *The Journal of Geology* 94, 261-282.

1206 Raith, M., Raase, P., Ackermant, D., Lal, R.K., 1983. Regional geothermobarometry in  
1207 the granulite facies terrane of South India. *Transactions of the Royal Society of*  
1208 *Edinburgh: Earth Sciences* 73, 221-244.

1209 Rajesh et al., 2009. Evidence for an early Archaean granite from Bastar craton, India.  
 1210 Geological Society, London, Special Publications 166, 193-196.

1211 Ramakrishnan, M., Venkata Dasu, S.P., Kröner, A., 1994. Middle Archean ages of  
 1212 Sargur group by single grain zircon dating and geochemical evidences for the  
 1213 clastic origin of metaquartzite from J. C. Pura greenstone belt, Karnataka.  
 1214 Journal of the Geological Society of India, 44, 605–616.

1215 Ramakrishnan, M., 2009. Precambrian mafic magmatism in the Western Dharwar  
 1216 craton, Southern India. Journal of the Geological Society of India 73, 101-116.

1217 Rey, P.F., Phipps, P., Thébaud, N., 2003. Contribution of mantle plumes, crustal  
 1218 thickening and greenstone blanketing to the 2.75-2.65 Ga global crisis.  
 1219 Precambrian Research 127, 43-60.

1220 Rogers, J.J.W., Callahan, E.J., Dennen, K.O., Fullagar, P.D., Stroh, P.T., Wood, L.F.,  
 1221 1986. Chemical evolution of peninsular gneiss in the Western Dharwar craton,  
 1222 Southern India. The Journal of Geology 94, 233-246.

1223 Rollinson, H.R., Windley, B.F., Ramakrishnan, M., 1981. Contrasting high and  
 1224 intermediate pressures of metamorphism in the Archaean Sargur Schists of  
 1225 Southern India. Contributions in Mineralogy and Petrology 76, 420-429.

1226 Santosh, M., Tanaka, K., Yokoyama, K., Collins, A.S., 2005. Late Neoproterozoic-  
 1227 Cambrian Felsic Magmatism Along Transcrustal Shear Zones in Southern  
 1228 India: U-Pb Electron Microprobe Ages and Implications for the Amalgamation  
 1229 of the Gondwana Supercontinent. Gondwana Research 8, 31-42.

1230 Santosh, M., Morimoto, T., Tsutsumi, Y., 2006. Geochronology of the khondalite belt  
 1231 of Trivandrum, Southern India: Electron probe ages and implications for  
 1232 Gondwana tectonics. Gondwana Research 9, 261-278.



- 1233 Santosh, M., Yang, Q.-Y., Shaji, E., Ram Mohan, M., Tsunogae, T., Satyanarayanan,  
1234 M., 2016. Oldest rocks from Peninsular India: Evidence for Hadean to  
1235 Neoarchean crustal evolution. *Gondwana Research* 29, 105-135.
- 1236 Sarkar, G., Corfu, F., Paul, D.K., McNaughton, N.J., Gupta, S.N., Bishui, P.K., 1993.  
1237 Early Archaean crust in Bastar craton, central India—a geochemical and  
1238 isotopic study. *Precambrian Research* 62, 127–137.
- 1239 Sarma, S.D., McNaughton, N.J., Belousova, E., Mohan, M.R., Fletcher, I.R., 2012.  
1240 Detrital zircon U-Pb ages and Hf-isotope systematics from the Gadag Greenston  
1241 Belt: Archean crustal growth in the western Dharwar Craton, India. *Gondwana*  
1242 *Research* 22, 843-854.
- 1243 Sato, K., Santosh, M., Tsunogae, T., Chetty, T.R.K., Hirata, T., 2011. Subduction-  
1244 accretion-collision history along the Gondwana suture in southern India: A laser  
1245 ablation ICP-MS study of zircon chronology. *Journal of Asian Earth Sciences*,  
1246 40, 162-171.
- 1247 Shand, S.J., 1943. Eruptive rocks. Their genesis, composition, classification, and their  
1248 relations to ore-deposits. Wiley, New York, 444pp.
- 1249 Scherer, E., Münker, C., Mezger, K., 2001. Calibration of the lutetium–hafnium clock.  
1250 *Science* 293, 683–687.
- 1251 Schoene, B., de Wit, M., Bowring, S.A., 2008. Mesoarchean assembly and stabilization  
1252 of the eastern Kaapvaal craton: A structural-thermochronological perspective.  
1253 *Tectonics* 27, 1-27.
- 1254 Sláma, J., Kosler, J., Condon, D.J., Crowley, J.L., Gerdes, A., Hanchar, J.M.,  
1255 Horstwood, M.S.A., Morris, G.A., Nasdala, L., Norberg, N., Schaltegger, U.,  
1256 Schoene, B., Tubrett, M.N., Whitehouse, M.J., 2008. Plešovice zircon – A new

1257 natural reference material for U–Pb and Hf isotopic microanalysis. *Chemical*  
 1258 *Geology* 249, 1–35.  
 1259  
 1260 Söderlund, U., Patchett, J.P., Vervoort, J.D., Isachsen, C.E., 2004. The  $^{176}\text{Lu}$  decay  
 1261 constant determined by Lu–Hf and U–Pb isotope systematics of Precambrian  
 1262 mafic intrusions. *Earth and Planetary Science Letters* 219, 311–324.  
 1263 Stroh, P.T., Monrad, J.R., Fullagar, P.D., Naqvi, S.M., Hussain, S.M., Rogers, J.J.W.,  
 1264 1983. 3,000 M.y.-old Halekote trondhjemite: A record of stabilization of the  
 1265 Dharwar craton. *Geological Society of India Memoirs* 4, 365–376.  
 1266 Stevenson, R.K., Patchett, P.J., 1990. Implications for the evolution of continental crust  
 1267 from Hf isotope systematics of Archean detrital zircons. *Geochimica et*  
 1268 *Cosmochimica Acta* 54, 1683–1697.  
 1269 Taylor, P.N., Chadwick, B., Moorbath, S., Ramakrishnan, M., Viswanatha, M.N., 1984.  
 1270 Petrography, chemistry, and isotopic ages of Peninsular Gneiss, Dharwar  
 1271 acidvolcanic rocks and the Chitradurga granite with special reference to the  
 1272 lateArchaean evolution of the Karnataka craton. *Precambrian Research* 23,  
 1273 349–375.  
 1274 Vavra, G., Schmid, R., Gebauer, D., 1999. Internal morphology, habit and U–Th–Pb  
 1275 microanalysis of amphibolite-to-granulite- facies zircons: geochronology of the  
 1276 Ivrea Zone (Southern Alps). *Contributions to Mineralogy and Petrology* 134,  
 1277 380–404.  
 1278 Wang, X., Griffin, W.L., Chen, J., Huang, P., Li, X., 2011. U and Th contents and Th/U  
 1279 ratios of zircon in felsic and mafic magmatic rocks: improved zircon-melt  
 1280 distribution coefficient. *Acta Geologica Sinica* 85, 164–174.

1281 Weihed, P., Arndt, N., Billström, K., Duchesne, J.-C., Eilu, P., Martinsson, O.,  
1282 Papunen, H., Lahtinen, R., 2005. Precambrian geodynamics and ore formation:  
1283 the Fennoscandian Shield. *Ore Geology Review* 27, 273–322.

1284 Whitmeyer, S.J., Karlstrom, K.E., 2007. Tectonic model for the Proterozoic growth of  
1285 North America. *Geosphere* 3, 220–259.

1286 Wiedenbeck, M., Allé, P., Corfu, F., Griffin, W.L., Meier, M., Oberli, F., von Quadt,  
1287 A., Roddick, J.C., Spiegel, W., 1995, Three natural zircon standards for U–Th–  
1288 Pb, Lu–Hf, trace element and REE analyses. *Geostandard Newsletters* 19, 1 –  
1289 23.

1290 Wiedenbeck M, Hanchar JM, Peck WH, Sylvester P, Valley J, Whitehouse M, Kronz  
1291 A, Morishita Y, Nasdala L, Fiebig J, Franchi I, Girard JP, Greenwood RC,  
1292 Hinton R, Kita N, Mason PRD, Norman M, Ogasawara M, Piccoli R, Rhede D,  
1293 Satoh H, Schulz-Dobrick B, Skår O, Spicuzza MJ, Terada K, Tindle A, Togashi  
1294 S, Vennemann T, Xie Q, Zheng Y-F (2004) Further characterization of the  
1295 91500 zircon crystal. *Geostandards and Geoanalytical Research* 28, 9-39.

1296 Woodhead, J.D., Hergt, J.M., 2005. A preliminary appraisal of seven natural zircon  
1297 reference materials for *in situ* Hf isotope determination. *Geostandards and*  
1298 *Geoanalytical Research* 29, 183-195.

1299 Yoshida, M., Arima, M., Kano, T., Kunugiza, K., Venkata-Rao, M., Shirahata, H.,  
1300 Sohma, T., Unnikrishnan-Warrier, C., Venkatesh-Ragavan, Yamaguchi, Y.,  
1301 1994. Geological survey in Southern to Eastern Peninsular India, 1992. *Journal*  
1302 *of Geosciences* 37, 31-54.

1303 Yoshida, M., Bindu, R.S., Kagami, H., Rajesham, T., Santosh, M., Shirahata, H., 1996.  
1304 Geochronologic constraints of granulite terranes of South India and their

1305 implications for the Precambrian assembly of Gondwana. Journal of Southeast  
 1306 Asian Earth Sciences, 14, 137–148.

1307 Zeh, A., Gerdes, A., Millonig, L., 2011. Hafnium isotope record of the Ancient Gneiss  
 1308 Complex, Swaziland, southern Africa: evidence for Archaean crust–mantle  
 1309 formation and crust reworking between 3.66 and 2.73 Ga. Journal of the  
 1310 Geological Society of London 168, 953–963.

1311

# 1312 **Figure captions**

1313 Table 1. Summary of the Archean geology of the Western Dharwar craton after [Naqvi](#)  
 1314 [and Rogers \(1987\)](#), [Yoshida et al. \(1994\)](#), [Naqvi et al. \(2009\)](#), and [Dey \(2013\)](#).

1315

1316 Table 2. Details of rock sampling location and petrography.

1317

1318 Table 3. Summary of U-Pb and Lu-Hf isotope results for Indian zircons analyzed by  
 1319 LA-ICP-MS and LA-MC-ICP-MS

1320

1321 Table 4. Interpreted U-Pb ages and Lu-Hf isotope systematics for Indian zircons  
 1322 analyzed herein

1323

1324 Figure 1. Detailed geological map of the Dharwar craton adapted from [Chardon et al.](#)  
 1325 [\(2008\)](#) and [Dey \(2013\)](#). WDC and EDC refer to Western and Eastern Dharwar Cratons,  
 1326 respectively. Major schist belts have been reported and names are indicated as follows;  
 1327 B for Banasandra, Bb for Bababudan, Ch for Chitradurga, G for Ghattihsahalli, Ga for  
 1328 Gadag, Ho for Holenarsipur, J for Jayachamarajapura (J.C. Pura), K for Kalyadi, Ku

for Kudremuh, N for Nuggihalli, S for Sandur, Sh for Shimoga, and Sg for Sargur. The inset shows where Figure 1 locates respective to India.

Figure 2. Merged geological and structural map of the Holenarsipur Schist Belt (Western Dharwar Craton, Southern India), from [Bouhallier et al. \(1993\)](#), with location of samples collected for this study (red dots).

Figure 3. Photos of sampling locations with corresponding thin section images in polarized and cross-polarized light for samples 13DC12 (Figs. 3A-3C) and 13DC13 (Figs. 3D-3F). Note the hammer and the chisel, with orange handle, for scale in 3A and 3D, respectively. Mineral names are reported as Qz for quartz, Plg for plagioclase, Kf for K-Feldspar (essentially microcline), Bt for biotite, and Ms for muscovite.

Figure 4. Diagrams presenting the major characteristics of samples 13DC12 and 13DC13 based on major and minor element concentrations. Figure A is an An-Ab-Or normative plot that discriminates granitoid types (after [O'Connor, 1965](#) and [Barker, 1979](#)). Figure B is a diagram that indicates granite chemical affinity according to the classification proposed by [Shand \(1943\)](#). Figure C is MALI index after [Frost et al. \(2001\)](#) with field compositions after [Martin and Moyen \(2012\)](#) and [Laurent et al. \(2014\)](#). Figure D is a classification of late-Archean granitoids proposed in [Laurent et al. \(2014\)](#). Figure E is a ternary diagram that presents the compositional field of melts produced by a range of possible sources (i.e., low-K and high-K mafic rocks, as well as tonalities and metasediments). This diagram can be used to infer granite sources using major element concentrations (after [Laurent et al., 2014](#)).

1354 Figure 5. Coupled U-Pb and Lu-Hf isotope results for zircons from sample 13DC12.  
1355 Dashed lines represent closed-system evolution of the Lu-Hf isotope system using the  
1356  $^{176}\text{Lu}/^{177}\text{Hf}$  indicated next to each line, which correspond to the lowest and highest  
1357 values measured for this zircon population, and assuming that the initial  $^{176}\text{Hf}/^{177}\text{Hf}$  is  
1358 the average of those visible in the inset. Note the general good match between  
1359 datapoints and evolution lines.

1360

1361 Figure 6. Summary of 13DC12 zircon U-Pb geochronology. Figure A is a Concordia  
1362 plot displaying the most concordant and oldest least discordant U-Pb data from  
1363 13DC12. Figure B presents the weighted average  $^{207}\text{Pb}/^{206}\text{Pb}$  age for U-Pb data shown  
1364 in Figure A. Figure C is a Concordia diagram that shows U-Pb data for all other zircons  
1365 from 13DC12.

1366

1367 Figure 7. Coupled U-Pb and Lu-Hf isotope results for zircons from sample 13DC13.  
1368 As in Figure 4, dashed lines represent closed-system evolution of the Lu-Hf isotope  
1369 system using the  $^{176}\text{Lu}/^{177}\text{Hf}$  indicated next to each line, which correspond to the lowest  
1370 and highest values measured, and assuming that the initial  $^{176}\text{Hf}/^{177}\text{Hf}$  is the average of  
1371 the oldest zircons.

1372

1373 Figure 8. Coupled U-Pb and Lu-Hf isotope results for zircons from sample 13DC15.  
1374 The dashed line represents closed-system evolution of the Lu-Hf isotope system using  
1375 the  $^{176}\text{Lu}/^{177}\text{Hf}$  measured in 13DC15\_1b and the initial  $^{176}\text{Hf}/^{177}\text{Hf}$  from 13DC15\_1a.

1376

1377 Figure 9. Compilation of available U-Pb and Lu-Hf isotope data for detrital zircons  
1378 from the Western Dharwar Craton ([Sarma et al., 2012](#); [Lancaster et al., 2015](#); [Maibam](#)

et al., 2016), combined with data from this study, and those for Gorur gneiss from Bhaskar Rao et al. (2008). Also shown is the age range for Sargur-group komatiites analyzed by Jayananda et al. (2008) using the Sm-Nd isotope system. Bulk Silicate Earth (BSE) parameters are those from Iizuka et al. (2015) and arc-mantle evolution is deduced from a present-day  $\epsilon_{\text{Hf}}$  of +13.3 (Dhuime et al., 2011; Iizuka et al., 2013). Dashed lines indicate the evolution paths for reservoirs with mafic ( $^{176}\text{Lu}/^{177}\text{Hf} = 0.02$ ) and felsic (TTG;  $^{176}\text{Lu}/^{177}\text{Hf} = 0.005$ ) compositions. See text for details.

Captions to supplementary Figures and Tables:

Table S1. Major and minor oxide abundances for the orthogneisses analyzed in this study

Table S2. LA-ICP-MS and LA-MC-ICP-MS operating conditions

Table S3. U-Pb isotope results for the zircon standard 91500 analyzed by LA-ICP-MS.

Table S4. U-Pb isotope results for Indian zircons analyzed by LA-ICP-MS.

Table S5: Lu-Hf isotope results for zircon standards analyzed by LA-MC-ICP-MS

Table S6. Lu-Hf isotope results for Indian zircons analyzed by LA-MC-ICP-MS

Figure S1. Concordia plot and weighted average  $^{207}\text{Pb}/^{206}\text{Pb}$  for the zircon standard 91500 that was used as a quality check in this study.

Figure S2. Plots showing the accuracy of Hf isotope measurements performed on standards in this study.  $\epsilon_{\text{Hf}}$  values presented in this figure correspond to those visible in Table S5 which were calculated by normalization to the accepted values of the corresponding zircon standard also provided in Table S5.

Figure S3. Concordia plot for zircons from the granitic gneiss (13DC12) with corresponding cathodo-luminescence images.

Figure S4. Concordia plot for zircons from the trondhjemitic gneiss (13DC13) with corresponding cathodo-luminescence images.

Figure S5. Concordia plot of all U-Pb data for 13DC13 zircons (A) and  $^{207}\text{Pb}/^{206}\text{Pb}$  age vs. Th/U plot for corresponding zircons (B). White-filled symbols correspond to low-Th/U zircons whereas those filled with grey and black correspond to zircons with Th/U that comply with the common magmatic range and high-Th/U zircons, respectively.

Figure S6. Concordia plot for zircons from 13DC15 with corresponding transmitted light and cathodo-luminescence images.



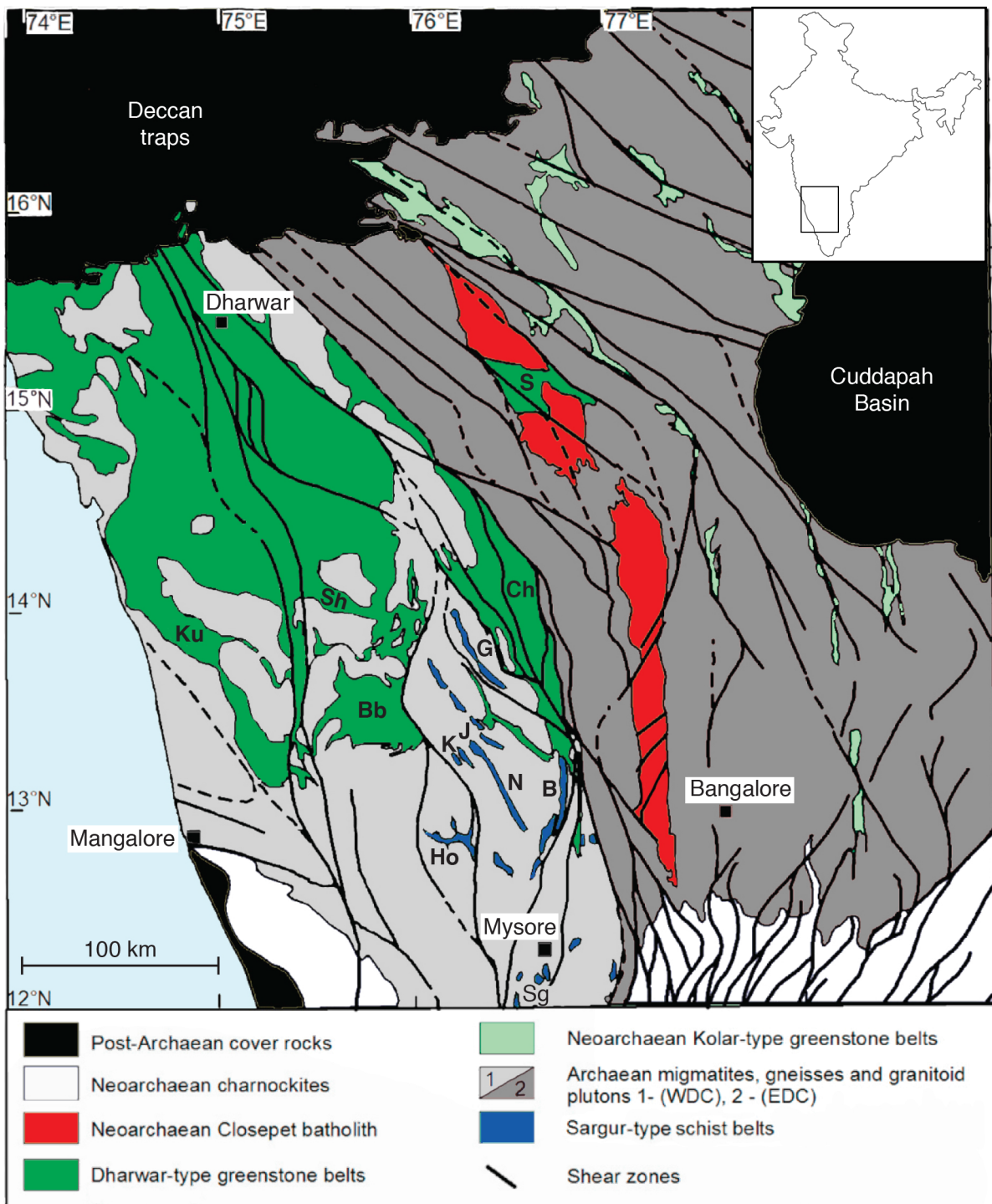


Figure 1

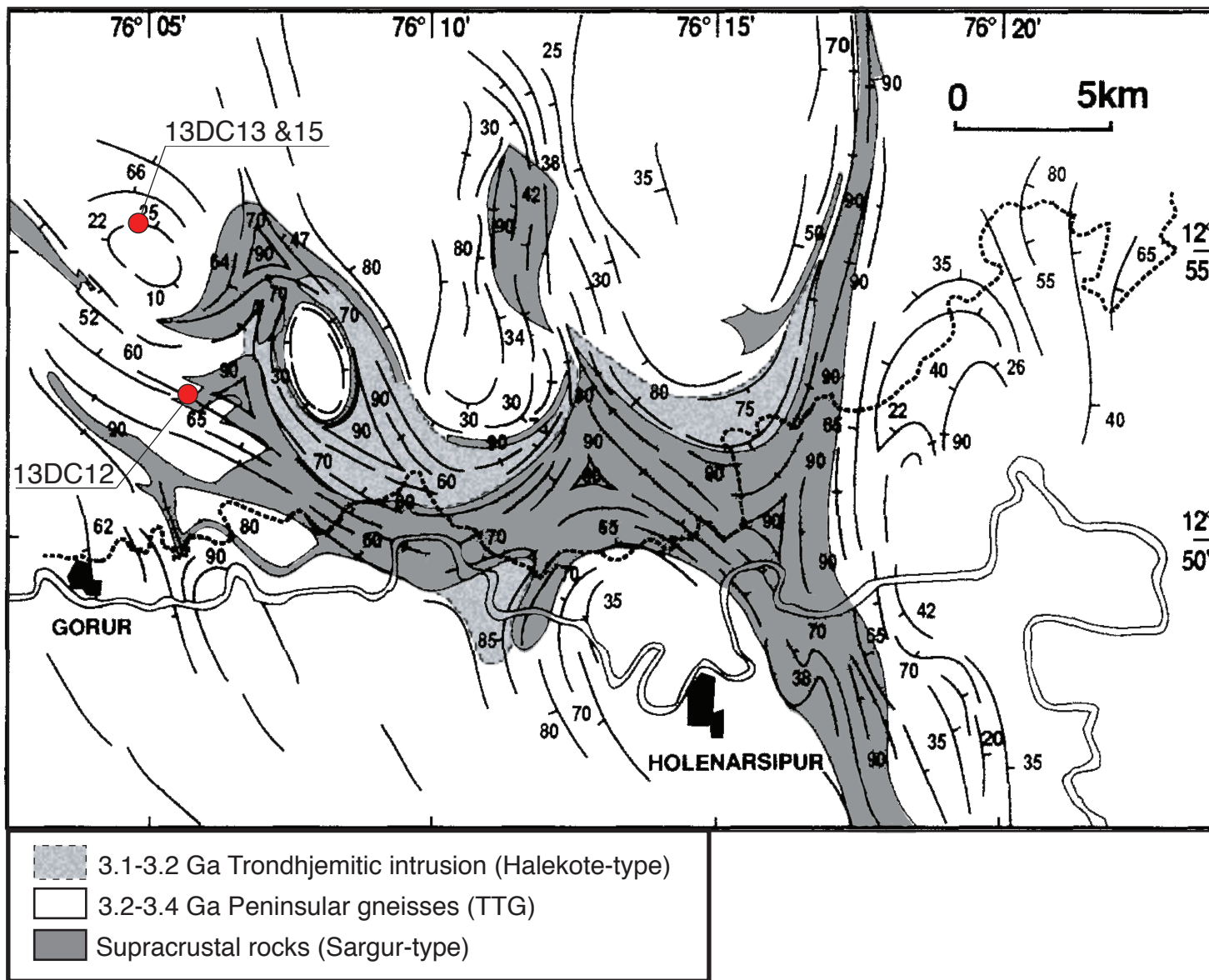


Figure 2



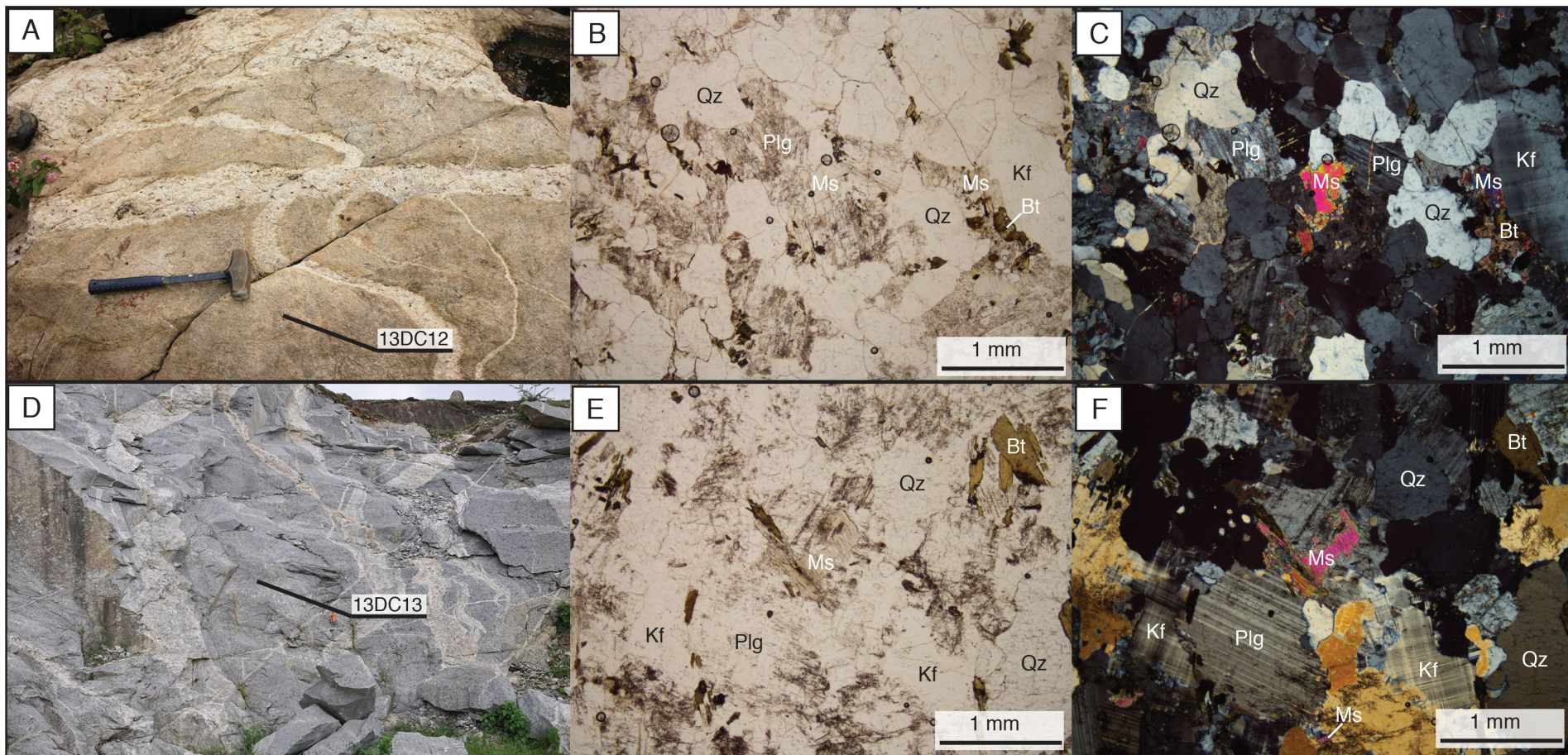


Figure 3

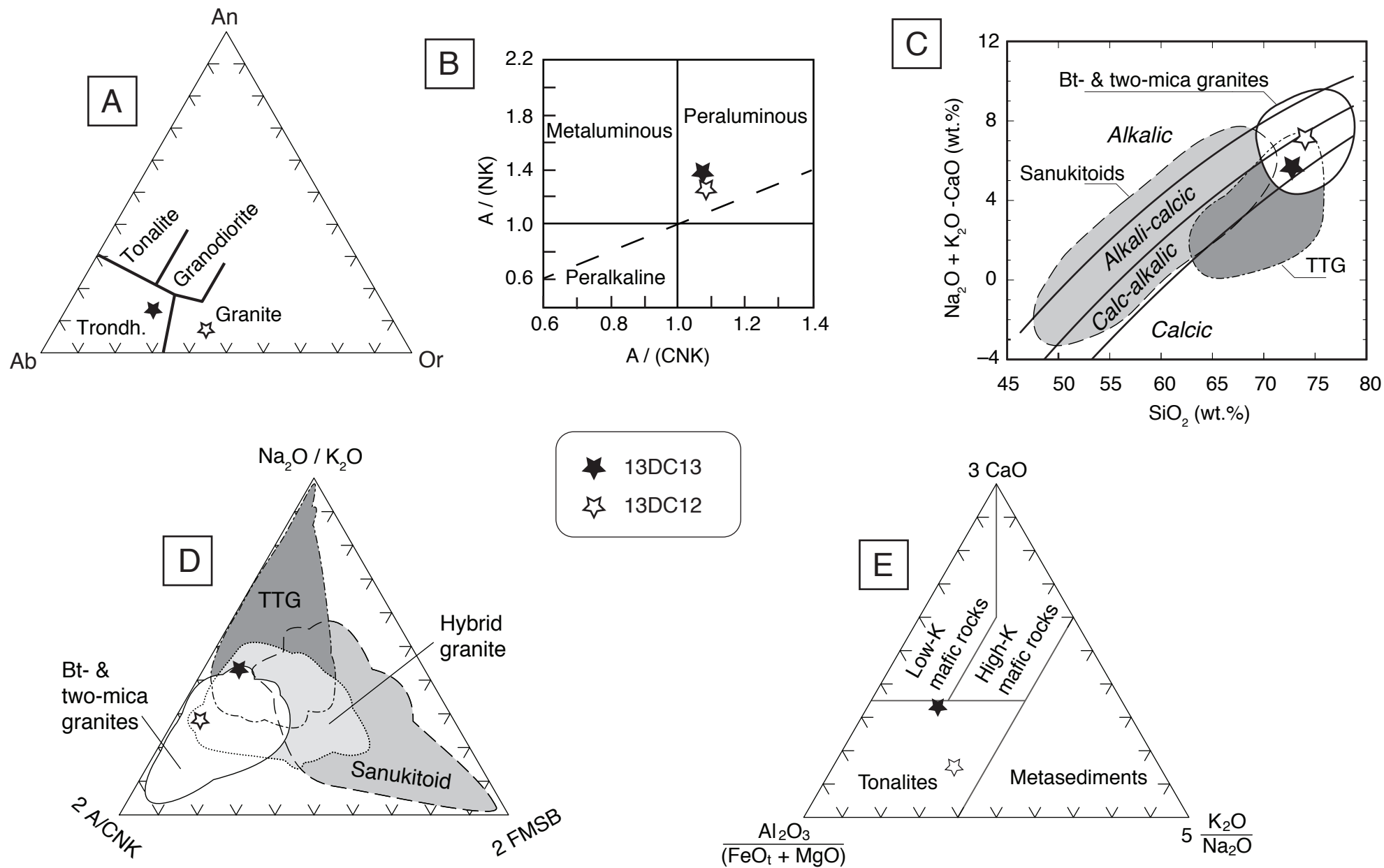
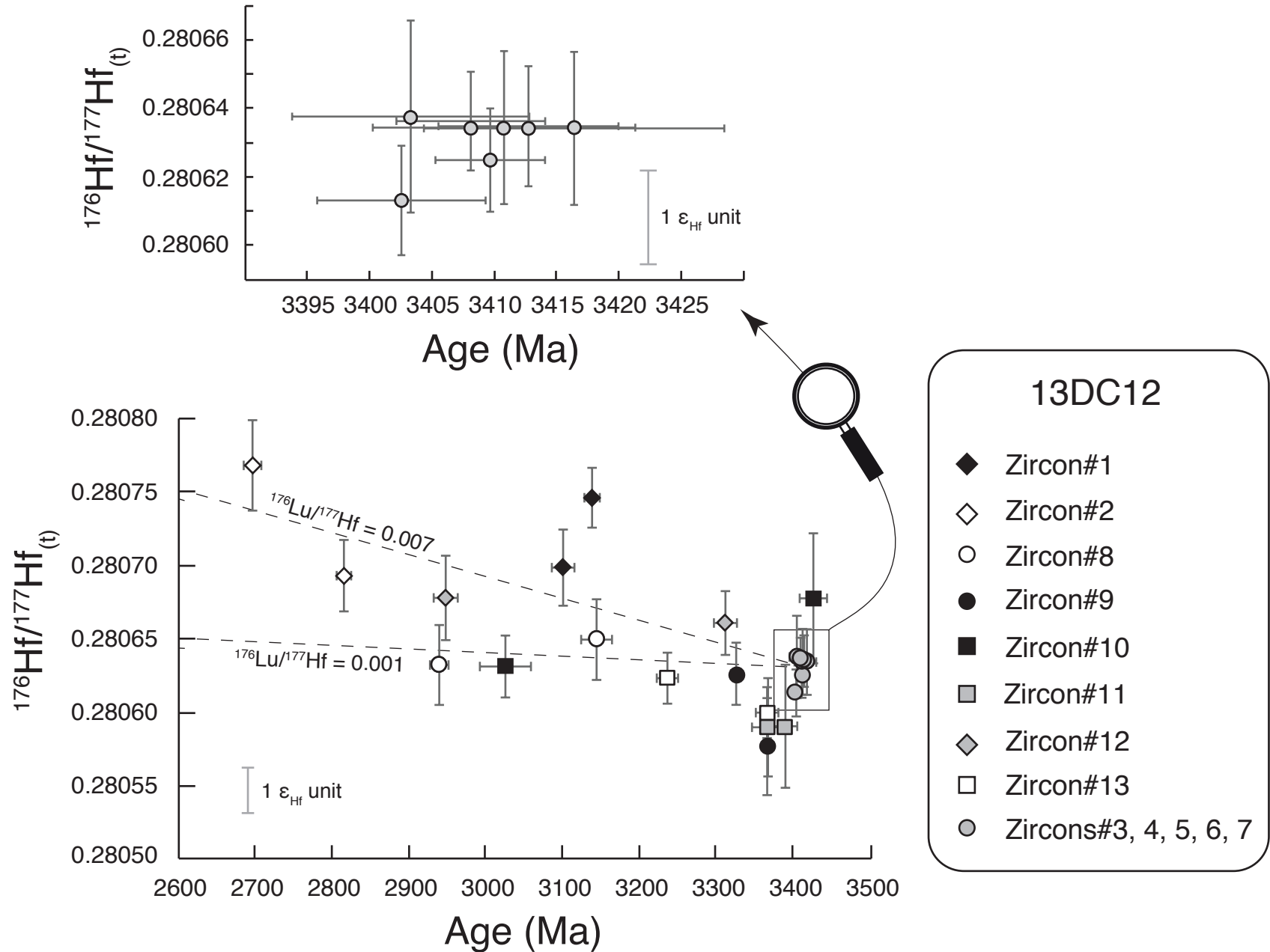


Figure 4

Figure 5





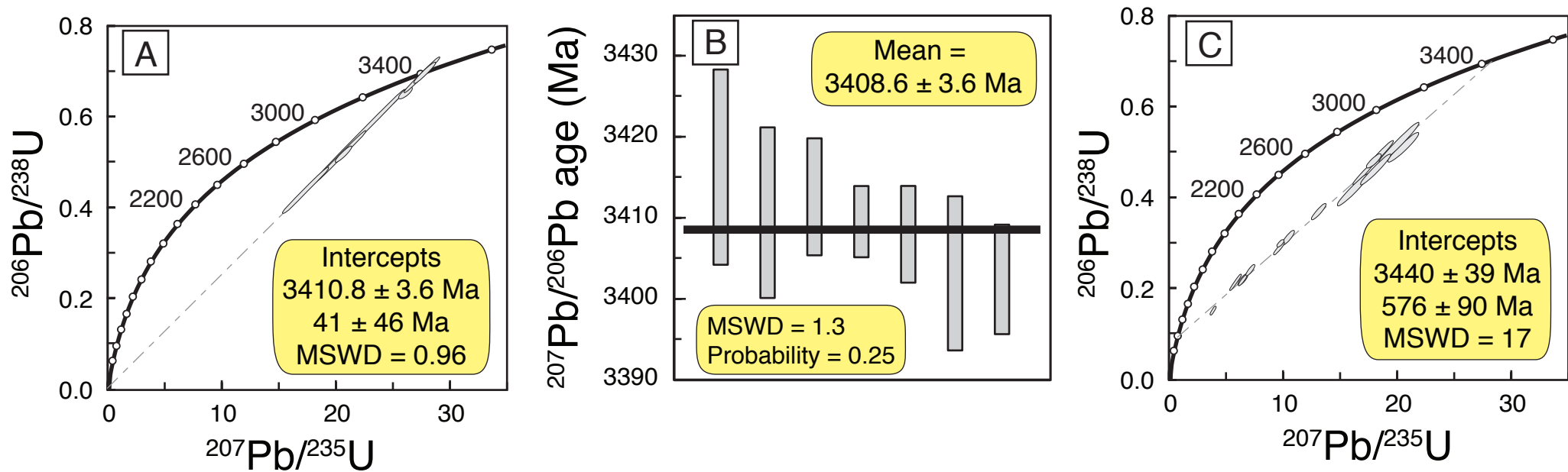


Figure 6

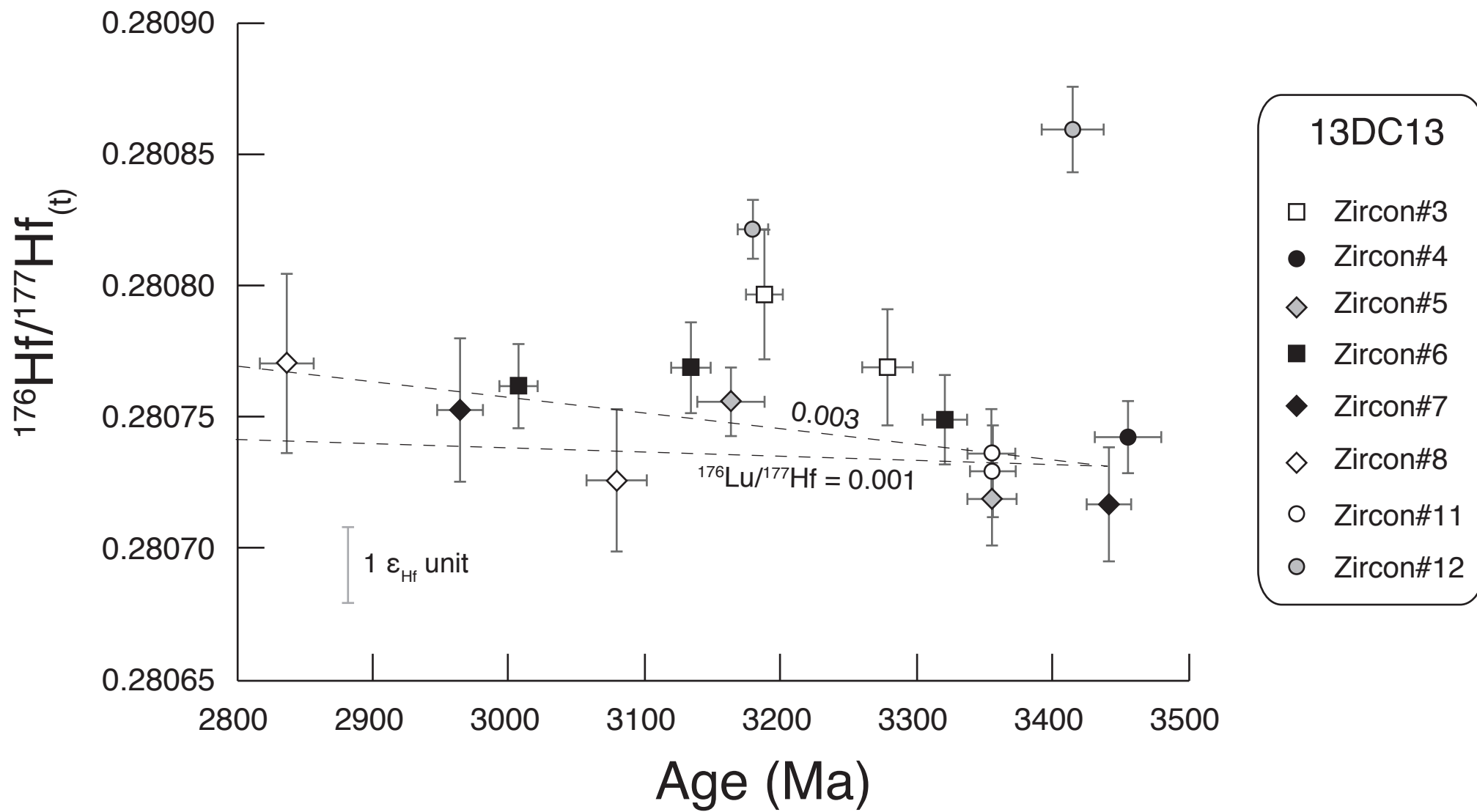


Figure 7

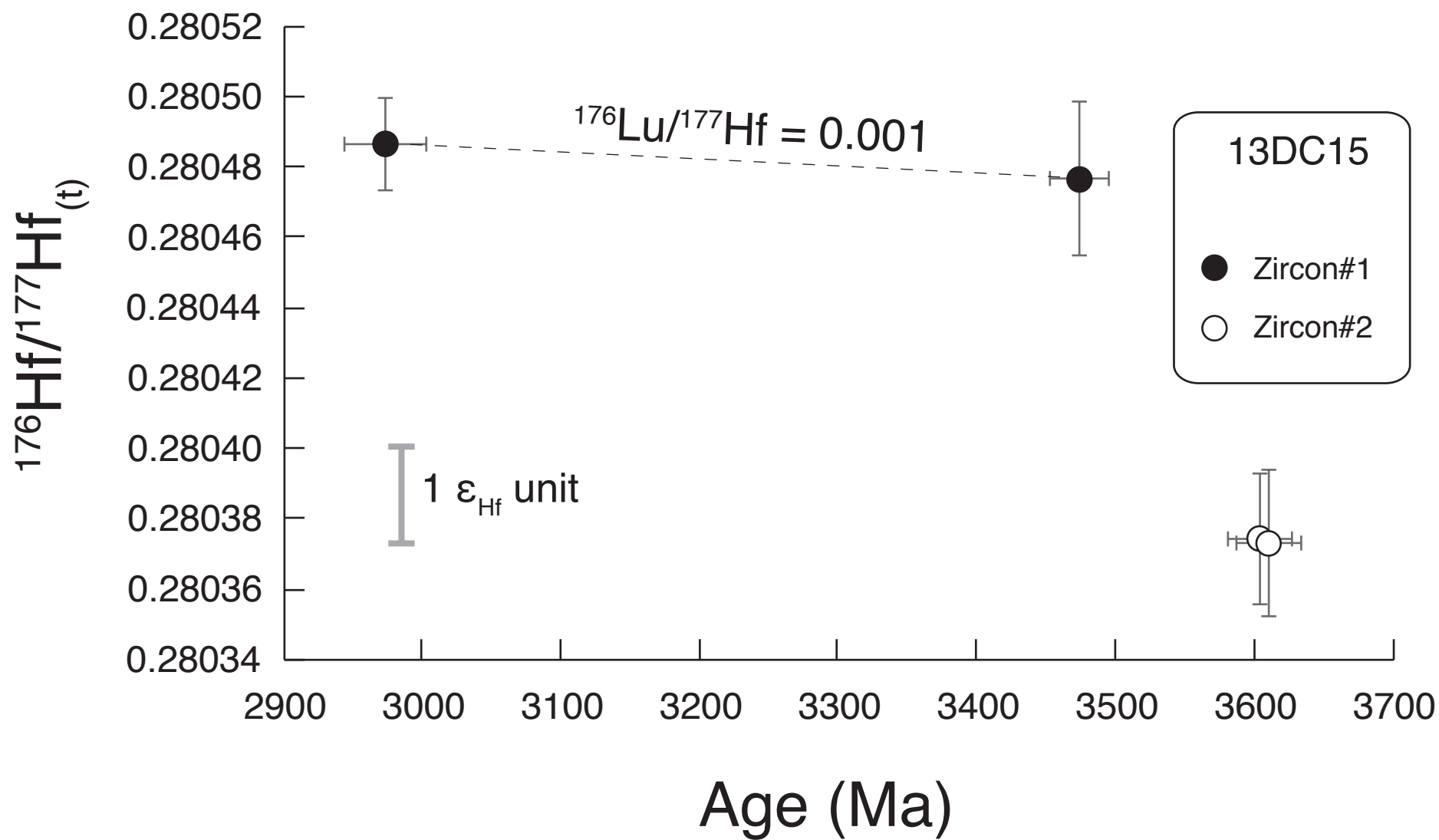


Figure 8



Figure 9

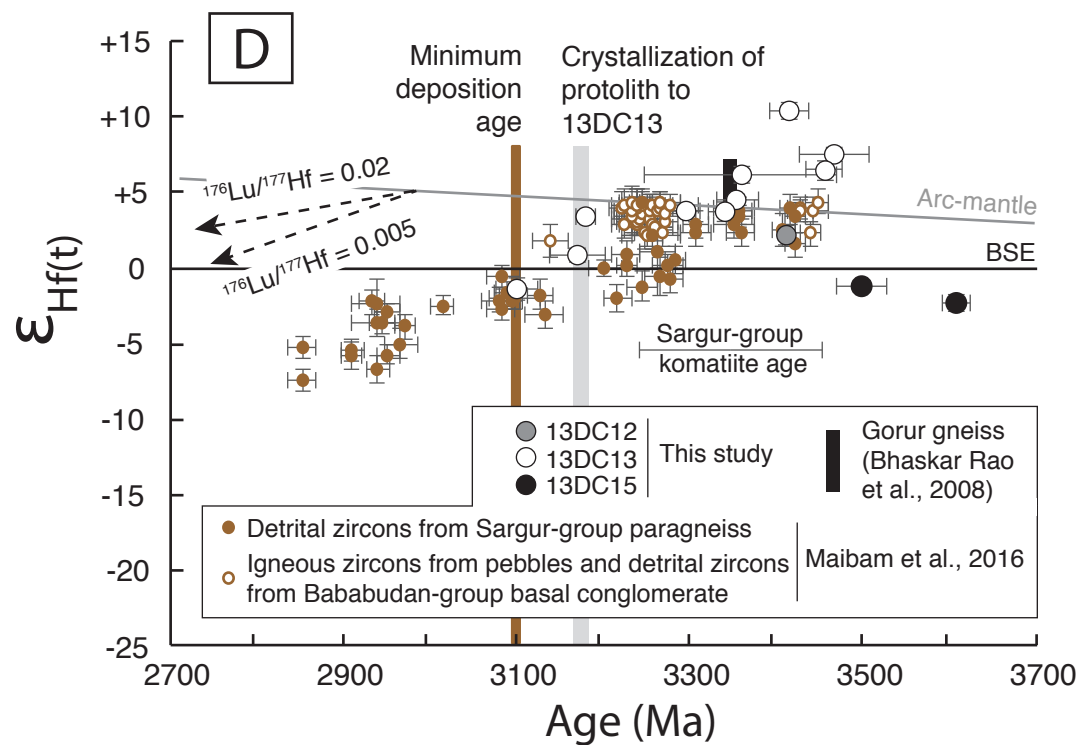
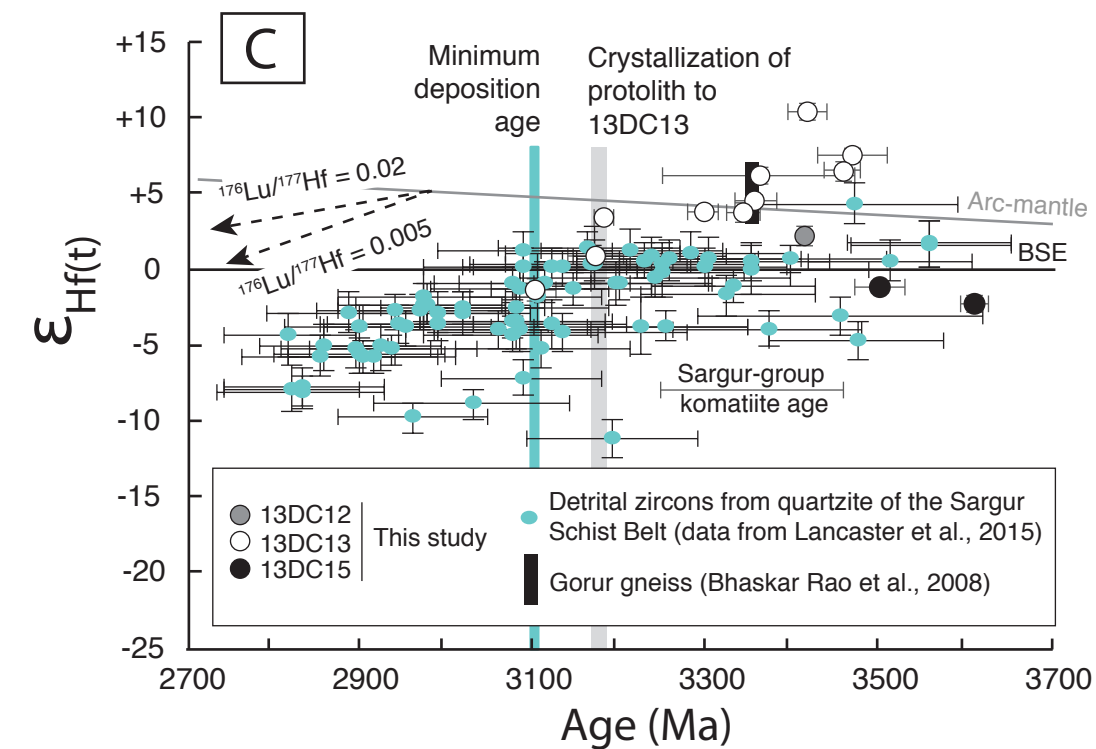
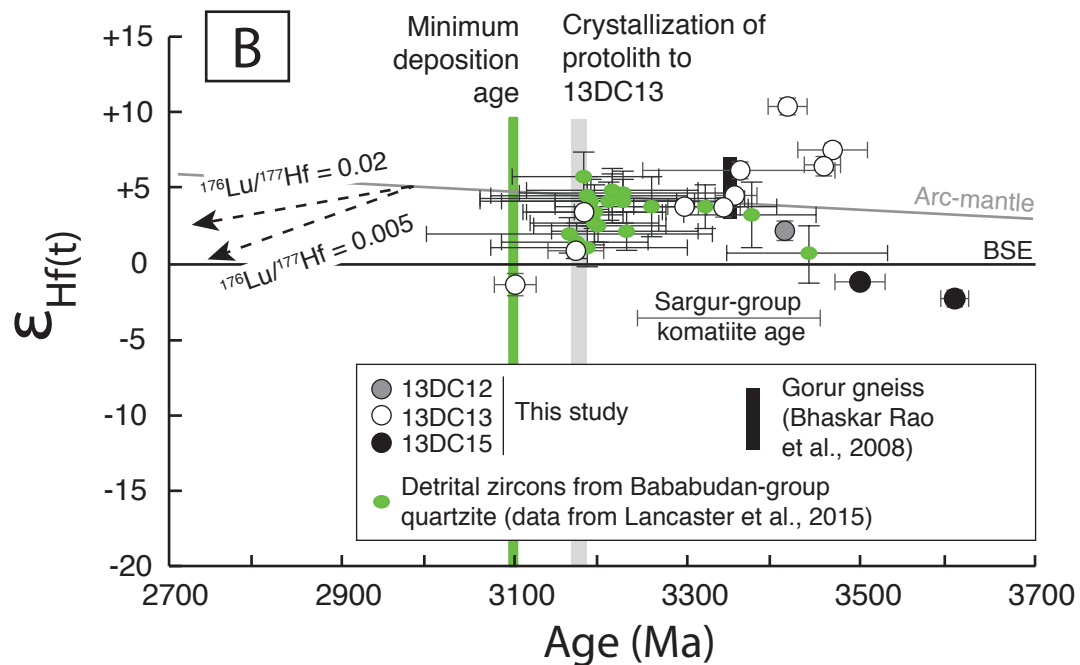
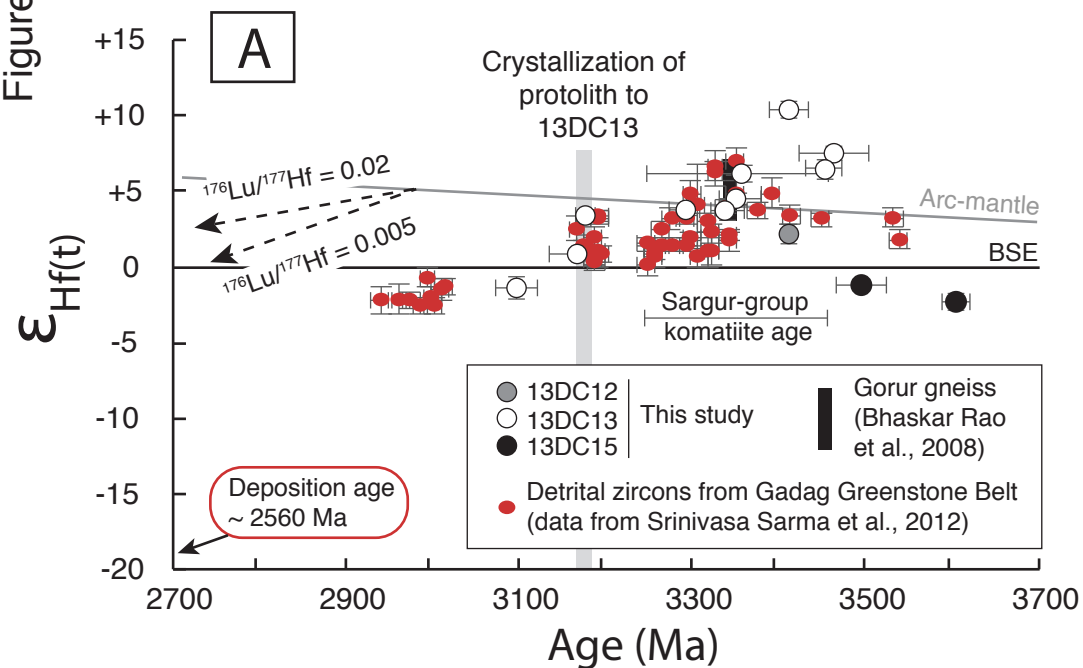


Table 1. Summary of the Archean geology of the Western Dharwar craton after Naqvi and Rogers (1987), Yoshida et al. (1994), Naqvi et al. (2009), and Dey (2013)

| Supracrustal rocks  | Granitic rocks                                     | Lithologies   | Additional information  |
|---|--|---|---|
|   | <b>Closepet granite<br/>(~2500 to ~2600 Ma)</b>    | K-rich granite  |   |
| <b>Dharwar Supergroup<br/>(~2500 to ~2900 Ma)</b>                   |  |   |   |
| <b>Chitradurga group</b><br>-----Unconformity-----<br>-             |  | Conglomerate, quartzite, greywacke, pelite, BIF, basalt                             | Oldest reported detrital zircon in Gadag greenstone belt: $3542 \pm 9$ Ma (Sarma et al., 2012)  |
| <b>Bababudan group (3.2-3.0 Ga?)</b><br>-----Unconformity-----<br>- |  | Conglomerate, quartzite, basalt, BIF  | Oldest reported detrital zircon: $3634 \pm 10$ Ma (Bhaskar Rao et al., 2008)  |
|   | <b>Diapiric bodies<br/>(~3100 to ~3200 Ma)</b>     | Trondhjemite (Halekote) and granite/granodiorite (Chikmagalur)                      | Contains remnants of older greenstones and basement gneisses (e.g., Meen et al., 1992; Jayananda et al., 2015; this study). Inherited igneous zircon: $3607 \pm 16$ Ma (this study)   |
| <b>Sargur group<br/>(~3000 to ~3400 Ma)</b>                         |  | Quartzite, pelite, calc-silicate, basalt, komatiite, BIF, layered mafic-ultramafics | Oldest age of $3352 \pm 110$ Ma from komatiites (Jayananda et al., 2008). Detrital zircons indicate a range from 3580 to 3130 Ma (Nutman et al., 1992). Lancaster et al. (2015) reported an oldest detrital zircon age of $3555 \pm 95$ Ma. |
|   | <b>Peninsular gneisses<br/>(~3200 to ~3400 Ma)</b> | Tonalite-trondhjemite-granodiorite and granite                                      | Oldest generations: $3342 \pm 6$ Ma (Gorur gneiss; Beckinsale et al., 1980; Jayananda et al., 2015), $3350 \pm 9$ Ma (Chikmagalur gneiss; Jayananda et al., 2015), and $3410.8 \pm 3.6$ Ma (this study)                                     |
|   | <b>Older basement<br/>( up to ~3600 Ma)</b>        | TTG?  | Existence inferred from detrital and inherited zircons (e.g., Nutman et al., 1992; Bhaskar Rao et al., 2008; Lancaster et al., 2015; this study)  |

Table 2. Sample locations and petrographic details of the samples analyzed in this study

| Sample name | Locality                      | GPS Coordinates |              | Rock type                     |
|-------------|-------------------------------|-----------------|--------------|-------------------------------|
| 13DC12      | Near Byadarahalli (Karnataka) | N12°52.463'     | E076°05.686' | Granitic gneiss               |
| 13DC13      | Near Javenahalli (Karnataka)  | N12°55.461'     | E076°04.809' | Trondhjemitic gneiss          |
| 13DC15      | Near Javenahalli (Karnataka)  | N12°55.461'     | E076°04.809' | Bt-rich enclave within 13DC13 |

\* Qz is for quartz, Plg for plagioclase, K-Feld for alkali feldspar, Bt for biotite, Msc for muscovite, Op for opaque pha

|                   |
|-------------------|
| <b>Mineralogy</b> |
|-------------------|

Qz, Plg, K-Feld, Bt, Msc, ± Op

Qz, Plg, K-Feld, Bt, Msc, ± Op

Bt, Qz, Plg, ± K-Feld, ± Msc, ± Chl

ases, and Chl for chlorite

Table 3. Summary of U-Pb and Lu-Hf isotope results for Indian zircons analyzed by LA-ICP-MS

| Sample               | U     | Th   | Pb   | Th/U <sub>c</sub> | Age (Ma) | 2σ | Disc. | <sup>176</sup> Hf/ <sup>177</sup> Hf | 2 σ                  | <sup>176</sup> Lu/ <sup>177</sup> Hf |
|----------------------|-------|------|------|-------------------|----------|----|-------|--------------------------------------|----------------------|--------------------------------------|
|                      | (ppm) |      |      |                   | (Ma)     |    |       |                                      | (x10 <sup>-6</sup> ) |                                      |
| Granitic gneiss      |       |      |      |                   |          |    |       |                                      |                      |                                      |
| 13DC12_1a            | 1334  | 257  | 561  | 0.41              | 3137     | 10 | 54%   | 0.281023                             | 18                   | 0.00460                              |
| 13DC12_1b            | 1691  | 394  | 751  | 0.44              | 3100     | 15 | 51%   | 0.280990                             | 22                   | 0.00489                              |
| 13DC12_2a            | 2837  | 1205 | 763  | 0.49              | 2696     | 11 | 71%   | 0.281124                             | 29                   | 0.00689                              |
| 13DC12_2b            | 2072  | 1762 | 720  | 0.61              | 2815     | 9  | 61%   | 0.280890                             | 23                   | 0.00365                              |
| 13DC12_3_1           | 538   | 201  | 442  | 0.51              | 3411     | 11 | 26%   | 0.280772                             | 21                   | 0.00209                              |
| 13DC12_3_2           | 260   | 119  | 292  | 0.61              | 3416     | 12 | 7%    | 0.280772                             | 21                   | 0.00209                              |
| 13DC12_4             | 253   | 48   | 230  | 0.39              | 3403     | 7  | 18%   | 0.280723                             | 15                   | 0.00167                              |
| 13DC12_5a            | 262   | 80   | 270  | 0.30              | 3413     | 7  | 0%    | 0.280757                             | 16                   | 0.00186                              |
| 13DC12_5b            | 302   | 99   | 311  | 0.30              | 3410     | 4  | 1%    | 0.280734                             | 14                   | 0.00165                              |
| 13DC12_6             | 1277  | 1155 | 994  | 0.63              | 3403     | 10 | 37%   | 0.280875                             | 24                   | 0.00361                              |
| 13DC12_7             | 471   | 631  | 504  | 0.99              | 3408     | 6  | 26%   | 0.280766                             | 12                   | 0.00198                              |
| 13DC12_8a            | 2849  | 1454 | 1027 | 0.71              | 2939     | 12 | 62%   | 0.280855                             | 25                   | 0.00394                              |
| 13DC12_8b            | 1352  | 463  | 640  | 0.46              | 3143     | 20 | 50%   | 0.281032                             | 24                   | 0.00633                              |
| 13DC12_9a            | 615   | 660  | 498  | 0.63              | 3324     | 7  | 33%   | 0.280767                             | 19                   | 0.00219                              |
| 13DC12_9b            | 456   | 284  | 462  | 0.48              | 3365     | 6  | 11%   | 0.280685                             | 32                   | 0.00167                              |
| 13DC12_10a           | 581   | 483  | 519  | 0.74              | 3425     | 18 | 25%   | 0.280884                             | 43                   | 0.00313                              |
| 13DC12_10b           | 1523  | 1530 | 550  | 0.56              | 3024     | 33 | 63%   | 0.280816                             | 20                   | 0.00317                              |
| 13DC12_11a           | 1088  | 827  | 856  | 0.63              | 3388     | 15 | 33%   | 0.280869                             | 36                   | 0.00426                              |
| 13DC12_11b           | 1060  | 802  | 805  | 0.66              | 3366     | 21 | 39%   | 0.280766                             | 30                   | 0.00272                              |
| 13DC12_12a           | 1328  | 1141 | 554  | 0.83              | 2947     | 16 | 58%   | 0.280886                             | 25                   | 0.00369                              |
| 13DC12_12b           | 1958  | 3334 | 742  | 0.13              | 3310     | 15 | 28%   | 0.280833                             | 15                   | 0.00271                              |
| 13DC12_13a           | 640   | 201  | 374  | 0.37              | 3235     | 14 | 43%   | 0.280733                             | 15                   | 0.00177                              |
| 13DC12_13b           | 271   | 86   | 218  | 0.52              | 3365     | 15 | 24%   | 0.280739                             | 13                   | 0.00214                              |
| Trondhjemitic gneiss |       |      |      |                   |          |    |       |                                      |                      |                                      |
| 13DC13_3a            | 348   | 292  | 363  | 1.02              | 3278     | 19 | 6%    | 0.280841                             | 20                   | 0.00114                              |
| 13DC13_3b            | 341   | 314  | 318  | 1.02              | 3187     | 14 | 10%   | 0.280885                             | 24                   | 0.00143                              |
| 13DC13_4_1           | 512   | 27   | 455  | 0.22              | 3424     | 17 | 10%   | 0.280856                             | 12                   | 0.00170                              |
| 13DC13_4_2           | 538   | 381  | 601  | 0.53              | 3455     | 24 | 3%    | 0.280856                             | 12                   | 0.00170                              |
| 13DC13_5a_1          | 2772  | 123  | 2057 | 0.11              | 3116     | 25 | 14%   | 0.280873                             | 11                   | 0.00191                              |
| 13DC13_5a_2          | 3668  | 459  | 3205 | 0.14              | 3163     | 25 | 2%    | 0.280873                             | 11                   | 0.00191                              |
| 13DC13_5b_1          | 1395  | 80   | 1044 | 0.08              | 3276     | 15 | 24%   | 0.280837                             | 16                   | 0.00182                              |
| 13DC13_5b_2          | 680   | 28   | 694  | 0.05              | 3355     | 18 | -7%   | 0.280837                             | 16                   | 0.00182                              |
| 13DC13_6a            | 1380  | 25   | 700  | 0.02              | 3133     | 15 | 40%   | 0.280893                             | 16                   | 0.00206                              |
| 13DC13_6b            | 122   | 83   | 154  | 0.58              | 3320     | 16 | -14%  | 0.280856                             | 15                   | 0.00167                              |
| 13DC13_6c            | 2410  | 55   | 933  | 0.03              | 3007     | 14 | 52%   | 0.280926                             | 14                   | 0.00284                              |
| 13DC13_7a            | 2222  | 342  | 801  | 0.11              | 2964     | 17 | 54%   | 0.280899                             | 26                   | 0.00256                              |
| 13DC13_7b            | 576   | 512  | 633  | 0.66              | 3441     | 16 | 5%    | 0.280948                             | 18                   | 0.00348                              |
| 13DC13_8a            | 2097  | 560  | 497  | 1.22              | 2836     | 20 | 80%   | 0.280872                             | 33                   | 0.00186                              |
| 13DC13_8b            | 615   | 259  | 268  | 1.21              | 3079     | 22 | 29%   | 0.280836                             | 26                   | 0.00186                              |
| 13DC13_11a           | 265   | 170  | 254  | 0.79              | 3354     | 18 | 14%   | 0.280888                             | 15                   | 0.00234                              |
| 13DC13_11b           | 225   | 156  | 234  | 0.82              | 3356     | 17 | 5%    | 0.280912                             | 16                   | 0.00283                              |
| 13DC13_12a           | 291   | 101  | 299  | 0.32              | 3414     | 23 | 0%    | 0.280929                             | 15                   | 0.00105                              |
| 13DC13_12b           | 232   | 12   | 191  | 0.05              | 3179     | 11 | 3%    | 0.280864                             | 9                    | 0.00069                              |
| Biotite-rich enclave |       |      |      |                   |          |    |       |                                      |                      |                                      |
| 13DC15_1a            | 241   | 75   | 240  | 0.43              | 3473     | 21 | 2%    | 0.280571                             | 21                   | 0.00140                              |
| 13DC15_1b            | 494   | 86   | 314  | 0.18              | 2973     | 30 | 23%   | 0.280548                             | 11                   | 0.00108                              |
| 13DC15_2a            | 293   | 177  | 320  | 0.47              | 3603     | 23 | 9%    | 0.280450                             | 17                   | 0.00109                              |
| 13DC15_2b            | 315   | 191  | 336  | 0.54              | 3610     | 23 | 11%   | 0.280475                             | 20                   | 0.00146                              |

# S and LA-MC-ICP-MS

| 2 $\sigma$<br>( $\times 10^{-5}$ ) | $^{176}\text{Hf}/^{177}\text{Hf}_{\text{in}}$ | 2 $\sigma$<br>( $\times 10^{-6}$ ) | $\varepsilon_{\text{Hf in}}$ | 2 $\sigma$ |
|------------------------------------|---|------------------------------------|------------------------------|------------|
|------------------------------------|---|------------------------------------|------------------------------|------------|

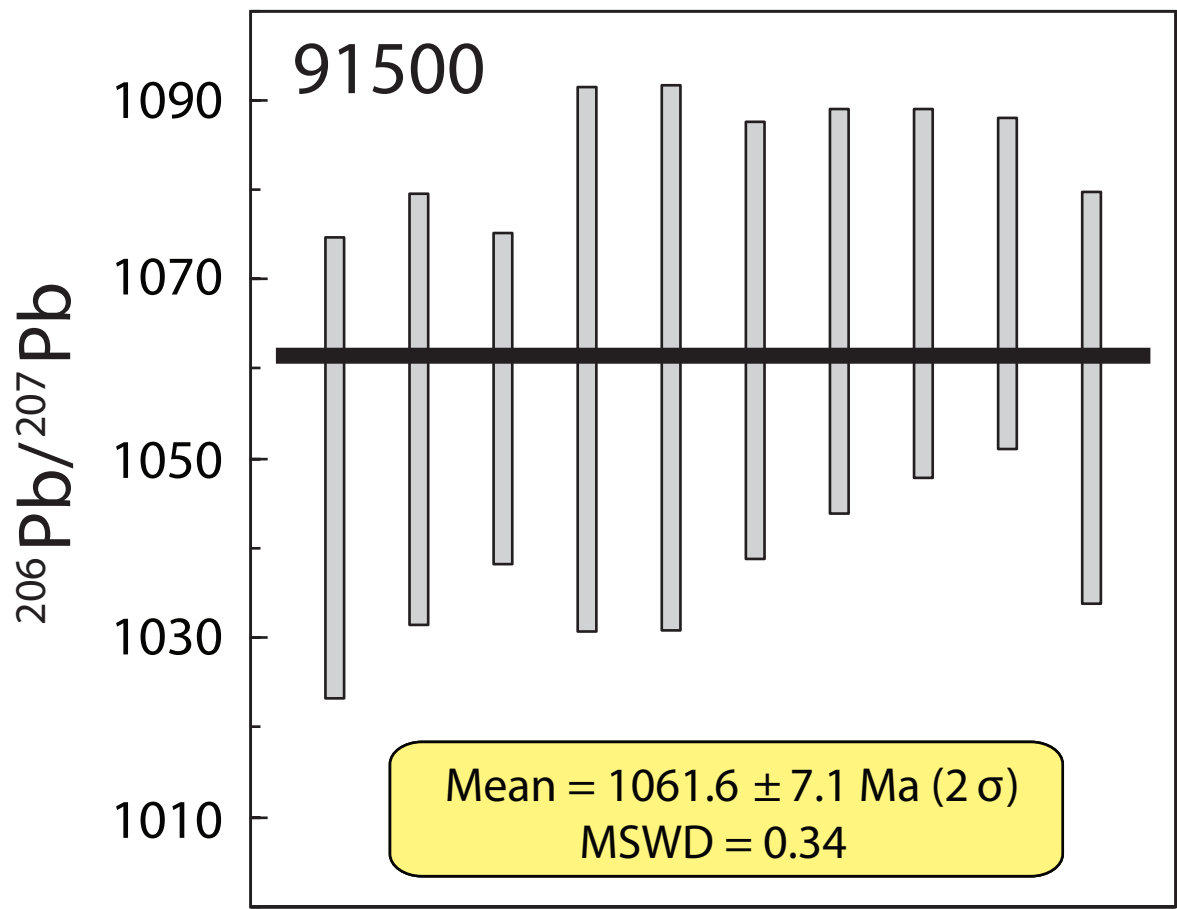
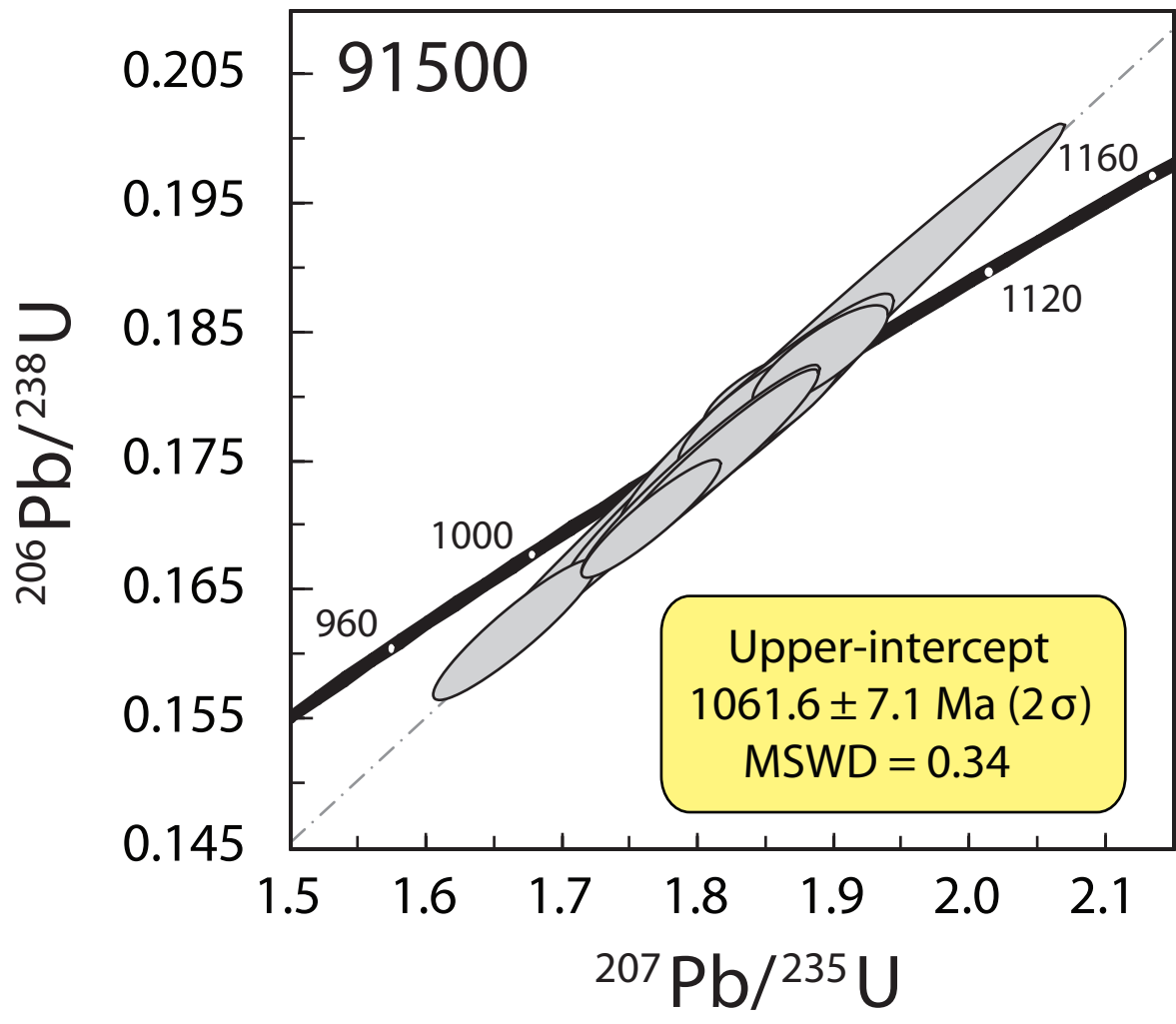
|    |          |          |     |
|----|----------|----------|-----|
| 13 | 0.280746 | 20 -0.3  | 0.7 |
| 21 | 0.280699 | 26 -2.9  | 0.9 |
| 14 | 0.280768 | 31 -10   | 1.1 |
| 8  | 0.280693 | 24 -9.8  | 0.9 |
| 9  | 0.280635 | 22 +2.3  | 0.8 |
| 9  | 0.280634 | 22 +2.4  | 0.8 |
| 5  | 0.280613 | 16 +1.3  | 0.6 |
| 7  | 0.280635 | 18 +2.3  | 0.6 |
| 3  | 0.280625 | 15 +1.9  | 0.5 |
| 20 | 0.280638 | 28 +2.2  | 1.0 |
| 9  | 0.280636 | 14 +2.3  | 0.5 |
| 14 | 0.280632 | 27 -9.1  | 1.0 |
| 21 | 0.280650 | 27 -3.6  | 1.0 |
| 12 | 0.280626 | 21 -0.1  | 0.8 |
| 5  | 0.280577 | 33 -0.9  | 1.2 |
| 10 | 0.280678 | 44 +4.1  | 1.6 |
| 6  | 0.280631 | 21 -7.1  | 0.8 |
| 31 | 0.280591 | 42 +0.2  | 1.5 |
| 20 | 0.280590 | 33 -0.4  | 1.2 |
| 23 | 0.280678 | 29 -7.2  | 1.0 |
| 23 | 0.280661 | 22 +0.8  | 0.8 |
| 10 | 0.280623 | 17 -2.3  | 0.6 |
| 15 | 0.280600 | 17 -0.1  | 0.6 |
| 9  | 0.280769 | 22 +3.9  | 0.8 |
| 6  | 0.280797 | 25 +2.7  | 0.9 |
| 6  | 0.280744 | 14 +6.5  | 0.5 |
| 6  | 0.280743 | 14 +7.2  | 0.5 |
| 4  | 0.280758 | 13 -0.4  | 0.5 |
| 4  | 0.280756 | 13 +0.7  | 0.5 |
| 7  | 0.280722 | 18 +2.2  | 0.6 |
| 7  | 0.280719 | 18 +4.0  | 0.6 |
| 4  | 0.280769 | 17 +0.4  | 0.6 |
| 6  | 0.280749 | 17 +4.2  | 0.6 |
| 7  | 0.280762 | 16 -2.8  | 0.6 |
| 13 | 0.280753 | 27 -4.2  | 1.0 |
| 17 | 0.280717 | 22 +5.9  | 0.8 |
| 7  | 0.280771 | 34 -6.6  | 1.2 |
| 7  | 0.280726 | 27 -2.4  | 1.0 |
| 7  | 0.280736 | 17 +4.6  | 0.6 |
| 7  | 0.280730 | 17 +4.3  | 0.6 |
| 3  | 0.280860 | 16 +10.4 | 0.6 |
| 3  | 0.280822 | 11 +3.4  | 0.4 |
| 6  | 0.280477 | 22 -1.8  | 0.8 |
| 2  | 0.280487 | 13 -13.4 | 0.5 |
| 9  | 0.280374 | 19 -2.4  | 0.7 |
| 4  | 0.280373 | 21 -2.3  | 0.7 |

Table 4. Interpreted U-Pb ages and Lu-Hf isotope systematics for Indian zircons analyzed here

| Sample                               | Age (Ma) | 2 $\sigma$ | $^{176}\text{Hf}/^{177}\text{Hf}_{\text{in}}$ | 2 $\sigma$ | $\epsilon_{\text{Hf in}}$ | 2 $\sigma$ |
|--------------------------------------|----------|------------|---|------------|---------------------------|------------|
| <b>Granitic gneiss (13DC12)</b>      | 3410.8   | 3.6        | 0.280631                                      | 0.000018   | +2.2                      | 0.6        |
| <b>Trondhjemitic gneiss (13DC13)</b> |          |            |   |            |                           |            |
| Zircon #4 (group 1)                  | 3468     | 41         | 0.280742                                      | 0.000014   | +7.5                      | 0.5        |
| Zircon #7 (group 1)                  | 3456     | 20         | 0.280721                                      | 0.000017   | +6.4                      | 0.6        |
| Zircon #12a (group 1)                | 3414     | 23         | 0.280860                                      | 0.000016   | +10.4                     | 0.6        |
| Zircon #3 (group 2)                  | 3359     | 110        | 0.280778                                      | 0.000016   | +6.1                      | 0.6        |
| Zircon #11 (group 2)                 | 3356     | 25         | 0.280733                                      | 0.000012   | +4.5                      | 0.4        |
| Zircon #5b (group 2)                 | 3342     | 19         | 0.280720                                      | 0.000018   | +3.7                      | 0.6        |
| Zircon #6 (group 3)                  | 3295     | 18         | 0.280752                                      | 0.000010   | +3.7                      | 0.4        |
| Zircon #5a (group 4)                 | 3170     | 32         | 0.280756                                      | 0.000013   | +0.8                      | 0.5        |
| Zircon #12b (group 4)                | 3179     | 11         | 0.280822                                      | 0.000011   | +3.4                      | 0.4        |
| Zircon #8 (group 5)                  | 3101     | 25         | 0.280739                                      | 0.000021   | -1.4                      | 0.7        |
| <b>Biotite-rich enclave (13DC15)</b> |          |            |   |            |                           |            |
| Zircon #1                            | 3499     | 29         | 0.280476                                      | 0.000011   | -1.3                      | 0.4        |
| Zircon #2                            | 3607     | 16         | 0.280374                                      | 0.000014   | -2.3                      | 0.5        |

in





Deviation from accepted  $^{176}\text{Hf}/^{177}\text{Hf}_{(t)}$  in epsilon units

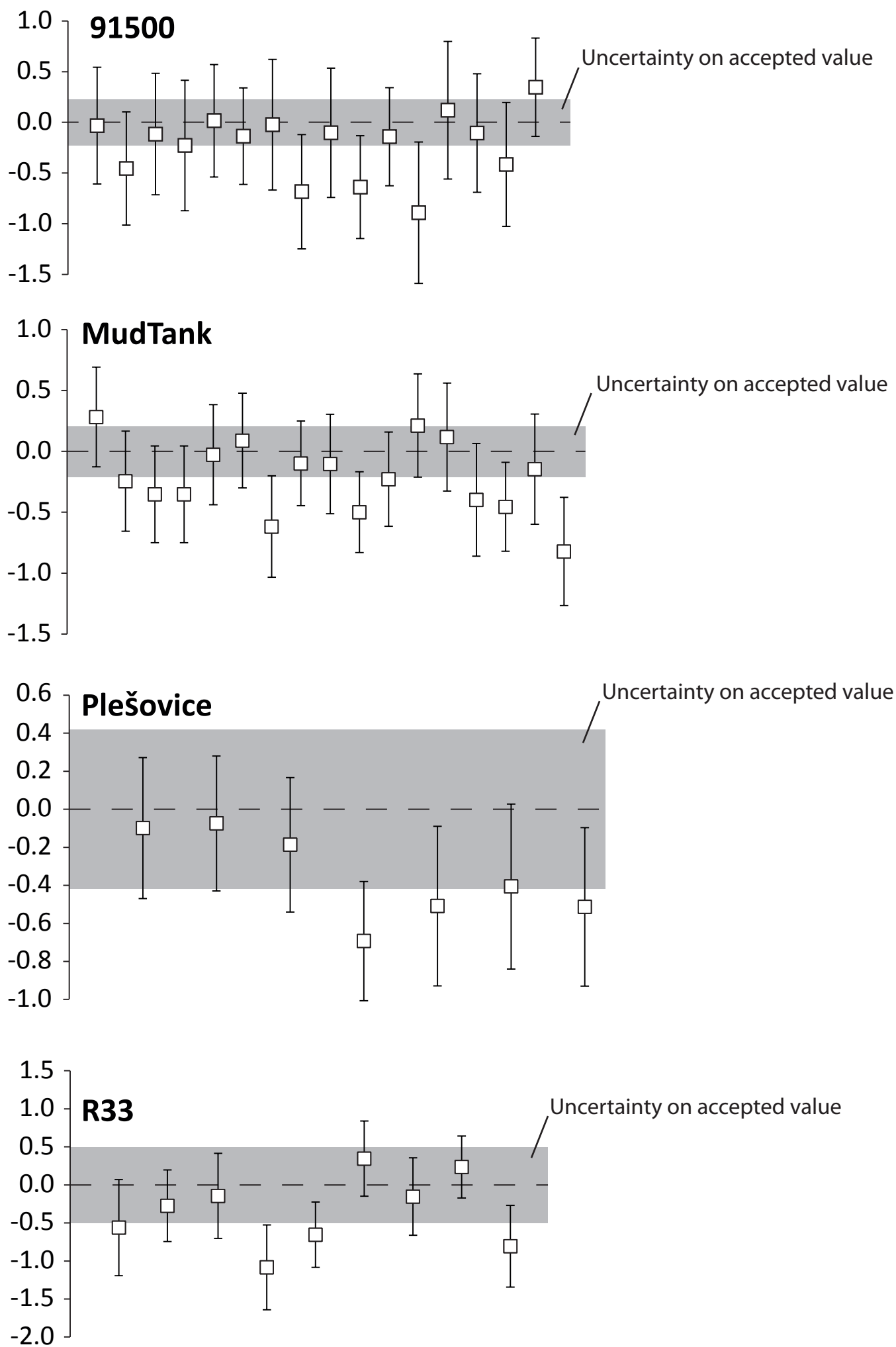


Figure S2

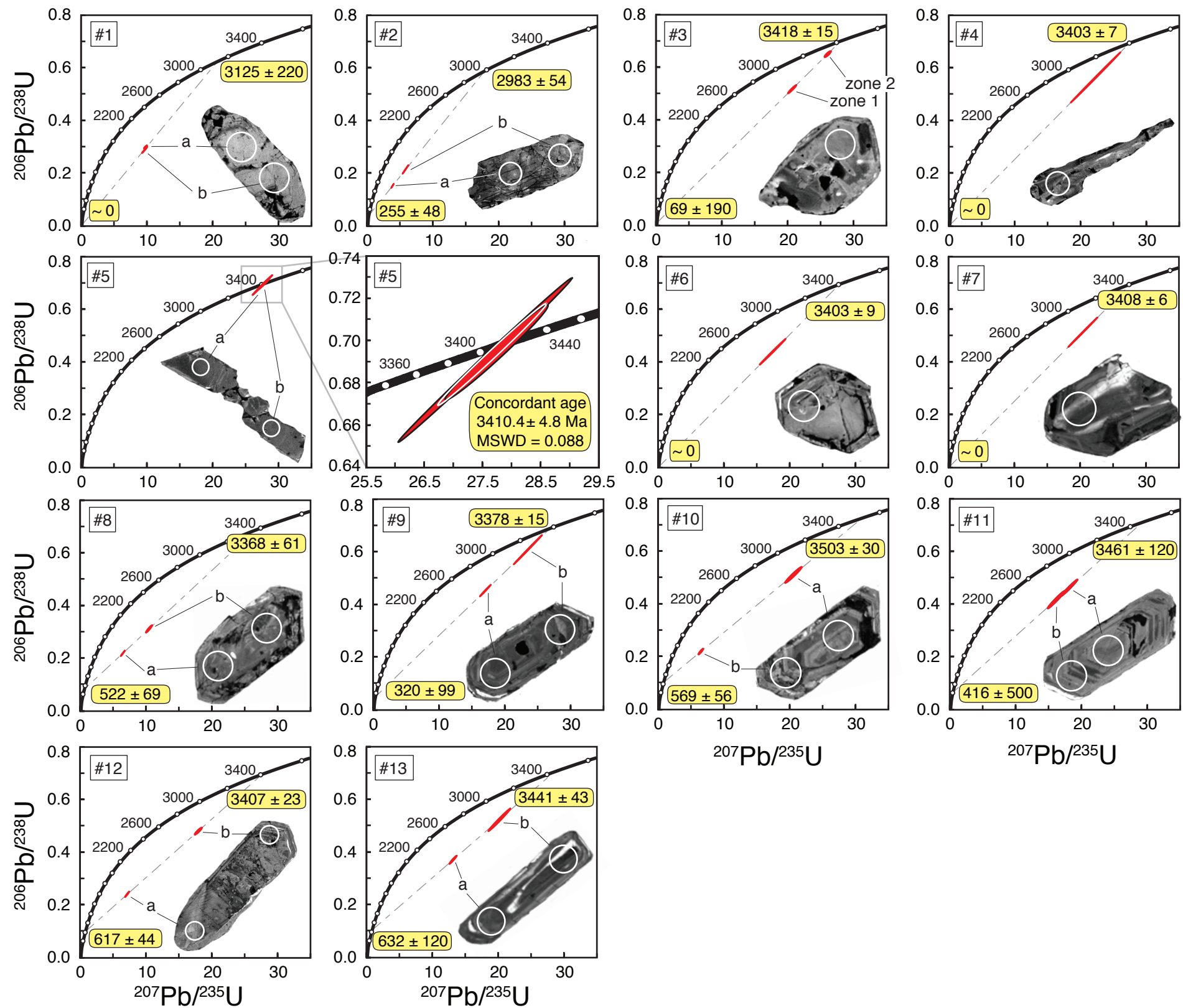


Figure S3

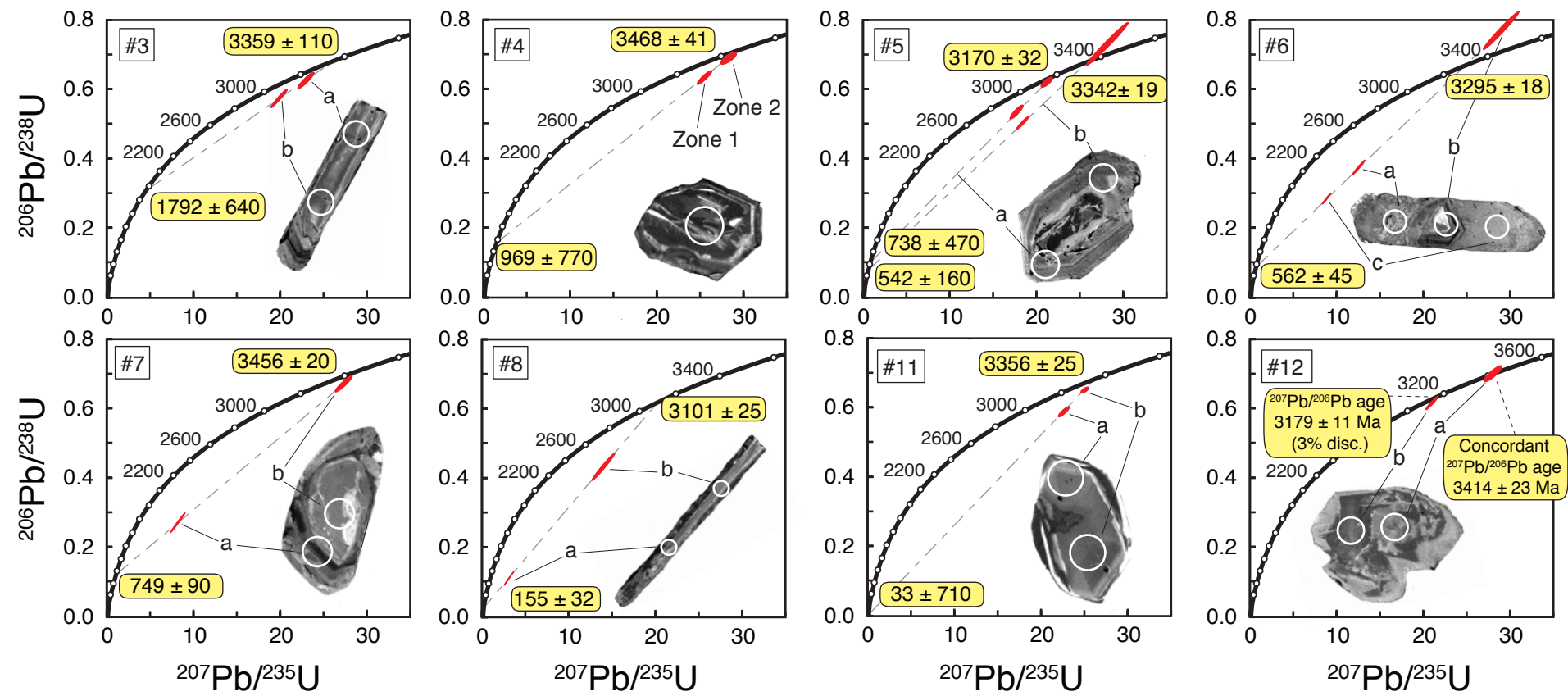


Figure S4

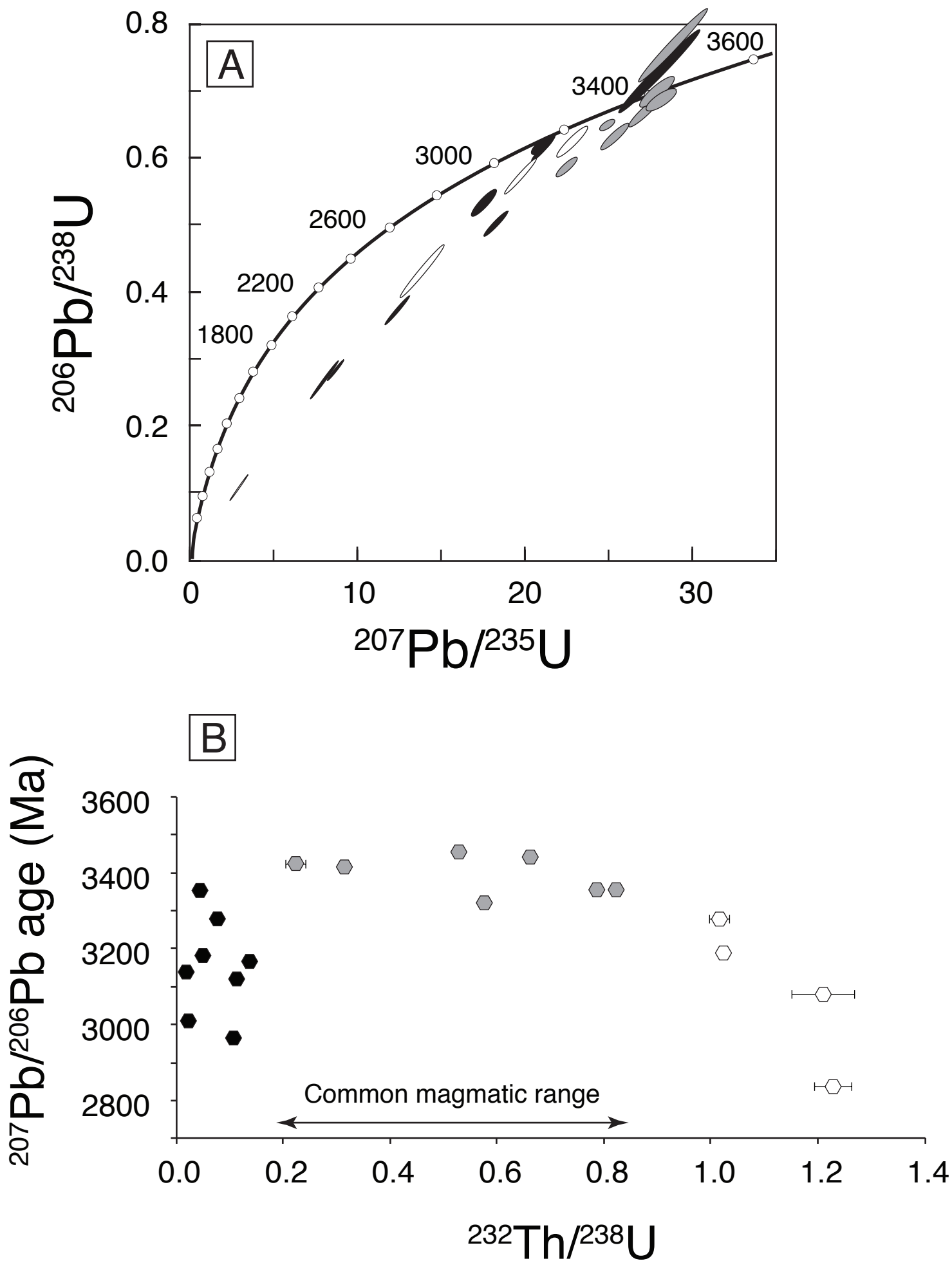


Figure S5

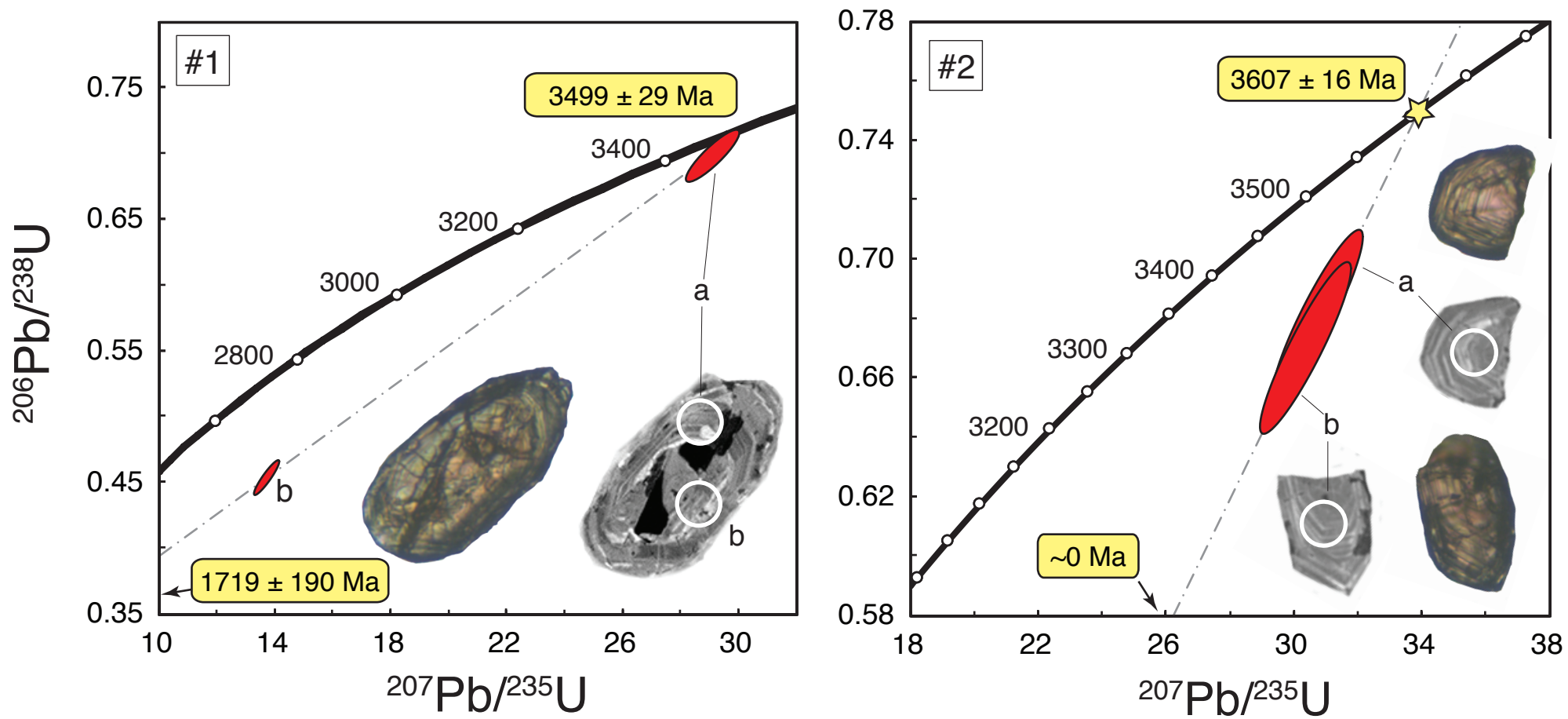


Figure S6

Table S1. Major and minor oxide abundances for the orthogneisses analyzed in this study

|                                | 13DC12 | 13DC13 |
|--------------------------------|--------|--------|
| SiO <sub>2</sub>               | 74.01  | 72.57  |
| TiO <sub>2</sub>               | 0.11   | 0.27   |
| Al <sub>2</sub> O <sub>3</sub> | 13.85  | 15.04  |
| Fe <sub>2</sub> O <sub>3</sub> | 1.47   | 1.69   |
| MnO                            | 0.02   | 0.02   |
| MgO                            | 0.19   | 0.50   |
| CaO                            | 0.95   | 1.82   |
| Na <sub>2</sub> O              | 3.94   | 4.89   |
| K <sub>2</sub> O               | 4.31   | 2.54   |
| P <sub>2</sub> O <sub>5</sub>  | 0.11   | 0.08   |
| Ba                             | 0.048  | 0.051  |
| Sr                             | 0.009  | 0.041  |
| L.O.I.                         | 0.83   | 0.55   |
| Total                          | 99.85  | 100.06 |
| Or                             | 0.41   | 0.24   |
| Ab                             | 0.53   | 0.64   |
| An                             | 0.06   | 0.12   |
| A/(CNK)                        | 1.1    | 1.1    |
| A/(NK)                         | 1.2    | 1.4    |

Table S2. LA-ICP-MS and LA-MC-ICP-MS operating conditions

| <b>Analysis</b>          | <i>U-Pb geochronology</i>   | <i>Lu-Hf isotope system</i>     |
|--------------------------|-----------------------------|---------------------------------|
| <b>Laboratory</b>        | University of New Hampshire | Université Blaise Pascal        |
| ICP-MS model             | Nu Instruments AttoM        | Thermo Neptune +                |
| Forward Power            | 1300 W                      | 1200 W                          |
| Auxiliary gas (Ar)       | ~0.8 l/min                  | 0.66 l/min                      |
| Ar sample                | ~0.7 l/min                  | 0.86 l/min                      |
| Oxide ThO/Th             | ~0.5%                       | -                               |
| Additional gas           | -                           | N <sub>2</sub>                  |
| Additional gas flow      | -                           | 4.5 ml/min                      |
| <b>Laser model</b>       | New Wave Research UP-213    | Resonetics Resolution M-50      |
| Wavelength               | 213 nm                      | 193 nm                          |
| Pulse duration           | <4 ns                       | <4 ns                           |
| Energy                   | 50% / ~0.07 mJ              | ~3.2 mJ                         |
| Fluence                  | 9-10 J/cm <sup>2</sup>      | ~3.8 J/cm <sup>2</sup>          |
| Frequency                | 5 Hz                        | 6 Hz                            |
| Spot size                | 30 µm                       | 40 µm                           |
| Carrier gas              | He                          | He                              |
| Carrier gas flow         | ~0.8 l/min                  | 0.7 l/min                       |
| <b>Data acquisition</b>  |                             | <b>Data acquisition</b>         |
| Protocol                 | Time resolved analysis      | Time resolved analysis          |
| Scanning mode            | Peak-jumping                | Static multi-collection         |
| Dwell time per isotope   | 4 ms                        | 1 s                             |
| Sweeps per cycle         | 10                          | -                               |
| Dead-time correction     | 14 ns                       | -                               |
| Settling time            | 20 µs                       | -                               |
| Background counting time | 30 s                        | 20s                             |
| Sample measurement time  | 60 s                        | 50s                             |
| Measurement type         | Standard bracketing         | Internal normalization          |
| External standard        | AS3, 91500                  | 91500, Mud Tank, Plešovice, R33 |



Table S3. U-Pb isotope results for the zircon standard 91500 analyzed by LA-ICP-MS.

| Sample name  | % $^{206}\text{Pb}_{\text{rad}}$ | <i>Isotope Ratio</i>             |            |                                  |            |
|--------------|----------------------------------|----------------------------------|------------|----------------------------------|------------|
|              |                                  | $^{207}\text{Pb}/^{235}\text{U}$ | 2 $\sigma$ | $^{206}\text{Pb}/^{238}\text{U}$ | 2 $\sigma$ |
| <b>91500</b> |                                  |                                  |            |                                  |            |
| 91500_1      | 99.05                            | 1.666                            | 0.050      | 0.162                            | 0.004      |
| 91500_3      | 99.67                            | 1.765                            | 0.042      | 0.171                            | 0.004      |
| 91500_5      | 99.61                            | 1.792                            | 0.072      | 0.174                            | 0.007      |
| 91500_6      | 99.23                            | 1.813                            | 0.061      | 0.175                            | 0.006      |
| 91500_7      | 99.68                            | 1.890                            | 0.041      | 0.183                            | 0.003      |
| 91500_8      | 98.94                            | 1.802                            | 0.072      | 0.174                            | 0.007      |
| 91500_9      | 98.92                            | 1.847                            | 0.036      | 0.180                            | 0.003      |
| 91500_10     | 99.44                            | 1.847                            | 0.051      | 0.179                            | 0.004      |
| 91500_11     | 99.49                            | 1.843                            | 0.083      | 0.179                            | 0.008      |
| 91500_12     | 99.75                            | 1.846                            | 0.183      | 0.180                            | 0.018      |

| <i>ios</i>                           |     |                                      |     |  |     | <i>Ages (Ma)</i>                    |     |                                     |
|--------------------------------------|-----|--------------------------------------|-----|--|-----|-------------------------------------|-----|-------------------------------------|
| <sup>207</sup> Pb/ <sup>206</sup> Pb | 2 σ | <sup>208</sup> Pb/ <sup>206</sup> Pb | 2 σ | <sup>232</sup> Th/ <sup>238</sup> U <sub>C</sub> | 2 σ | <sup>207</sup> Pb/ <sup>235</sup> U | 2 σ | <sup>206</sup> Pb/ <sup>238</sup> U |

|        |        |        |        |       |       |      |    |      |
|--------|--------|--------|--------|-------|-------|------|----|------|
| 0.0746 | 0.0009 | 0.1099 | 0.0025 | 0.365 | 0.009 | 996  | 19 | 968  |
| 0.0750 | 0.0007 | 0.1112 | 0.0023 | 0.369 | 0.008 | 1033 | 15 | 1016 |
| 0.0746 | 0.0007 | 0.1112 | 0.0020 | 0.369 | 0.008 | 1043 | 26 | 1036 |
| 0.0750 | 0.0008 | 0.1112 | 0.0025 | 0.369 | 0.009 | 1050 | 22 | 1041 |
| 0.0748 | 0.0009 | 0.1112 | 0.0028 | 0.369 | 0.010 | 1077 | 14 | 1084 |
| 0.0749 | 0.0008 | 0.1094 | 0.0030 | 0.363 | 0.011 | 1046 | 26 | 1036 |
| 0.0743 | 0.0010 | 0.1118 | 0.0035 | 0.371 | 0.013 | 1062 | 13 | 1069 |
| 0.0747 | 0.0011 | 0.1106 | 0.0034 | 0.367 | 0.013 | 1062 | 18 | 1063 |
| 0.0747 | 0.0011 | 0.1125 | 0.0042 | 0.373 | 0.015 | 1061 | 29 | 1061 |
| 0.0745 | 0.0009 | 0.1106 | 0.0025 | 0.367 | 0.009 | 1062 | 63 | 1065 |

|                |             |             |
|----------------|-------------|-------------|
| <i>Average</i> | <i>0.37</i> | <i>0.01</i> |
|----------------|-------------|-------------|

|              |              |                                |
|--------------|--------------|--------------------------------|
| <i>0.344</i> | <i>0.001</i> | <i>Wiedenbeck et al., 1995</i> |
| <i>0.38</i>  | <i>0.09</i>  | <i>Wiedenbeck et al., 2004</i> |

| <i>1a)</i>                            |  |            |                    | <i>Semi-quantitative estimates</i> |                   |                    |                    |                    |                   |
|---------------------------------------|--|------------|--------------------|------------------------------------|-------------------|--------------------|--------------------|--------------------|-------------------|
| <b>2 σ</b>                            | <b><sup>207</sup>Pb/<sup>206</sup>Pb</b> | <b>2 σ</b> | <b>Discordance</b> | <b>Pb (ppm)</b>                    | <b>2 σ</b>        | <b>U (ppm)</b>     | <b>2 σ</b>         | <b>Th (ppm)</b>    | <b>2 σ</b>        |
| 25                                    | 1057                                     | 23         | 9%                 | 9.0                                | 2.0               | 42.4               | 9.6                | 13.0               | 1.7               |
| 21                                    | 1070                                     | 18         | 5%                 | 13.2                               | 2.4               | 59.7               | 7.9                | 21.0               | 2.8               |
| 38                                    | 1057                                     | 19         | 2%                 | 19.7                               | 1.7               | 84.5               | 5.8                | 34.6               | 1.1               |
| 31                                    | 1069                                     | 20         | 3%                 | 11.9                               | 0.8               | 52.5               | 6.2                | 16.0               | 0.9               |
| 18                                    | 1063                                     | 24         | -2%                | 17.4                               | 0.9               | 72.1               | 3.3                | 26.8               | 0.8               |
| 37                                    | 1067                                     | 23         | 3%                 | 15.3                               | 2.6               | 68.3               | 10.3               | 21.1               | 2.8               |
| 14                                    | 1049                                     | 26         | -2%                | 13.2                               | 0.9               | 56.4               | 4.1                | 18.6               | 1.1               |
| 23                                    | 1061                                     | 30         | 0%                 | 16.0                               | 2.6               | 70.0               | 10.0               | 21.8               | 2.6               |
| 41                                    | 1061                                     | 30         | 0%                 | 17.2                               | 1.5               | 73.2               | 5.4                | 24.1               | 0.9               |
| 97                                    | 1056                                     | 24         | -1%                | 14.2                               | 3.3               | 61.1               | 11.4               | 18.8               | 1.7               |
| <b><i>Average</i></b>                 |  |            |                    | <b><i>14.4</i></b>                 | <b><i>2.1</i></b> | <b><i>66.3</i></b> | <b><i>7.9</i></b>  | <b><i>23.0</i></b> | <b><i>4.5</i></b> |
|                                       |  |            |                    | <b><i>15.0</i></b>                 | <b><i>4.0</i></b> | <b><i>80.0</i></b> | <b><i>16.0</i></b> | <b><i>29.9</i></b> | <b><i>4.2</i></b> |
| <b><i>Wiedenbeck et al., 2004</i></b> |  |            |                    |                                    |                   |                    |                    |                    |                   |

Table S4. U-Pb isotope results for Indian zircons analyzed by LA-ICP-MS.

|                      |                                    | Isotope Ratios                      |     |                                     |       |                                      |        |
|----------------------|------------------------------------|-------------------------------------|-----|-------------------------------------|-------|--------------------------------------|--------|
| Sample name          | % <sup>206</sup> Pb <sub>rad</sub> | <sup>207</sup> Pb/ <sup>235</sup> U | 2 σ | <sup>206</sup> Pb/ <sup>238</sup> U | 2 σ   | <sup>207</sup> Pb/ <sup>206</sup> Pb | 2 σ    |
| Granitic gneiss      |                                    |                                     |     |                                     |       |                                      |        |
| 13DC12_1a            | 99.3                               | 9.7                                 | 0.3 | 0.289                               | 0.010 | 0.2426                               | 0.0015 |
| 13DC12_1b            | 99.3                               | 9.8                                 | 0.2 | 0.299                               | 0.005 | 0.2369                               | 0.0022 |
| 13DC12_2a            | 99.5                               | 3.9                                 | 0.2 | 0.152                               | 0.006 | 0.1847                               | 0.0013 |
| 13DC12_2b            | 99.2                               | 5.9                                 | 0.4 | 0.214                               | 0.014 | 0.1986                               | 0.0012 |
| 13DC12_3_1           | 99.6                               | 20.7                                | 0.5 | 0.519                               | 0.013 | 0.2887                               | 0.0020 |
| 13DC12_3_2           | 99.6                               | 26.1                                | 0.4 | 0.653                               | 0.009 | 0.2898                               | 0.0023 |
| 13DC12_4             | 99.9                               | 22.5                                | 3.0 | 0.567                               | 0.077 | 0.2872                               | 0.0012 |
| 13DC12_5a            | 99.9                               | 27.7                                | 0.7 | 0.696                               | 0.018 | 0.2891                               | 0.0013 |
| 13DC12_5b            | 99.9                               | 27.5                                | 1.2 | 0.692                               | 0.031 | 0.2885                               | 0.0008 |
| 13DC12_6             | 99.8                               | 17.4                                | 1.6 | 0.439                               | 0.040 | 0.2873                               | 0.0018 |
| 13DC12_7             | 99.9                               | 20.4                                | 1.8 | 0.513                               | 0.046 | 0.2882                               | 0.0011 |
| 13DC12_8a            | 98.1                               | 6.5                                 | 0.3 | 0.219                               | 0.008 | 0.2143                               | 0.0016 |
| 13DC12_8b            | 99.7                               | 10.5                                | 0.4 | 0.312                               | 0.011 | 0.2435                               | 0.0031 |
| 13DC12_9a            | 99.4                               | 17.1                                | 0.7 | 0.453                               | 0.018 | 0.2732                               | 0.0012 |
| 13DC12_9b            | 99.9                               | 23.5                                | 1.8 | 0.608                               | 0.045 | 0.2803                               | 0.0011 |
| 13DC12_10a           | 99.8                               | 21.2                                | 1.1 | 0.527                               | 0.027 | 0.2913                               | 0.0034 |
| 13DC12_10b           | 98.9                               | 7.0                                 | 0.4 | 0.224                               | 0.011 | 0.2261                               | 0.0047 |
| 13DC12_11a           | 99.3                               | 18.1                                | 1.0 | 0.462                               | 0.026 | 0.2846                               | 0.0028 |
| 13DC12_11b           | 99.5                               | 16.2                                | 1.1 | 0.418                               | 0.027 | 0.2805                               | 0.0038 |
| 13DC12_12a           | 99.3                               | 7.2                                 | 0.3 | 0.241                               | 0.009 | 0.2154                               | 0.0021 |
| 13DC12_12b           | 99.8                               | 17.9                                | 0.5 | 0.481                               | 0.011 | 0.2708                               | 0.0026 |
| 13DC12_13a           | 99.5                               | 13.2                                | 0.5 | 0.370                               | 0.013 | 0.2581                               | 0.0023 |
| 13DC12_13b           | 99.9                               | 20.2                                | 1.4 | 0.522                               | 0.035 | 0.2803                               | 0.0026 |
| Trondhjemitic gneiss |                                    |                                     |     |                                     |       |                                      |        |
| 13DC13_3a            | 99.9                               | 22.9                                | 0.7 | 0.625                               | 0.019 | 0.2652                               | 0.0032 |
| 13DC13_3b            | 99.9                               | 19.8                                | 0.8 | 0.573                               | 0.022 | 0.2504                               | 0.0022 |
| 13DC13_4_1           | 99.9                               | 25.4                                | 0.7 | 0.633                               | 0.016 | 0.2911                               | 0.0032 |
| 13DC13_4_2           | 99.9                               | 28.2                                | 0.7 | 0.687                               | 0.014 | 0.2971                               | 0.0047 |
| 13DC13_5a_1          | 99.6                               | 17.6                                | 0.6 | 0.534                               | 0.017 | 0.2394                               | 0.0038 |
| 13DC13_5a_2          | 99.6                               | 21.1                                | 0.5 | 0.620                               | 0.012 | 0.2466                               | 0.0039 |
| 13DC13_5b_1          | 99.8                               | 18.3                                | 0.6 | 0.502                               | 0.016 | 0.2649                               | 0.0025 |
| 13DC13_5b_2          | 99.9                               | 28.1                                | 2.0 | 0.730                               | 0.051 | 0.2786                               | 0.0032 |
| 13DC13_6a            | 99.9                               | 12.5                                | 0.6 | 0.373                               | 0.018 | 0.2420                               | 0.0022 |
| 13DC13_6b            | 99.9                               | 28.9                                | 1.7 | 0.769                               | 0.044 | 0.2725                               | 0.0029 |
| 13DC13_6c            | 99.9                               | 8.8                                 | 0.4 | 0.285                               | 0.013 | 0.2236                               | 0.0020 |
| 13DC13_7a_1          | 99.8                               | 8.1                                 | 0.7 | 0.270                               | 0.023 | 0.2177                               | 0.0023 |
| 13DC13_7b            | 99.9                               | 27.2                                | 0.8 | 0.671                               | 0.019 | 0.2944                               | 0.0031 |
| 13DC13_8a            | 98.7                               | 3.0                                 | 0.4 | 0.109                               | 0.016 | 0.2012                               | 0.0025 |
| 13DC13_8b            | 98.9                               | 13.9                                | 1.1 | 0.432                               | 0.033 | 0.2339                               | 0.0033 |
| 13DC13_11a           | 99.9                               | 22.6                                | 0.5 | 0.587                               | 0.012 | 0.2785                               | 0.0032 |
| 13DC13_11b           | 99.9                               | 25.0                                | 0.4 | 0.650                               | 0.007 | 0.2787                               | 0.0030 |
| 13DC13_12a           | 99.9                               | 27.9                                | 0.8 | 0.700                               | 0.018 | 0.2894                               | 0.0043 |
| 13DC13_12b           | 99.9                               | 21.1                                | 0.6 | 0.615                               | 0.015 | 0.2491                               | 0.0018 |
| Biotite-rich enclave |                                    |                                     |     |                                     |       |                                      |        |
| 13DC15_1a            | 99.9                               | 28.9                                | 0.7 | 0.697                               | 0.015 | 0.3006                               | 0.0042 |
| 13DC15_1b            | 99.2                               | 13.7                                | 0.7 | 0.454                               | 0.022 | 0.2189                               | 0.0041 |
| 13DC15_2a            | 99.9                               | 30.7                                | 1.2 | 0.681                               | 0.023 | 0.3271                               | 0.0050 |

|           |      |      |     |       |       |        |        |
|-----------|------|------|-----|-------|-------|--------|--------|
| 13DC15_2b | 99.9 | 30.4 | 1.2 | 0.670 | 0.024 | 0.3285 | 0.0050 |
|-----------|------|------|-----|-------|-------|--------|--------|

|                                      |        |                                     |       | <i>Ages (Ma)</i>                    |     |                                     |     |                                      |     |
|--------------------------------------|--------|-------------------------------------|-------|-------------------------------------|-----|-------------------------------------|-----|--------------------------------------|-----|
| <sup>208</sup> Pb/ <sup>206</sup> Pb | 2 σ    | <sup>232</sup> Th/ <sup>238</sup> U | 2 σ   | <sup>207</sup> Pb/ <sup>235</sup> U | 2 σ | <sup>206</sup> Pb/ <sup>238</sup> U | 2 σ | <sup>207</sup> Pb/ <sup>206</sup> Pb | 2 σ |
| 0.1097                               | 0.0021 | 0.410                               | 0.008 | 2403                                | 31  | 1635                                | 49  | 3137                                 | 10  |
| 0.1171                               | 0.0026 | 0.44                                | 0.01  | 2415                                | 18  | 1689                                | 26  | 3100                                 | 15  |
| 0.1344                               | 0.0092 | 0.49                                | 0.03  | 1609                                | 33  | 913                                 | 35  | 2696                                 | 11  |
| 0.1653                               | 0.0028 | 0.61                                | 0.01  | 1955                                | 54  | 1249                                | 73  | 2815                                 | 9   |
| 0.1349                               | 0.0050 | 0.51                                | 0.02  | 3124                                | 25  | 2697                                | 55  | 3411                                 | 11  |
| 0.1603                               | 0.0037 | 0.61                                | 0.01  | 3350                                | 15  | 3240                                | 35  | 3416                                 | 12  |
| 0.1016                               | 0.0018 | 0.39                                | 0.01  | 3204                                | 123 | 2897                                | 323 | 3403                                 | 7   |
| 0.0791                               | 0.0025 | 0.30                                | 0.01  | 3410                                | 25  | 3405                                | 68  | 3413                                 | 7   |
| 0.0802                               | 0.0022 | 0.304                               | 0.009 | 3403                                | 43  | 3392                                | 118 | 3410                                 | 4   |
| 0.1653                               | 0.0049 | 0.63                                | 0.02  | 2957                                | 85  | 2346                                | 183 | 3403                                 | 10  |
| 0.2601                               | 0.0050 | 0.99                                | 0.02  | 3110                                | 82  | 2670                                | 197 | 3408                                 | 6   |
| 0.1918                               | 0.0047 | 0.71                                | 0.02  | 2042                                | 34  | 1277                                | 45  | 2939                                 | 12  |
| 0.1221                               | 0.0042 | 0.46                                | 0.02  | 2478                                | 35  | 1751                                | 56  | 3143                                 | 20  |
| 0.1662                               | 0.0160 | 0.63                                | 0.06  | 2938                                | 38  | 2407                                | 81  | 3324                                 | 7   |
| 0.1274                               | 0.0047 | 0.48                                | 0.02  | 3248                                | 70  | 3063                                | 185 | 3365                                 | 6   |
| 0.1939                               | 0.0086 | 0.74                                | 0.03  | 3146                                | 49  | 2728                                | 114 | 3425                                 | 18  |
| 0.1519                               | 0.0091 | 0.56                                | 0.04  | 2111                                | 46  | 1305                                | 58  | 3024                                 | 33  |
| 0.1673                               | 0.0060 | 0.63                                | 0.02  | 2997                                | 53  | 2449                                | 115 | 3388                                 | 15  |
| 0.1733                               | 0.0153 | 0.66                                | 0.06  | 2886                                | 61  | 2251                                | 123 | 3366                                 | 21  |
| 0.2243                               | 0.0061 | 0.83                                | 0.02  | 2131                                | 33  | 1391                                | 46  | 2947                                 | 16  |
| 0.0337                               | 0.0025 | 0.127                               | 0.009 | 2987                                | 24  | 2531                                | 49  | 3310                                 | 15  |
| 0.0989                               | 0.0063 | 0.37                                | 0.02  | 2691                                | 33  | 2028                                | 60  | 3235                                 | 14  |
| 0.1370                               | 0.0070 | 0.52                                | 0.03  | 3099                                | 63  | 2706                                | 149 | 3365                                 | 15  |
|                                      |        |                                     |       |                                     |     |                                     |     |                                      |     |
| 0.2704                               | 0.0086 | 1.02                                | 0.03  | 3221                                | 31  | 3130                                | 75  | 3278                                 | 19  |
| 0.2734                               | 0.0060 | 1.02                                | 0.02  | 3082                                | 37  | 2922                                | 91  | 3187                                 | 14  |
| 0.0590                               | 0.0098 | 0.22                                | 0.04  | 3325                                | 26  | 3163                                | 62  | 3424                                 | 17  |
| 0.1390                               | 0.0048 | 0.53                                | 0.02  | 3425                                | 25  | 3373                                | 53  | 3455                                 | 24  |
| 0.0305                               | 0.0012 | 0.114                               | 0.005 | 2969                                | 33  | 2757                                | 70  | 3116                                 | 25  |
| 0.0377                               | 0.0012 | 0.141                               | 0.005 | 3142                                | 24  | 3110                                | 47  | 3163                                 | 25  |
| 0.0205                               | 0.0014 | 0.077                               | 0.005 | 3008                                | 31  | 2624                                | 68  | 3276                                 | 15  |
| 0.0120                               | 0.0017 | 0.045                               | 0.006 | 3421                                | 67  | 3535                                | 191 | 3355                                 | 18  |
| 0.0052                               | 0.0006 | 0.020                               | 0.002 | 2640                                | 45  | 2045                                | 84  | 3133                                 | 15  |
| 0.1528                               | 0.0061 | 0.58                                | 0.02  | 3450                                | 56  | 3678                                | 163 | 3320                                 | 16  |
| 0.0068                               | 0.0007 | 0.025                               | 0.003 | 2314                                | 40  | 1614                                | 64  | 3007                                 | 14  |
| 0.0291                               | 0.0017 | 0.108                               | 0.006 | 2244                                | 74  | 1543                                | 117 | 2964                                 | 17  |
| 0.1744                               | 0.0042 | 0.66                                | 0.02  | 3392                                | 29  | 3310                                | 72  | 3441                                 | 16  |
| 0.3320                               | 0.0225 | 1.22                                | 0.08  | 1414                                | 106 | 667                                 | 93  | 2836                                 | 20  |
| 0.3256                               | 0.0317 | 1.21                                | 0.12  | 2745                                | 70  | 2314                                | 148 | 3079                                 | 22  |
| 0.2083                               | 0.0053 | 0.79                                | 0.02  | 3208                                | 22  | 2979                                | 48  | 3354                                 | 18  |
| 0.2180                               | 0.0053 | 0.82                                | 0.02  | 3307                                | 15  | 3228                                | 27  | 3356                                 | 17  |
| 0.0831                               | 0.0045 | 0.32                                | 0.02  | 3416                                | 29  | 3420                                | 70  | 3414                                 | 23  |
| 0.0138                               | 0.0029 | 0.05                                | 0.01  | 3145                                | 25  | 3091                                | 62  | 3179                                 | 11  |
|                                      |        |                                     |       |                                     |     |                                     |     |                                      |     |
| 0.0491                               | 0.0027 | 0.43                                | 0.01  | 3450                                | 24  | 3410                                | 56  | 3473                                 | 21  |
| 0.1137                               | 0.0101 | 0.18                                | 0.04  | 2729                                | 48  | 2413                                | 99  | 2973                                 | 30  |
| 0.1222                               | 0.0081 | 0.47                                | 0.03  | 3510                                | 36  | 3349                                | 91  | 3603                                 | 23  |

0.1414 0.0048

0.54 0.02

3498 37

3307 92

3610 23

|       | <i>Semi-quantitative estimates</i> |            |         |            |          |            |
|-------|------------------------------------|------------|---------|------------|----------|------------|
| Disc. | Pb (ppm)                           | 2 $\sigma$ | U (ppm) | 2 $\sigma$ | Th (ppm) | 2 $\sigma$ |
| 54%   | 561.1                              | 54.2       | 1334.2  | 75.5       | 257.1    | 24.1       |
| 51%   | 750.8                              | 69.0       | 1691.0  | 97.5       | 393.6    | 21.5       |
| 71%   | 762.7                              | 58.6       | 2836.9  | 138.0      | 1205.3   | 56.3       |
| 61%   | 719.5                              | 82.0       | 2072.4  | 128.7      | 1761.5   | 119.7      |
| 26%   | 441.7                              | 31.8       | 537.6   | 26.3       | 201.2    | 7.2        |
| 7%    | 291.9                              | 28.6       | 259.7   | 20.9       | 119.2    | 6.5        |
| 18%   | 229.6                              | 35.6       | 252.7   | 25.7       | 47.9     | 8.1        |
| 0%    | 270.3                              | 24.3       | 262.1   | 14.3       | 79.6     | 4.3        |
| 1%    | 311.2                              | 144.1      | 301.8   | 64.9       | 99.1     | 35.8       |
| 37%   | 994.0                              | 459.5      | 1277.1  | 279.2      | 1155.2   | 416.1      |
| 26%   | 503.5                              | 232.0      | 470.9   | 100.2      | 630.9    | 224.8      |
| 62%   | 1026.5                             | 476.1      | 2848.9  | 611.6      | 1453.8   | 519.7      |
| 50%   | 639.5                              | 299.2      | 1351.8  | 293.4      | 463.4    | 168.2      |
| 33%   | 498.3                              | 58.6       | 615.0   | 31.8       | 659.5    | 34.4       |
| 11%   | 462.0                              | 63.7       | 455.9   | 36.4       | 283.8    | 24.0       |
| 25%   | 519.1                              | 65.7       | 581.2   | 30.2       | 483.1    | 30.4       |
| 63%   | 549.7                              | 70.8       | 1523.3  | 87.3       | 1529.7   | 84.0       |
| 33%   | 856.2                              | 118.6      | 1088.2  | 70.1       | 827.2    | 53.2       |
| 39%   | 804.5                              | 383.7      | 1060.1  | 255.7      | 802.4    | 316.6      |
| 58%   | 554.2                              | 264.1      | 1328.0  | 317.9      | 1141.1   | 473.1      |
| 28%   | 742.4                              | 355.2      | 1958.5  | 473.3      | 3333.7   | 665.8      |
| 43%   | 373.6                              | 181.5      | 640.1   | 154.4      | 201.4    | 81.2       |
| 24%   | 217.8                              | 26.1       | 271.2   | 28.5       | 86.3     | 11.8       |
| 6%    | 362.9                              | 36.3       | 348.2   | 22.4       | 291.7    | 16.8       |
| 10%   | 318.5                              | 34.0       | 341.1   | 24.9       | 314.0    | 17.9       |
| 10%   | 454.9                              | 60.5       | 512.0   | 16.6       | 27.1     | 3.4        |
| 3%    | 601.3                              | 127.5      | 537.8   | 54.1       | 380.8    | 44.1       |
| 14%   | 2056.7                             | 251.9      | 2772.3  | 171.0      | 123.0    | 9.9        |
| 2%    | 3204.9                             | 609.0      | 3668.1  | 425.6      | 459.0    | 62.8       |
| 24%   | 1043.6                             | 64.4       | 1395.5  | 35.8       | 80.5     | 4.2        |
| -7%   | 693.8                              | 178.2      | 679.7   | 34.8       | 28.3     | 4.5        |
| 40%   | 700.3                              | 67.2       | 1380.3  | 55.6       | 24.8     | 1.6        |
| -14%  | 153.6                              | 20.8       | 122.4   | 7.6        | 83.0     | 7.3        |
| 52%   | 933.0                              | 156.1      | 2409.8  | 204.5      | 54.9     | 4.3        |
| 54%   | 800.6                              | 416.3      | 2221.8  | 334.3      | 342.3    | 35.0       |
| 5%    | 633.2                              | 23.9       | 576.3   | 13.3       | 512.3    | 9.6        |
| 80%   | 497.2                              | 163.9      | 2097.3  | 130.5      | 560.3    | 34.1       |
| 29%   | 267.8                              | 50.0       | 615.1   | 65.1       | 259.1    | 34.6       |
| 14%   | 254.4                              | 37.7       | 265.0   | 18.6       | 169.7    | 20.1       |
| 5%    | 234.5                              | 34.5       | 224.7   | 15.6       | 155.7    | 18.4       |
| 0%    | 299.1                              | 46.4       | 290.7   | 21.1       | 101.5    | 12.7       |
| 3%    | 191.0                              | 11.8       | 232.3   | 5.1        | 12.1     | 1.4        |
| 2%    | 239.9                              | 28.6       | 240.6   | 24.3       | 75.1     | 9.4        |
| 23%   | 313.6                              | 24.1       | 494.5   | 20.9       | 86.1     | 9.8        |
| 9%    | 320.1                              | 18.1       | 292.7   | 10.4       | 177.2    | 4.5        |



|     |       |      |       |     |       |     |
|-----|-------|------|-------|-----|-------|-----|
| 11% | 336.1 | 10.8 | 314.8 | 7.4 | 191.2 | 4.0 |
|-----|-------|------|-------|-----|-------|-----|

Table S5: Lu-Hf isotope results for zircon standards analyzed by LA-MC-ICP-MS

| Standard name    | Age (Ma)    | 176Hf/177Hf 2 ste | 176Lu/177Hf 2 ste                 | 176Yb/177Hf          |
|------------------|-------------|-------------------|-----------------------------------|----------------------|
| <i>91500</i>     | <i>1065</i> | <i>0.282305</i>   | <i>0.000006 0.000121–0.000381</i> | <i>0.0036–0.0095</i> |
| 91500_1          |             | 0.282305          | 0.000016 0.000418                 | 0.014910             |
| 91500_2          |             | 0.282293          | 0.000016 0.000438                 | 0.015459             |
| 91500_3          |             | 0.282302          | 0.000017 0.000407                 | 0.014321             |
| 91500_4          |             | 0.282299          | 0.000018 0.000409                 | 0.014367             |
| 91500_5          |             | 0.282307          | 0.000016 0.000437                 | 0.015457             |
| 91500_6          |             | 0.282302          | 0.000013 0.000423                 | 0.014444             |
| 91500_7          |             | 0.282305          | 0.000018 0.000420                 | 0.014222             |
| 91500_8          |             | 0.282286          | 0.000016 0.000390                 | 0.013120             |
| 91500_9          |             | 0.282302          | 0.000018 0.000383                 | 0.012902             |
| 91500_10         |             | 0.282286          | 0.000014 0.000356                 | 0.011996             |
| 91500_11         |             | 0.282301          | 0.000014 0.000374                 | 0.012674             |
| 91500_12         |             | 0.282280          | 0.000020 0.000386                 | 0.012975             |
| 91500_13         |             | 0.282309          | 0.000019 0.000390                 | 0.013130             |
| 91500_14         |             | 0.282302          | 0.000016 0.000386                 | 0.012839             |
| 91500_15         |             | 0.282294          | 0.000017 0.000414                 | 0.013977             |
| 91500_16         |             | 0.282315          | 0.000014 0.000405                 | 0.013517             |
| Average          |             | 0.282299          | 0.000018 0.000402                 | 0.013769             |
|                  |             |                   |                                   |                      |
| <i>Mud tank</i>  | <i>570</i>  | <i>0.282507</i>   | <i>0.000006 0.000042 -</i>        | <i>0.0012</i>        |
| MudTank_1        |             | 0.282515          | 0.000012 0.000018                 | 0.000780             |
| MudTank_2        |             | 0.282500          | 0.000012 0.000017                 | 0.000746             |
| MudTank_3        |             | 0.282497          | 0.000011 0.000020                 | 0.000854             |
| MudTank_4        |             | 0.282497          | 0.000011 0.000020                 | 0.000854             |
| MudTank_5        |             | 0.282506          | 0.000012 0.000019                 | 0.000814             |
| MudTank_6        |             | 0.282509          | 0.000011 0.000023                 | 0.000948             |
| MudTank_7        |             | 0.282489          | 0.000012 0.000017                 | 0.000745             |
| MudTank_8        |             | 0.282504          | 0.000010 0.000018                 | 0.000737             |
| MudTank_9        |             | 0.282504          | 0.000012 0.000017                 | 0.000703             |
| MudTank_10       |             | 0.282493          | 0.000009 0.000017                 | 0.000707             |
| MudTank_11       |             | 0.282500          | 0.000011 0.000017                 | 0.000708             |
| MudTank_12       |             | 0.282513          | 0.000012 0.000018                 | 0.000759             |
| MudTank_13       |             | 0.282510          | 0.000013 0.000018                 | 0.000723             |
| MudTank_14       |             | 0.282496          | 0.000013 0.000017                 | 0.000727             |
| MudTank_15       |             | 0.282494          | 0.000010 0.000020                 | 0.000805             |
| MudTank_16       |             | 0.282503          | 0.000013 0.000018                 | 0.000766             |
| MudTank_17       |             | 0.282484          | 0.000013 0.000018                 | 0.000732             |
| Average          |             | 0.282501          | 0.000017 0.000018                 | 0.000771             |
|                  |             |                   |                                   |                      |
| <i>Plešovice</i> | <i>337</i>  | <i>0.282482</i>   | <i>0.000012 0.000042–0.000141</i> | <i>0.0012–0.0041</i> |
| Plešovice_gr1_1  |             | 0.282479          | 0.000010 0.000079                 | 0.004115             |
| Plešovice_gr1_2  |             | 0.282480          | 0.000010 0.000088                 | 0.004563             |
| Plešovice_gr1_3  |             | 0.282476          | 0.000010 0.000085                 | 0.004391             |
| Plešovice_gr1_4  |             | 0.282462          | 0.000009 0.000088                 | 0.004573             |
| Plešovice_gr1_5  |             | 0.282467          | 0.000012 0.000085                 | 0.004412             |
| Plešovice_gr1_6  |             | 0.282470          | 0.000012 0.000106                 | 0.005312             |
| Plešovice_gr1_7  |             | 0.282467          | 0.000012 0.000087                 | 0.004454             |
| Average          |             | 0.282472          | 0.000013 0.000088                 | 0.004546             |
|                  |             |                   |                                   |                      |
| <i>R33</i>       | <i>419</i>  | <i>0.282764</i>   | <i>0.000014 0.001989 -</i>        | <i>0.052</i>         |

|           |          |          |          |          |          |
|-----------|----------|----------|----------|----------|----------|
| R33_gr1_1 | 0.282749 | 0.000018 | 0.002085 | 0.000063 | 0.076698 |
| R33_gr1_2 | 0.282755 | 0.000013 | 0.001832 | 0.000091 | 0.067295 |
| R33_gr1_3 | 0.282757 | 0.000016 | 0.001660 | 0.000056 | 0.059885 |
| R33_gr1_4 | 0.282728 | 0.000016 | 0.001249 | 0.000050 | 0.044724 |
| R33_gr1_5 | 0.282740 | 0.000012 | 0.001351 | 0.000011 | 0.047085 |
| R33_gr2_1 | 0.282785 | 0.000014 | 0.003456 | 0.000014 | 0.120370 |
| R33_gr2_2 | 0.282771 | 0.000014 | 0.003375 | 0.000016 | 0.117759 |
| R33_gr2_3 | 0.282785 | 0.000012 | 0.003821 | 0.000033 | 0.135503 |
| R33_gr2_4 | 0.282747 | 0.000015 | 0.002672 | 0.000039 | 0.094189 |
| Average   | 0.282757 | 0.000039 | 0.002389 | 0.001943 | 0.084834 |

\* Present day value normalized to the respective zircon standard best average  $^{176}\text{Hf}/^{177}\text{Hf}$  as provided by the q

| 2 ste                            | 178Hf/177Hf | 2 ste    | $\epsilon_{\text{Hf}}(\text{ref})^*$ | 2 ste | Reference |
|----------------------------------|-------------|----------|--------------------------------------|-------|-----------|
| <i>Blichert-Toft (2008)</i>      |             |          |                                      |       |           |
| 0.000109                         | 1.467259    | 0.000047 | 0.0                                  | 0.6   |           |
| 0.000094                         | 1.467260    | 0.000031 | -0.5                                 | 0.6   |           |
| 0.000087                         | 1.467289    | 0.000037 | -0.1                                 | 0.6   |           |
| 0.000081                         | 1.467286    | 0.000044 | -0.2                                 | 0.6   |           |
| 0.000091                         | 1.467252    | 0.000040 | 0.0                                  | 0.6   |           |
| 0.000129                         | 1.467262    | 0.000037 | -0.1                                 | 0.5   |           |
| 0.000114                         | 1.467275    | 0.000043 | 0.0                                  | 0.6   |           |
| 0.000103                         | 1.467261    | 0.000032 | -0.7                                 | 0.6   |           |
| 0.000095                         | 1.467261    | 0.000042 | -0.1                                 | 0.6   |           |
| 0.000101                         | 1.467288    | 0.000032 | -0.6                                 | 0.5   |           |
| 0.000095                         | 1.467239    | 0.000038 | -0.1                                 | 0.5   |           |
| 0.000116                         | 1.467256    | 0.000040 | -0.9                                 | 0.7   |           |
| 0.000093                         | 1.467282    | 0.000035 | 0.1                                  | 0.7   |           |
| 0.000053                         | 1.467292    | 0.000036 | -0.1                                 | 0.6   |           |
| 0.000096                         | 1.467308    | 0.000037 | -0.4                                 | 0.6   |           |
| 0.000099                         | 1.467261    | 0.000039 | 0.3                                  | 0.5   |           |
| 0.002056                         | 1.467271    | 0.000036 | 0.4                                  | 0.7   |           |
| <i>Woodhead and Hergt (2005)</i> |             |          |                                      |       |           |
| 0.000009                         | 1.467283    | 0.000024 | 0.3                                  | 0.4   |           |
| 0.000008                         | 1.467256    | 0.000026 | -0.2                                 | 0.4   |           |
| 0.000013                         | 1.467266    | 0.000030 | -0.4                                 | 0.4   |           |
| 0.000013                         | 1.467266    | 0.000030 | -0.4                                 | 0.4   |           |
| 0.000007                         | 1.467258    | 0.000029 | 0.0                                  | 0.4   |           |
| 0.000006                         | 1.467275    | 0.000021 | 0.1                                  | 0.4   |           |
| 0.000006                         | 1.467268    | 0.000023 | -0.6                                 | 0.4   |           |
| 0.000007                         | 1.467276    | 0.000025 | -0.1                                 | 0.3   |           |
| 0.000005                         | 1.467293    | 0.000026 | -0.1                                 | 0.4   |           |
| 0.000007                         | 1.467280    | 0.000027 | -0.5                                 | 0.3   |           |
| 0.000006                         | 1.467272    | 0.000025 | -0.2                                 | 0.4   |           |
| 0.000010                         | 1.467314    | 0.000034 | 0.2                                  | 0.4   |           |
| 0.000005                         | 1.467279    | 0.000027 | 0.1                                  | 0.4   |           |
| 0.000011                         | 1.467256    | 0.000031 | -0.4                                 | 0.5   |           |
| 0.000005                         | 1.467266    | 0.000032 | -0.5                                 | 0.4   |           |
| 0.000007                         | 1.467283    | 0.000034 | -0.1                                 | 0.5   |           |
| 0.000006                         | 1.467281    | 0.000026 | -0.8                                 | 0.4   |           |
| 0.000132                         | 1.467275    | 0.000029 | -0.2                                 | 0.6   |           |
| <i>Sláma et al. (2008)</i>       |             |          |                                      |       |           |
| 0.000043                         | 1.467261    | 0.000029 | -0.1                                 | 0.4   |           |
| 0.000035                         | 1.467280    | 0.000032 | -0.1                                 | 0.4   |           |
| 0.000100                         | 1.467276    | 0.000021 | -0.2                                 | 0.4   |           |
| 0.000035                         | 1.467276    | 0.000024 | -0.7                                 | 0.3   |           |
| 0.000016                         | 1.467257    | 0.000026 | -0.5                                 | 0.4   |           |
| 0.000048                         | 1.467278    | 0.000026 | -0.4                                 | 0.4   |           |
| 0.000070                         | 1.467278    | 0.000028 | -0.5                                 | 0.4   |           |
| 0.000741                         | 1.467272    | 0.000019 | -0.4                                 | 0.5   |           |

*Fisher et al. (2014)*

|          |          |          |      |     |
|----------|----------|----------|------|-----|
| 0.003340 | 1.467262 | 0.000031 | -0.6 | 0.6 |
| 0.004302 | 1.467280 | 0.000031 | -0.3 | 0.5 |
| 0.001717 | 1.467243 | 0.000037 | -0.1 | 0.6 |
| 0.002176 | 1.467269 | 0.000025 | -1.1 | 0.6 |
| 0.000720 | 1.467270 | 0.000033 | -0.7 | 0.4 |
| 0.000759 | 1.467256 | 0.000027 | 0.3  | 0.5 |
| 0.000502 | 1.467293 | 0.000031 | -0.2 | 0.5 |
| 0.000336 | 1.467277 | 0.000026 | 0.2  | 0.4 |
| 0.000906 | 1.467256 | 0.000035 | -0.8 | 0.5 |
| 0.067200 | 1.467267 | 0.000030 | -0.3 | 0.9 |

quoted reference

Table S6. Lu-Hf isotope results for Indian zircons analyzed by LA-MC-ICP-MS

| Name                        | Age (Ma) | 2 $\sigma$ | Discordance (%) | 176Hf/177Hf | 2 $\sigma$ | 176Lu/177Hf |
|-----------------------------|----------|------------|-----------------|-------------|------------|-------------|
| <i>Granitic gneiss</i>      |          |            |                 |             |            |             |
| 13DC12_1a                   | 3137     | 10         | 54%             | 0.281023    | 0.000018   | 0.00460     |
| 13DC12_1b                   | 3100     | 15         | 51%             | 0.280990    | 0.000022   | 0.00489     |
| 13DC12_2a                   | 2696     | 11         | 71%             | 0.281124    | 0.000029   | 0.00689     |
| 13DC12_2b                   | 2815     | 9          | 61%             | 0.280890    | 0.000023   | 0.00365     |
| 13DC12_3                    | 3411     | 11         | 26%             | 0.280772    | 0.000021   | 0.00209     |
| 13DC12_3                    | 3416     | 12         | 7%              | 0.280772    | 0.000021   | 0.00209     |
| 13DC12_4                    | 3403     | 7          | 18%             | 0.280723    | 0.000015   | 0.00167     |
| 13DC12_5a                   | 3413     | 7          | 0%              | 0.280757    | 0.000016   | 0.00186     |
| 13DC12_5b                   | 3410     | 4          | 1%              | 0.280734    | 0.000014   | 0.00165     |
| 13DC12_6                    | 3403     | 10         | 37%             | 0.280875    | 0.000024   | 0.00361     |
| 13DC12_7                    | 3408     | 6          | 26%             | 0.280766    | 0.000012   | 0.00198     |
| 13DC12_8a                   | 2939     | 12         | 62%             | 0.280855    | 0.000025   | 0.00394     |
| 13DC12_8b                   | 3143     | 20         | 50%             | 0.281032    | 0.000024   | 0.00633     |
| 13DC12_9a                   | 3324     | 7          | 33%             | 0.280767    | 0.000019   | 0.00219     |
| 13DC12_9b                   | 3365     | 6          | 11%             | 0.280685    | 0.000032   | 0.00167     |
| 13DC12_10a                  | 3425     | 18         | 25%             | 0.280884    | 0.000043   | 0.00313     |
| 13DC12_10b                  | 3024     | 33         | 63%             | 0.280816    | 0.000020   | 0.00317     |
| 13DC12_11a                  | 3388     | 15         | 33%             | 0.280869    | 0.000036   | 0.00426     |
| 13DC12_11b                  | 3366     | 21         | 39%             | 0.280766    | 0.000030   | 0.00272     |
| 13DC12_12a                  | 2947     | 16         | 58%             | 0.280886    | 0.000025   | 0.00369     |
| 13DC12_12b                  | 3310     | 15         | 28%             | 0.280833    | 0.000015   | 0.00271     |
| 13DC12_13a                  | 3235     | 14         | 43%             | 0.280733    | 0.000015   | 0.00177     |
| 13DC12_13b                  | 3365     | 15         | 24%             | 0.280739    | 0.000013   | 0.00214     |
| <i>Trondhjemitic gneiss</i> |          |            |                 |             |            |             |
| 13DC13_3a                   | 3278     | 19         | 6%              | 0.280841    | 0.000020   | 0.00114     |
| 13DC13_3b                   | 3187     | 14         | 10%             | 0.280885    | 0.000024   | 0.00143     |
| 13DC13_4_1                  | 3424     | 17         | 10%             | 0.280856    | 0.000012   | 0.00170     |
| 13DC13_4_2                  | 3455     | 24         | 3%              | 0.280856    | 0.000012   | 0.00170     |
| 13DC13_5a_1                 | 3116     | 25         | 14%             | 0.280873    | 0.000011   | 0.00191     |
| 13DC13_5a_2                 | 3163     | 25         | 2%              | 0.280873    | 0.000011   | 0.00191     |
| 13DC13_5b_1                 | 3276     | 15         | 24%             | 0.280837    | 0.000016   | 0.00182     |
| 13DC13_5b_2                 | 3355     | 18         | -7%             | 0.280837    | 0.000016   | 0.00182     |
| 13DC13_6a                   | 3133     | 15         | 40%             | 0.280893    | 0.000016   | 0.00206     |
| 13DC13_6b                   | 3320     | 16         | -14%            | 0.280856    | 0.000015   | 0.00167     |
| 13DC13_6c                   | 3007     | 14         | 52%             | 0.280926    | 0.000014   | 0.00284     |
| 13DC13_7a                   | 2964     | 17         | 54%             | 0.280899    | 0.000026   | 0.00256     |
| 13DC13_7b                   | 3441     | 16         | 5%              | 0.280948    | 0.000018   | 0.00348     |
| 13DC13_8a                   | 2836     | 20         | 80%             | 0.280872    | 0.000033   | 0.00186     |
| 13DC13_8b                   | 3079     | 22         | 29%             | 0.280836    | 0.000026   | 0.00186     |
| 13DC13_11a                  | 3354     | 18         | 14%             | 0.280888    | 0.000015   | 0.00234     |
| 13DC13_11b                  | 3356     | 17         | 5%              | 0.280912    | 0.000016   | 0.00283     |
| 13DC13_12a                  | 3414     | 23         | 0%              | 0.280929    | 0.000015   | 0.00105     |
| 13DC13_12b                  | 3179     | 11         | 3%              | 0.280864    | 0.000009   | 0.00069     |
| <i>Biotite-rich enclave</i> |          |            |                 |             |            |             |
| 13DC15_1a                   | 3473     | 21         | 2%              | 0.280571    | 0.000021   | 0.00140     |
| 13DC15_1b                   | 2973     | 30         | 23%             | 0.280548    | 0.000011   | 0.00108     |
| 13DC15_2a                   | 3603     | 23         | 9%              | 0.280450    | 0.000017   | 0.00109     |

|           |      |    |     |          |          |         |
|-----------|------|----|-----|----------|----------|---------|
| 13DC15_2b | 3610 | 23 | 11% | 0.280475 | 0.000020 | 0.00146 |
|-----------|------|----|-----|----------|----------|---------|

| 2 $\sigma$ | 176Yb/177Hf 2 $\sigma$ |        | 178Hf/177Hf 2 $\sigma$ |         | 176Hf/177Hf in 2 $\sigma$ |          |
|------------|------------------------|--------|------------------------|---------|---------------------------|----------|
| 0.00013    | 0.1756                 | 0.0061 | 1.46728                | 0.00004 | 0.280746                  | 0.000020 |
| 0.00021    | 0.1899                 | 0.0100 | 1.46726                | 0.00004 | 0.280699                  | 0.000026 |
| 0.00014    | 0.2782                 | 0.0068 | 1.46728                | 0.00004 | 0.280768                  | 0.000031 |
| 0.00008    | 0.1358                 | 0.0034 | 1.46727                | 0.00006 | 0.280693                  | 0.000024 |
| 0.00009    | 0.0784                 | 0.0041 | 1.46723                | 0.00003 | 0.280635                  | 0.000022 |
| 0.00009    | 0.0784                 | 0.0041 | 1.46723                | 0.00003 | 0.280634                  | 0.000022 |
| 0.00005    | 0.0580                 | 0.0016 | 1.46731                | 0.00003 | 0.280613                  | 0.000016 |
| 0.00007    | 0.0644                 | 0.0026 | 1.46727                | 0.00002 | 0.280635                  | 0.000018 |
| 0.00003    | 0.0593                 | 0.0011 | 1.46727                | 0.00003 | 0.280625                  | 0.000015 |
| 0.00020    | 0.1296                 | 0.0104 | 1.46728                | 0.00004 | 0.280638                  | 0.000028 |
| 0.00009    | 0.0694                 | 0.0037 | 1.46727                | 0.00002 | 0.280636                  | 0.000014 |
| 0.00014    | 0.1406                 | 0.0058 | 1.46729                | 0.00004 | 0.280632                  | 0.000027 |
| 0.00021    | 0.2515                 | 0.0068 | 1.46726                | 0.00004 | 0.280650                  | 0.000027 |
| 0.00012    | 0.0684                 | 0.0040 | 1.46730                | 0.00007 | 0.280626                  | 0.000021 |
| 0.00005    | 0.0522                 | 0.0024 | 1.46729                | 0.00005 | 0.280577                  | 0.000033 |
| 0.00010    | 0.1032                 | 0.0028 | 1.46723                | 0.00005 | 0.280678                  | 0.000044 |
| 0.00006    | 0.1167                 | 0.0044 | 1.46730                | 0.00004 | 0.280631                  | 0.000021 |
| 0.00031    | 0.1539                 | 0.0125 | 1.46728                | 0.00005 | 0.280591                  | 0.000042 |
| 0.00020    | 0.0952                 | 0.0086 | 1.46734                | 0.00008 | 0.280590                  | 0.000033 |
| 0.00023    | 0.1298                 | 0.0093 | 1.46725                | 0.00003 | 0.280678                  | 0.000029 |
| 0.00023    | 0.0833                 | 0.0052 | 1.46728                | 0.00002 | 0.280661                  | 0.000022 |
| 0.00010    | 0.0596                 | 0.0027 | 1.46731                | 0.00003 | 0.280623                  | 0.000017 |
| 0.00015    | 0.0828                 | 0.0080 | 1.46729                | 0.00003 | 0.280600                  | 0.000017 |
| 0.00009    | 0.0401                 | 0.0037 | 1.46729                | 0.00004 | 0.280769                  | 0.000022 |
| 0.00006    | 0.0489                 | 0.0022 | 1.46733                | 0.00004 | 0.280797                  | 0.000025 |
| 0.00006    | 0.0559                 | 0.0020 | 1.46729                | 0.00003 | 0.280744                  | 0.000014 |
| 0.00006    | 0.0559                 | 0.0020 | 1.46729                | 0.00003 | 0.280743                  | 0.000014 |
| 0.00004    | 0.0680                 | 0.0006 | 1.46728                | 0.00002 | 0.280758                  | 0.000013 |
| 0.00004    | 0.0680                 | 0.0006 | 1.46728                | 0.00002 | 0.280756                  | 0.000013 |
| 0.00007    | 0.0569                 | 0.0021 | 1.46728                | 0.00003 | 0.280722                  | 0.000018 |
| 0.00007    | 0.0569                 | 0.0021 | 1.46728                | 0.00003 | 0.280719                  | 0.000018 |
| 0.00004    | 0.0587                 | 0.0018 | 1.46732                | 0.00004 | 0.280769                  | 0.000017 |
| 0.00006    | 0.0587                 | 0.0024 | 1.46727                | 0.00003 | 0.280749                  | 0.000017 |
| 0.00007    | 0.0832                 | 0.0010 | 1.46731                | 0.00003 | 0.280762                  | 0.000016 |
| 0.00013    | 0.0769                 | 0.0033 | 1.46724                | 0.00009 | 0.280753                  | 0.000027 |
| 0.00017    | 0.1165                 | 0.0060 | 1.46729                | 0.00003 | 0.280717                  | 0.000022 |
| 0.00007    | 0.0601                 | 0.0020 | 1.46733                | 0.00005 | 0.280771                  | 0.000034 |
| 0.00007    | 0.0592                 | 0.0019 | 1.46728                | 0.00006 | 0.280726                  | 0.000027 |
| 0.00007    | 0.0838                 | 0.0030 | 1.46727                | 0.00003 | 0.280736                  | 0.000017 |
| 0.00007    | 0.0985                 | 0.0020 | 1.46723                | 0.00003 | 0.280730                  | 0.000017 |
| 0.00003    | 0.0336                 | 0.0010 | 1.46729                | 0.00003 | 0.280860                  | 0.000016 |
| 0.00003    | 0.0223                 | 0.0012 | 1.46726                | 0.00003 | 0.280822                  | 0.000011 |
| 0.00006    | 0.0415                 | 0.0016 | 1.46730                | 0.00004 | 0.280477                  | 0.000022 |
| 0.00002    | 0.0349                 | 0.0004 | 1.46730                | 0.00003 | 0.280487                  | 0.000013 |
| 0.00009    | 0.0354                 | 0.0037 | 1.46726                | 0.00005 | 0.280374                  | 0.000019 |



0.00004      0.0502      0.0010      1.46726      0.00005      0.280373      0.000021

| $\epsilon_{\text{Hf in}}$ | $2\sigma$ |
|---------------------------|-----------|
| -0.3                      | 0.7       |
| -2.9                      | 0.9       |
| -10.0                     | 1.1       |
| -9.8                      | 0.9       |
| 2.3                       | 0.8       |
| 2.4                       | 0.8       |
| 1.3                       | 0.6       |
| 2.3                       | 0.6       |
| 1.9                       | 0.5       |
| 2.2                       | 1.0       |
| 2.3                       | 0.5       |
| -9.1                      | 1.0       |
| -3.6                      | 1.0       |
| -0.1                      | 0.8       |
| -0.9                      | 1.2       |
| 4.1                       | 1.6       |
| -7.1                      | 0.8       |
| 0.2                       | 1.5       |
| -0.4                      | 1.2       |
| -7.2                      | 1.0       |
| 0.8                       | 0.8       |
| -2.3                      | 0.6       |
| -0.1                      | 0.6       |
| 3.9                       | 0.8       |
| 2.7                       | 0.9       |
| 6.5                       | 0.5       |
| 7.2                       | 0.5       |
| -0.4                      | 0.5       |
| 0.7                       | 0.5       |
| 2.2                       | 0.6       |
| 4.0                       | 0.6       |
| 0.4                       | 0.6       |
| 4.2                       | 0.6       |
| -2.8                      | 0.6       |
| -4.2                      | 1.0       |
| 5.9                       | 0.8       |
| -6.6                      | 1.2       |
| -2.4                      | 1.0       |
| 4.6                       | 0.6       |
| 4.3                       | 0.6       |
| 10.4                      | 0.6       |
| 3.4                       | 0.4       |
| -1.8                      | 0.8       |
| -13.4                     | 0.5       |
| -2.4                      | 0.7       |

-2.3

0.7